DOCTOR OF PHILOSOPHY

Visible Light Positioning for Indoor and Outdoor Applications

Mahmoud, Abdulrahman

Award date:
2022

Awarding institution:
Coventry University

Visible Light Positioning for Indoor and Outdoor Applications

By

Abdulrahman A. Mahmoud

PhD

April, 2022

Visible Light Positioning for Indoor and Outdoor Applications

A thesis submitted in partial fulfilment of the University's requirements for the degree of Doctor of Philosophy

April, 2022

Supervisors: Dr. Olivier Haas, Dr. Zahir Ahmad, Dr. Sujan Rajbhandari

Coventry University

Certificate of Ethical Approval

Applicant:	Abdulrahman Mahmoud
Project Title:	Visible Light Positioning for Indoor and Outdoor Applications

This is to certify that the above named applicant has completed the Coventry University Ethical Approval process and their project has been confirmed and approved as Low Risk

Date of approval:	03 Jun 2021
Project Reference Number:	P122558

[redacted]

Declaration

All sentences or passages quoted in this document from other people's work have been specifically acknowledged by clear cross-referencing to author, work and page(s). Any illustrations that are not the work of the author of this report have been used with the explicit permission of the originator and are specifically acknowledged. I understand that failure to do this amounts to plagiarism and will be considered grounds for failure.

Name: Abdulrahman A. Mahmoud

Signature: [redacted]

Date: April 14, 2022

Abstract

Traditional approaches to three-dimensional (3-D) visible light positioning (VLP) suffers significantly in the presence of multipath propagation. This thesis overcomes such challenges by adopting a novel spatial and angular diversity receivers and combining them with various machine learning (ML) algorithms for indoor, dark, passive and outdoor VLP. This thesis uses light emitting diode (LED)s as transmitters and photodiode (PD)s as receivers. To ensure that realistic channel models are used, the VLP model includes line-of-sight (LOS), non-LOS (NLOS) for all indoor applications. Only LOS path is considered in the outdoor as the effect of NLOS from the road is ignored. However, the outdoor applications consider the impact of weather condition. A range of ML approaches were considered, however, it is found that multi-layer perceptron (MLP) network offers the best performance and the lowest complexity for VLP applications. Using Levenberg Marquardt, the MLP hyper-parameters are tuned for each application to ensure good performance and generalisability.

The results for each indoor application demonstrates the benefit of combining ML technique with received signal strength (RSS) based VLP. The ML technique offers good 3-D indoor VLP that is further improved using spatial receiver diversity, resulting in a positioning error of 0.021 m in a 5 m^3 room. The application to dark VLP, which uses a very low duty cycle pulse width modulation (PWM), resulted in a slightly higher positioning error of 0.06 m, which is still a 52% positioning accuracy improvement compared to state-of-the-art dark VLP techniques. The more challenging passive VLP led to an RMS error of 0.23 m for a solution involving 9 transmitters and 21 receivers placed on the ceiling and walls in a 5 m $\times$5 m $\times$3 m room dimension.

MLs are demonstrated for outdoor vehicular applications with traffic lights and streetlights. The two-dimensional VLP using angular and spatial receiver diversity is able to overcome the streetlight collinearity condition resulting in 0.22 m RMS error in the presence of direct sunlight, 0.29 m for dense fog and 0.14 m at night. Traffic light VLP with two receivers facing the direction of travel led to positioning errors of 1.33 m and 0.21 m using a single and double traffic light on the road, respectively. This represented a 77% and 47% improvement with the state-of-the-art traffic light-based VLP technique. These results highlight the degrading effect of NLOS and weather conditions in VLP and how ML techniques, together with spatial and angular receiver diversity scheme can be used to offer improved accuracy for outdoor and indoor applications.

Acknowledgement

Working as a PhD student at Coventry University was a magnificent and challenging experience. Several people have been directly or indirectly, instrumental in shaping up my academic career throughout the years. It was hardly possible for me to blossom in my doctoral work without the continued aid of these personalities. Here is a small tribute to them all.

Alhamdulillah, I praise and thank Allah SWT for His greatness and for giving me the strength and courage to complete this thesis.

I want to extend my sincere gratitude to the petroleum technology development fund (PTDF) for providing me with the funding to conduct this research.

I want to thank all my supervisors named in this document for their relentless effort in giving me the hope, courage and support needed to complete this thesis. One could not wish for a better team to govern his/her research pathway.

In my research group, I was fortunate and blessed with cheerful friends. A special thanks to all my office colleagues for their invaluable assistance.

My parents, Abdullahi Mahmud Gaya and Salma Rabiu Abdullahi deserve special mention for their inseparable support and prayers. They have, in countless ways, been responsible for the man I am today, and words fail to show my appreciation towards them. Finally, I would like to thank Mahmoud Abdullahi for his support in ensuring the graphical content of this thesis is up to par.

Contents

List of Figures

List of Tables

Abbreviations

1-D	One-dimensional
2-D	Two-dimensional
3-D	Three-dimensional
5G	Fifth generation
ALOHA	Additive links on-line hawaii
ANN	Artificial Neural Network
AOA	Angle of arrival
APD	Avalanche Photo-Diode
AWGN	Additive White Gaussian Noise
BPSK	Binary phase shift keying
CDF	Cumulative distributive function
CI	Confidence interval
CMD	Cayley Menger determinant
DD	Direct detection
dGPS	differential GPS
DNN	Deep neural network
DTMF	Dual-tone multi-frequency
FDM	Frequency Division Multiplexing
FOV	Field of view
FPGA	Field-programmable gate array
GNSS	Global Navigation Satellite System
GPS	Global positioning system
GRU	Gated recurrent unit
I2V	Infrastructure to vehicle
IMU	Inertial measurement unit
IM	Intensity Modulation
IPS	Indoor positioning system
ITS	Intelligent Transport System
LBS	Location-based services
LD	Laser Diode
LED	Light Emitting Diode
LLS	Linear least squares
LOS	Line-of-sight

LSTM Long short-term memory
ML Machine learning
MLP Multi-layer perceptron
MSE Mean squared error
NLOS Non line-of-sight
NN Neural network
OFDM Orthogonal frequency division multiplexing
OIR Object impulse response
OOC Optical symmetrical code
OW Optical Wireless
OWC Optical Wireless Communication
PC-LED Phosphor Converted LED
PD Photo-diode
PIR Passive infrared sensor
POA Phase of arrival
PPM Pulse-position modulation
PSO Particle swarm optimisation
PWM Pulse width modulation
QPSK Quadrature phase shift keying
RF Radio-frequency
RFID Radio-frequency identification
RMS Root mean square
RNN Recurrent neural network
RSS Received signal strength
SLP Single-layer perceptron
SNR Signal-to-noise ratio
SSL Solid-state lighting
TDM Time Division Multiplexing
TDOA Time difference of arrival
TOA Time of arrival
TOF Time of flight
UWB Ultra-Wide Band
V2I Vehicle to infrastructure
V2V Vehicle-to-vehicle
VLC Visible Light Communication
VLP Visible Light Positioning
WiGig Wireless Gigabit Alliance

List of Symbols

$\bar{x}$	Sample mean
β_λ	Atmospheric attenuation
ΔA	Wall reflectors
η	Fixed capacitance of the PD
η_{qe}	Quantum efficiency
Γ	FET channel noise factor
λ	Wavelength
λ_0	Solar band maximum spectrum
$*$	Hadamard product in LSTM
$\mathbf{b_c}$	Current memory state in LSTM
$\mathbf{b_f}$	Forget gate in LSTM
$\mathbf{b_h}$	Hidden bias vector in RNN
$\mathbf{b_i}$	Bias of the input gate in LSTM
$\mathbf{b_l}$	Output gate in LSTM
$\mathbf{b_m}$	Bias of the current memory state in GRU
$\mathbf{b_o}$	Output bias vector in RNN
$\mathbf{b_r}$	Reset gate in GRU
$\mathbf{b_z}$	Update gate in GRU
$\mathbf{h_{t-1}}$	Previous state in LSTM
$\mathbf{h_{t-1}}$	Previous state in RNN
$\mathbf{U_c}$	Current memory state in LSTM
$\mathbf{U_f}$	Forget gate in LSTM
$\mathbf{U_h}$	Hidden weight matrices of the current memory state in GRU
$\mathbf{U_h}$	Hidden weight matrix in RNN
$\mathbf{U_i}$	Hidden weight matrices of the input gate in LSTM
$\mathbf{U_o}$	Output gate in LSTM
$\mathbf{U_r}$	Reset gate in GRU
$\mathbf{U_z}$	Update gate in GRU
$\mathbf{W_f}$	Forget gate in LSTM
$\mathbf{W_h}$	Weight matrices of the current memory state in GRU
$\mathbf{W_i}$	Weight matrices of the input gate in LSTM
$\mathbf{W_o}$	Output gate in LSTM
$\mathbf{W_r}$	Reset gate in GRU

$\mathbf{W_x}$	Input matrix in RNN
$\mathbf{W_z}$	Update gate in GRU
μ	Newton update
$\omega^2_{thermal,j}$	Thermal noise
$\omega^2_{shot,j}$	Shot noise
$\overline{SNR}$	Average SNR
ϕ	Irradiance angle
Ψ	FOV
ψ	Incidence angle
ρ	Reflection coefficient
$\mathbf{X}_k$	Levenberg-Marquardt algorithm
$\widehat{d}$	Calculated distance
$\widehat{x}$	Estimated receiver location in x axis
$\widehat{y}$	Estimated receiver location in y axis
$\widehat{z}$	Estimated receiver location in z axis
$a(t)$	Period
A_{coll}	Lens collection area
A_{eff}	Detector active area of a PD
A_d	Detector physical area of a PD
B	Bandwidth
$c(h)$	Cost function
D	Duty cycle
e	Vector of the networks error
g	Optical concentrator gain
G	Open-loop gain
g_m	FET trans-conductance
g_r	Gradient
H	Hessian matrix
H_{los}	Line of sight DC gain
H_{nlos}	Non-line of sight DC gain
I	Optical intensity at a given distance
I_{bg}	Background current
I_{ph}	APD un-multiplied photo-current
I_0	Optical intensity at zero distance
I_2	Noise bandwidth factor
I_T	Average photo-current
J	Jacobian matrix
k	Boltzmann's constant
L	Hidden layer
m	Lambertian emission order
M	Number of transmitters
n	Sample size

N	Number of receivers
n_c	Refractive index
0	Computational complexity
O_e	Number of epochs
O_e	Number of training samples
P_r	Received power
P_t	Transmitted power
q	Electronic charge
r	Point in coordinate system
R_0	Angular distribution
R_p	Receiver responsivity
s	Confidence level
$S(\phi)$	Radiant intensity
T_{PWM}	PWM signal
T_{th}	2% Visual threshold
T_k	Absolute temperature
$T_s(\psi)$	Optical filter
V	Visibility
w	Visible – NIR wavelengths
x	Actual receiver position in x axis
y	Actual receiver position in y axis
z	Actual receiver position in z axis

Chapter 1

Introduction

1.1 Overall scenario

In recent years, there has been an increase in demand for location-based services (LBSs) for underground parking, autonomous vehicle control, shopping centres, health applications and several more [1–4]. LBSs is a vital aspect of mobile experience and opens a broader platform for navigation and travel, geo-social networking, real estate and retail searches, mobile marketing and advertising. Whether used for finding the nearest restaurant, neighbourhood advertisement or locating friends, LBSs provides end-users with up-to-date information about their surroundings and enables businesses to offer updates to potential customers. The first couple of stages in the evolution of LBSs is to enhance location applications (e.g. location of shops) and location-based (navigation) applications where the actual geographical position is provided. The development of hybrid technology between the intrinsic location and location information services improved reliability, accuracy and the number of services that can be delivered. This has in turn, caused a significant amount of deployment in mission-specific applications such as vehicle navigation.

Global positioning system (GPS) is a mature technology that provides accurate positioning in most outdoor locations. However, due to multipath propagation and signal path-loss, the performance of GPS degrades in areas such as tunnel, multi-storey car parks, indoor environments and locations within GPS dead zone areas [5]. This happens when the beams from a single transmitter hit a surface, and the signal either deflects, diffracts or terminates [6]. The current market on LBSs focuses on indoor applications by using a fusion of geomagnetic field, beacons and wireless sensors to complement GPS. The resulting indoor positioning system (IPS) from these applications are based on radio frequency identification (RFID) [7,8], Bluetooth [9,10], Wi-Fi [11,12] and ultra-wide band (UWB) [13,14]. The methods for radio-frequency (RF) based positioning algorithms can be categorised into two, namely: range free and range-based methods. RFID positioning techniques exploit the range free category, which utilises the targets proximity rather than the geometric relationship for positioning. The targets position is determined with the received signal, thus revealing the vicinity of the transmitter. In a room with several transmitters, the target chooses the strongest signal, and pinpointing its relative location. Range free methods can only provide an approximate location. In a range-based approach, the positioning process is divided into three phases. a) one or multiple of the received signal strength (RSS), time of arrival (TOA) or phase of arrival (POA) information are obtained. These are methods of measuring signals from the transmitter, which are detailed in the following Chapter 2. b) determine the distance between the transmitter and the receiver based on the signal measured in step one. c) a trilateration or similar algorithm is used to determine the receiver's position based on values calculated in step two. Bluetooth and Wi-Fi-based positioning methods use this process with positioning accuracy ranging from decimetres to metres. Walls and furniture situated in an indoor environment add uncertainties to the channel model for the RF-based positioning, which deteriorates the positioning accuracy [15]. To reduce the effect of multipath propagation in RF-based positioning, correction algorithms or pre-calibration can be done, which can be computationally complex and labour intensive. UWB is reported to have good positioning accuracy (in centimetre range) by estimating the time of flight (TOF) of narrow pulses, which are less vulnerable to multipath propagation [13]; this utilizes bandwidths larger than 500 MHz which makes it easier to be measured precisely. This is because higher bandwidths result in higher data rates, thus resulting in more precise calculation. With UWB, the signal is transmitted with low power, preventing interference with other systems using the radio spectrum such as cell phones and police radios. This is only achievable at a higher cost of implementation [16].

Traditional fluorescent and incandescent lighting are beginning to be replaced by solid-state lighting (SSL) LEDs and laser Diode (LD). This has led to the extensive development of a new communication technique, namely Visible Light Communication (VLC), which uses modulated light to transmit information. VLC is a promising communication technique with the capability of attaining multi-Gbits/s data rates [17]. Its promising nature has led to the development of a new research topic, VLP.

VLP is a positioning technique using visible light. VLP has numerous advantages over RF-based positioning systems [18] such as a) the effect of multipath propagation in VLP is less than that in RF-based positioning [19], b) locations including hospitals and airports with RF restricted areas can successfully deploy VLP, c) VLP systems can leverage the existing lighting infrastructure; hence, its deployment should be low cost and ubiquitous, d) VLP can be deployed to work with VLC seamlessly, thus providing positioning and communication services simultaneously [16]. However, existing VLP techniques show that there is a need for distributed transmitters, which can be difficult in heterogeneous environments, e.g. intelligent transport system (ITS), which has linear array of light sources. With the advantages mentioned above, the following section list the motivations of this work.

1.2 Research Motivation

In the field of VLP, researchers have explored different system designs and algorithms. Although there are several reported solutions in the literature, which address the challenges that arise in VLP, some current issues are still yet to be solved (mentioned below) to fully understand the VLP system and provide high accuracy for users. Hence, this thesis is motivated by the need to design the VLP solutions, thereby tackling the issues that have not been considered and critically evaluated in the literature.

In a typical indoor environment, existing VLP techniques worsen in the presence of multipath propagation. This has been stated in the literature for two-dimensional (2-D) applications, but a majority of the existing studies in three-dimensional (3-D) VLP do not consider its effect. Therefore, this thesis investigates the multipath propagation effect in 3-D environment and potential methods or algorithms to improve VLP accuracy.

In a conventional VLP system, it is always assumed that the LEDs are turned on all the time. However, illumination is not always necessary, e.g. during the day when natural light illuminates the building or during out of office hours where the lights are turned off. Hence, it is of great importance to investigate the feasibility of a highly accurate VLP system when the lights appear 'OFF' to the human eye.

Contrary to active positioning systems, passive positioning offers unprecedented flexibility and can provide for new potential applications such as tracking without the need for users participating in the process. Existing simulation based studies fail to use an accurate channel model. Hence this thesis investigates the use of an appropriate technique to obtain the passive VLP channel and apply an appropriate positioning algorithm to track objects and evaluate its performance.

For outdoor applications, ITS aim to provide innovative services to make safer, smarter, and more coordinated use of transport, which is also directly related to human and material safety. This focuses on using different technologies to reduce casualties and prevent loss of lives. VLP can complement or supplement GPS in specific areas such as underground parking, tunnels and GPS dead zone areas. The already existing lighting infrastructure and the European Union's policy measures banning the sale of inefficient lighting technologies makes VLP relatively easy to deploy. Though these events provide ease in the deployment of VLP, challenges arise due to the lack of distributed transmitters for the purpose of positioning in an outdoor environment. Though streetlights are dynamically available, they are placed collinearly of each other, which makes it difficult to apply positioning methods. Since the traditional algorithms fail to provide positioning for a linear array of transmitters, and installing or modifying the existing streetlight design is not practical or cost-effective, there is a need to explore this research area and analyse its novel applications.

Based on these motivations, aims and objectives are listed to narrow down the direction of the thesis.

1.3 Aims and Objectives

This work explores the feasibility of VLP for ITS and indoor applications.

The major challenge in deploying VLP for outdoor application is the lack of distributed transmitters (as streetlights are in a linear format) and the impact of weather conditions on the positioning accuracy as VLP can be prone to ambient noise. The challenge for indoor 3-D VLP is the avoidance of a realistic channel model, which leads to limitations in providing various studies in VLP, i.e. non line-of-sight (NLOS) is ignored. As a result, the following themes are explored in this thesis:

- Design and critically evaluate a simplified/optimised machine learning (ML) algorithm and structure for 3-D indoor VLP.
- Evaluate the effect of the multipath channel on the 3-D VLP.
- Design and critically evaluate a diversity scheme with ML-based VLP algorithms to provide accurate 3-D positioning with multipath signal prorogation.
- Design and evaluate 3-D dark VLP in an indoor environment using ML and diversity receiver.
- Design and evaluate 2-D passive VLP using ML with a realistic channel model.
- Explore the use of streetlights and traffic light as transmitters and PD as a receiver for outdoor VLP.
- Investigate spatial and angular receiver diversity scheme for streetlight-based 2-D outdoor VLP and investigate ML with diversity technique to provide accurate positioning using collinearity source.
- Investigate the effect of different weather conditions in outdoor VLP.

1.4 Original Contributions

Figure 1.1 summarises the challenges, the existing and the proposed solutions for VLP for indoor and outdoor applications.

The major contributions in the thesis are detailed below:

- **3-D indoor position using receiver diversity with ANN**: Proposed and studied receiver diversity with Artificial Neural Network (ANN) for highly accurate indoor 2-D and 3-D VLP. The performance of the proposed solution is evaluated in line-of-sight (LOS) and NLOS propagation. This study demonstrates the improved positioning accuracy compared to existing solution.

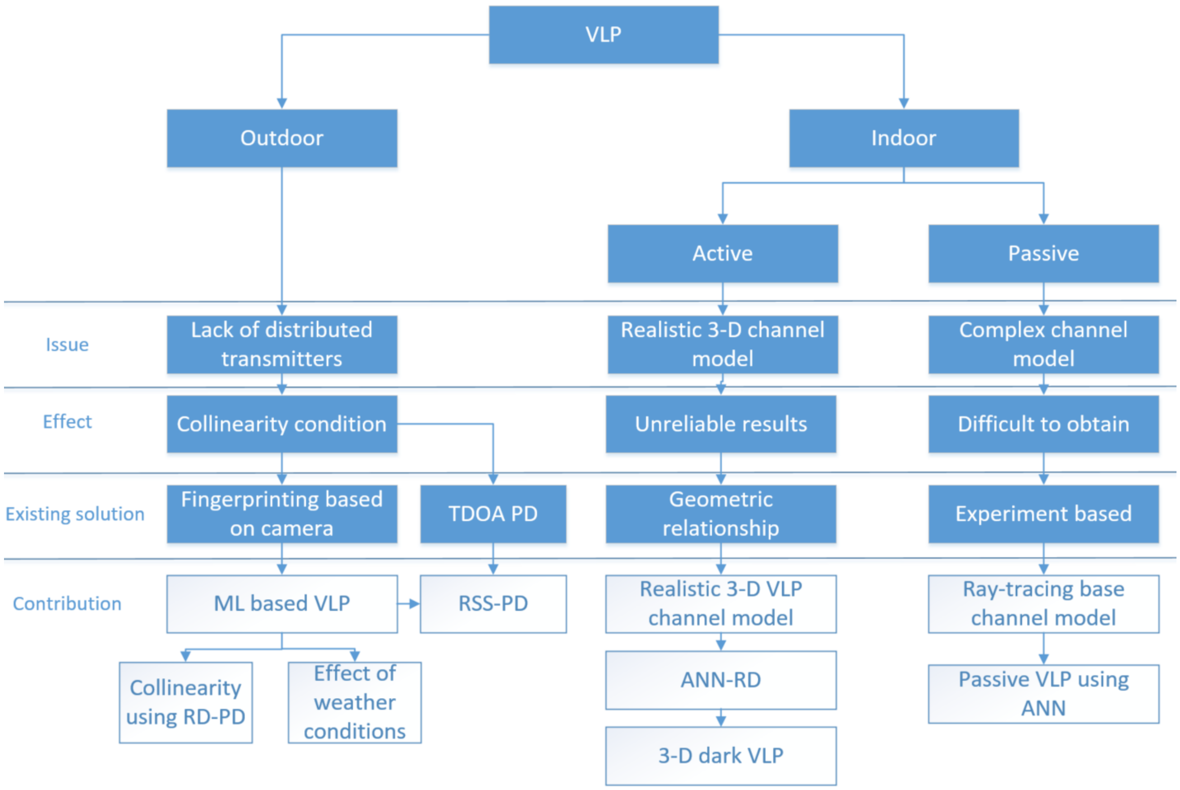

Figure 1.1: *The summary of the challenges, the existing and the proposed solutions for VLP in the indoor and outdoor environment.*

- **RSS-based 3-D dark VLP**: Proposed the use of low duty cycle pulse width modulation (PWM) to obtain an 'OFF' state LED and used apparent 'OFF' sources for indoor positioning. Demonstrated improved performance using ANN and its ability to establish positioning at a very low PWM duty cycle.

- **ML-based passive VLP**: Proposed the use of ML technique for passive VLP. Critically evaluated the performance of the system using a realistic channel model under different object sizes and reflections.

- **Outdoor VLP using streetlight for vehicular application**: Proposed and critically evaluated the ANN-based VLP accuracy using a linear array of transmitters with spatial and angular diversity receiver. By considering a variety of different road dimensions, the study demonstrates improved accuracy and robustness of the proposed solution in the presence of different weather conditions. Studied and demonstrated ANN to be the most suitable ML algorithm for outdoor VLP.

1.5 Thesis Organisation

This thesis is arranged into seven chapters which are structured as follows

- Chapter 1 highlighted the background, research motivation and summary of the major contribution in this thesis.

- Chapter 2 presents a comprehensive review on VLP, including channel model, transmitter and receiver system, VLP algorithms and applications. The review is then concluded by identifying the research gap in the literature and the rationale for selecting the approach adopted in the thesis.

- Chapter 3 provides an overview of the mathematical model for the VLP channel (LOS and NLOS). Various positioning algorithms such as CMD, ANN, gated recurrent unit (GRU), recurrent neural network (RNN) and Long short-term memory (LSTM) are detailed.

- Chapter 4 provides a review of related work that addressed NLOS channel followed by a rationale to use ANN for 3-D VLP. Next, a description of the proposed multi-layer perceptron (MLP)-ANN for indoor VLP is shown. Thereafter, the ANN and VLP system architecture is optimised. The chapter provides detailed studies of 2-D and 3-D VLP using receiver diversity. Finally, a comparative study is given with respect to similar work in the literature.

- Chapter 5 investigates the application of ML on passive VLP. Different transmitter-receiver scenarios are investigated to see their impact on VLP. The chapter entails a study on the effect of object size and object reflectivity. This sets a theory that the VLP channel can be modelled based on ray-tracing software.

- Chapter 6 proposes a new VLP technique for autonomous vehicle application using streetlights or traffic lights as transmitters and spacial and angular diversity receiver with ML. The chapter provides a brief review of the existing literature on outdoor VLP. Thereafter, proposed VLP with spatial and angular diversity receiver with ANN is described and system parameters are optimised for vehicular application. Different ML algorithms performance is compared for outdoor VLP using a linear array of transmitters. Computer simulations are carried out to study the system's performance under different road scenarios and weather conditions.

- Chapter 7 concludes the thesis and discusses possible future direction.

1.6 Publications

1.6.1 Journal

- A. A. Mahmoud, Z. Ahmad, U. Onyekpe, Y. Almadani, M. Ijaz, O. C. L. Haas, and S. Rajbhandari, “Vehicular Visible Light Positioning Using Receiver Diversity with Machine Learning,” Electronics, vol. 10, no. 23, p. 3023, Dec. 2021.

- A. Mahmoud, Z. U. Ahmad, O. C. L. Haas and S. Rajbhandari, ”Precision indoor three-dimensional visible light positioning using receiver diversity and multi-layer perceptron neural network,” in IET Optoelectronics, vol. 14, no. 6, pp. 440-446, 12 2020, doi: 10.1049/iet-opt.2020.0046.

1.6.2 Conference

- A. Mahmoud, Z. Ahmad, Y. Almadani, M. Ijaz, O. C. L. Haas and S. Rajbhandari, ”Outdoor Visible Light Positioning Using Artificial Neural Networks for Autonomous Vehicle Application, ”2020 12th International Symposium on Communication Systems, Networks and Digital Signal Processing (CSNDSP), Porto, Portugal, 2020, pp. 1-4, doi: 10.1109/CSNDSP49049.2020.9249440.

Chapter 2

Overview of Visible Light Positioning

2.1 Introduction

The exponential growth of electronic device technologies has led to different communication techniques being used and newer communication models being investigated for optimum efficiency. Various communication infrastructures and technologies including radio wireless and optical wireless communication (OWC) based techniques have been investigated for a number of applications. This includes underwater, satellite, free space and terrestrial environment to support the emerging sixth generation (6-G) of wireless communication and internet of things applications [20, 21]. OWC is the process of transmitting data in vacuum or air through optical (infrared, visible & ultraviolet) wavelengths. OWC has an array of advantages, such as an unlicensed and regulation-free large frequency spectrum [22]. VLC is a subset of OWC, that uses visible wavelength for communication. Graham Bell in 1880 demonstrated the first VLC system named Photophone to transmit voice signals over a 200 m distance using the sunlight. Visible light has been used for communication in different scenarios since ancient time such as marine lights for ships visibility and coded light signals [23]. However, it is only in the last few decades that significant research and development has been carried out in the field of VLC. The introduction of LED/LD, which has the capability of transmitting information/data at a high-speed of more than 32 Gb/s [24] has made this application more feasible.

Over the years, there has been an increase in demand for LBSs for shopping centres, underground parking, autonomous robot control and health applications. GPS is one of the successful means of tracking objects in outdoor environments. However, GPS signals suffer significant attenuation, path loss and multipath fading in an indoor and some outdoor environment scenarios such as urban roads with high buildings and tunnels. This can result in large positioning errors [25]. Though the accuracy requirement for indoor and outdoor environments is different, in most machine control applications, the guidance of industrial machines, robots and vehicles require cm-level accuracy [26]. There are several RF-based indoor positioning techniques such as Wi-Fi, Bluetooth, RFID which find application in the indoor environment but exhibit limitations such as low accuracy in decimeter range [27] due to the multipath propagation and RF interference of other sources. VLC and VLP on the other hand, are free from electromagnetic interference. The ubiquitous nature of illumination infrastructure has motivated the use of VLP.

This chapter introduces indoor and outdoor VLP, various VLP technologies and key challenges. It is organised as follows. Section 2.2 provides a description of VLC/VLP transmitters and receivers, their respective link configuration and an overview of existing indoor and outdoor VLP. Section 2.3 describes the existing VLP algorithms based on RSS, angle of arrival (AOA), TOA, TDOA and their positioning methods. Section 2.4 details the multiplexing techniques adopted by VLP. Section 2.5 provides detailed analysis in the justification of the methods and models adopted in this thesis to perform VLP for indoor and outdoor environments.

2.2 Visible Light Communication/Positioning

VLC uses visible light sources to transfer information to a targeted receiver. VLP, similar to VLC, has emerged due to the recent development of easily digitally modulated LEDs. VLP is a competitive IPS that is capable of providing accurate 2-D and 3-D positions to participating users. Light waves are confined by nature to the walls and objects in a room, which allows for the data transfer within the same bandwidth to be used in the room next door without interference. Moreover, the deployment of such a system is predicted to be low-priced as it will work with the existing lighting infrastructure. Figure 2.1 shows the electromagnetic spectrum and the visible light spectrum has a wavelength of $360 - 780$ nm [28]. Using the illumination infrastructure, it's possible to achieve illumination, communication and positioning. The block diagram of a typical VLC/VLP system is shown in Figure 2.2. The system consists of the transmitters containing driver circuit & modulator, free space channel and the receiver containing photodiode, amplifier, electrical filter & demodulator. The transmitter and receiver section are detailed in the following subsection.

2.2.1 Transmitter

Different sources have been developed for VLC and VLP over the years ranging from incandescent light, LD and LEDs. The use of LED in VLP is advantageous due to several positive reasons and little negativity to both the environment and humans. LED's advantages are long lifetime, low radiant heat, instantaneous light, design flexibility, low power consumption and fast switching [29].

This technology will soon be used both for outdoors and indoor application. LED can be used for illumination and data transmission including audio and video at multi

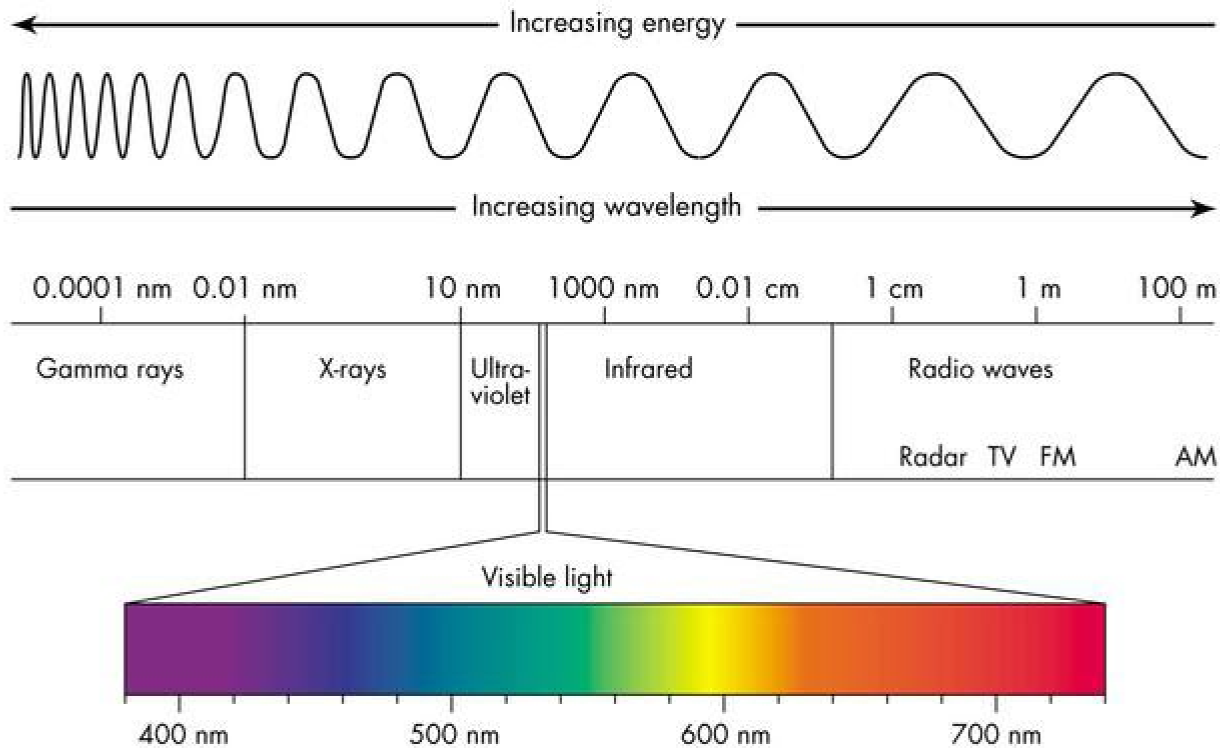

Figure 2.1: *Electromagnetic spectrum [28].*

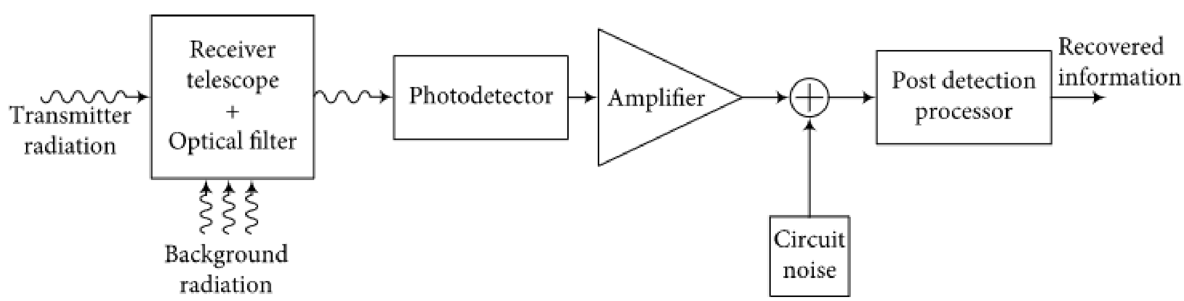

Figure 2.2: *VLC with DD block diagram [33].*

gigabits/sec [30, 31].

With this array of advantages, white LED sources are ideal for VLP and further aiding energy saving at a universal level. Furthermore, the application of VLP is not affected by electromagnetic interference [32]. Hence, VLP is eligible to be used in several institutions including hospitals.

2.2.2 Receiver

The receivers used in VLC are normally cameras and photo-detectors. For the purpose of this research, photo-detectors are adopted. Photo-detectors have the ability to turn light received into an electrical pulse. This works by converting photonic energy to electrical energy. Several available photo-detectors such as photo-transistors, photo-multipliers, photo-conductors, and PDs each have unique qualities. However, PDs are the preferred photo-detector due to their fast response, high sensitivity and small size. Avalanche Photo-Diode (APD) and P-I-N are the most common PDs used as photo-detector [33].

P-I-N photo-detector

The P-I-N PD consists of two p-type and n-type semi-conductor materials, which are separated by an intrinsic sparingly n-doped region. The schematic of a P-I-N PD is shown in Figure 2.3. The device operates when a large reverse bias voltage is applied. To convert the received photon into an electrical current, the band-gap energy has to be

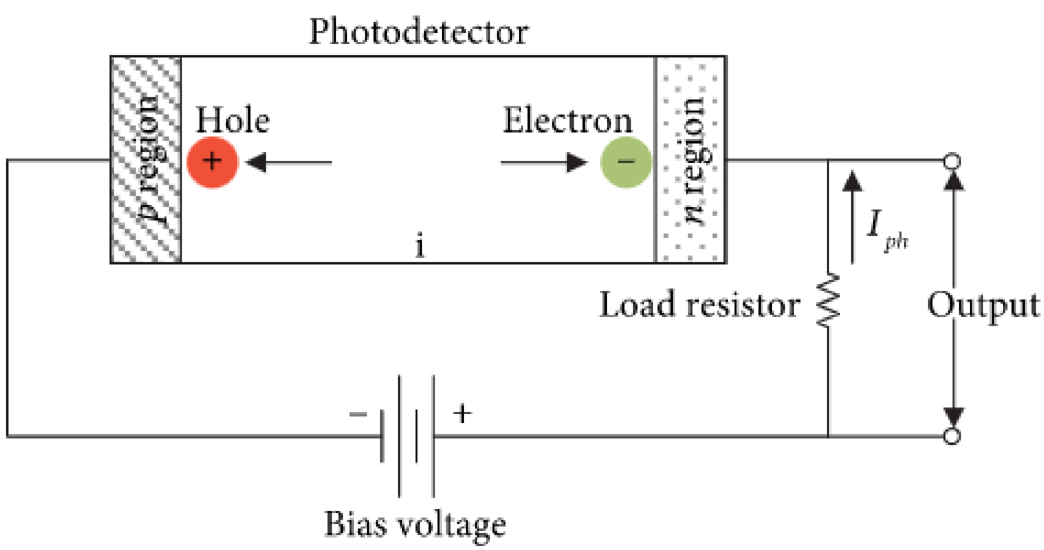

Figure 2.3: *Schematic of a P-I-N PD [34].*

equal or less than the incident photon. The energy from the electron excites the photon to the conduction band, which generates an electron-hole pair. The concentration of impinging light is under conventional conditions directed to the depleted intrinsic region. Due to the high electric field in the depleted area, the charge carriers are separated, which is accumulated across the reverse-biased junction. The process then leads to the current flowing across the resistor, as seen in Figure 2.3. For each generated pair, there is a single flow of electrons. For communication applications, a P-I-N PD has the capability of functioning at high bit rates over 100 Gbps [34]. However, due to packaging restrictions, most of the PD-based devices available in the market have a bandwidth of less than 20 GHz.

APD Photo-detector

The APD is slightly different for P-I-N as the current gain is supplied using a repeated electron ionization process. This results in a highly sensitive receiver due to the multiplication of photo-current before encountering the thermal noise of the receiver circuit. The APDs gain has an impact on the responsivity and given by due to standard gain values of the APD ranging between 50 and 300, the responsivity can be higher than unity [33]. This means that APD has more sensitivity when compared to P-I-N PD with a unity gain. However, APDs sensitive nature also makes it prone to noise as well as temperature due to the ionization process. These factors are to be considered in a practical component selection, as it is significant to the performance of the system.

2.2.3 Intensity Modulation/Direct Detection

Intensity modulation (IM)/DD is the process of transforming an optical signal carrying information into a corresponding electrical signal. Before the signal is transmitted, it is encoded on the frequency or radiation intensity of the optical source. For systems that utilize IM/DD, the radiated emission from the light source is directly modulated using the electric signal. Post-transmission, using optical fibre or free-space, the PDs convert the received optical intensity into photo-current, then the receiver system filters the signal. In OWC, among others, IM/DD and coherent detection with DD are the most used schemes due to their simplicity [17]. These attributes associate the data with the transmitted fields intensity variations. Figure 2.2 shows a receiver based on DD.

For a VLP channel, there exists a physical link configuration which is explained in the following section.

2.2.4 VLC link configuration

The VLC/VLP link configuration can be classified based on the directionality of the receiver and transmitter. VLC/VLP links can be directed, non-directed and hybrid as shown in Figure 2.4. In the directed configuration, a narrow divergence angle transmitter and a narrow FOV receiver are used, which are pointed to each other. This configuration requires precise link arrangement and a tracking system. Directed link configuration tends to have a higher power efficiency as it reduces geometrical propagation loss and noises from artificial and ambient light sources. In the non-directed configuration, a wide divergence angle transmitter and wide FOV receiver are used, which are not directed or focused at a specific point. However, this configuration requires high power levels to combat the high optical loss and the multipath-induced distortions. In the hybrid link configurations, the transmitter and receiver can have a variety of directionalities such as a wide FOV receiver to detect a narrow beam transmitter [17, 30]. Using these link configurations, indoor VLP can be deployed which is

Figure 2.4: *Channel configuration models a) Directed LOS configuration b) Hybrid LOS configuration c) Non-directed LOS configuration d) Directed Non-LOS configuration e) Hybrid Non-LOS configuration f) Non-directed Non-LOS configuration [30].*

discussed in the following section.

2.2.5 Indoor visible light positioning system

To implement indoor positioning, multiple operational techniques can be adopted such as Wi-Fi access point, RFID and VLP. In the application of VLP, which is the focus of this thesis, illumination sources serve as a transmitting unit [35]. Conventional light sources such as incandescent or fluorescent lamps have low bandwidth and are not suitable for VLC/VLP. Recently, LEDs based on SSL have emerged as a suitable and prominent replacement of conventional light sources with advantages mentioned in Section 2.2.1. The schematic of an indoor VLP system is shown in Figure 2.5. The

Figure 2.5: *A schematic of indoor VLP [46].*

light signal is transmitted from an LED in its modulated form carrying the information of the transmitter, which is then received by an image sensor or PD through a VLC channel. Thereafter, the position of the receiver is estimated based on the received signal attributes.

Indoor light positioning systems have been initiated by certain enterprises such as Carrefour in Lille, France (see Figure 2.6), which introduced intelligent lighting devices in 2015, to help customers track products within the supermarket [2,36]. A professional IPS was deployed in the same year (2015) by Acuity Brands [3]. The following year (2016), Qualcomm piloted an LED guiding system named Lumicast [37]. The Lumicast system was capable of achieving centimetre level accuracy in indoor environments. VLP systems can be deployed in the various scenarios, which are discussed below.

Indoor Public Spaces

VLP would be a valuable asset for guiding people in public settings such as museums, theatres, exhibition centres and opera houses where tourists and the general public can get lost, VLP can guide users to their desired locations [10]. This can also be used to navigate visitors to elevators, toilets, their respective seats, exits and emergency exits. Since the aforementioned places are already equipped with LED lights, the deployment of LED-based IPS should come at ease with minor additional modifications.

Figure 2.6: *LED-based indoor positioning by Philips, Carrefour France [2].*

Shopping Centers

IPS can support shoppers in shopping centres to navigate through the complex nature of supermarket floor plans where items are scattered throughout the building. The application of VLP in shopping centres could help customers navigate to their desired products in a timely manner. This would reduce the time spent in shops, increase shoppers throughput and ensure a shopper can keep a safe distance from other shoppers during the pandemic. This would also benefit merchants by exploiting VLC for coupons and advertisements to potential customers in the vicinity. Moreover, this would help promote a personalised shopping experience by sending users information on price comparisons on items for different brands. Furthermore, customer purchase behaviour can be studied to pinpoint sales hot spots, enabling shelf layout optimisation by the merchant.

Factories and Logistics

VLP can be used in factories and logistics where managers could efficiently locate assets and employees, thus improving management and security [38]. This could also be used for inventory storage by autonomous robots. Furthermore, deployment of VLP in factories and logistics can provide flexibility for rezoning and reconfiguration for changing mandates and needs, thus contributing to operational efficiency, as well as energy and maintenance savings [39].

Figure 2.7: *LED-based indoor positioning by Philips, EDEKA Paschmann supermarket, Germany [36]*

Healthcare Facilities

RF-based IPS are challenging to deploy in hospitals as they may interfere with critical care equipment such as ventilators and external pacemakers. As most hospitals are already equipped with LED luminaries, VLP can be deployed without the need for additional transmitters and their associated costs. VLP can be used in hospitals to track medical devices, wheelchairs, beds, provide more accessibility to emergency services and further navigate patients through wards.

Airports and Train Stations

In areas with a high volume of people like airports and train stations, VLP can be used to assist passengers in reaching boarding points, bus exits, trains, restrooms, booking offices and stores. This can be very helpful for the first time and foreign visitors. Similarly, this can be used in traffic control and information hub.

2.2.6 Outdoor light positioning system

Urgent positioning techniques are needed for vehicular navigation to provide service in urban and city centre locations where GPS offers poor performance [40] due to multipath propagation and signal path-loss. This is needed to effectively deploy and improve driver safety in ITS. The application of VLP for the outdoor environment is relatively in infancy. In [41], vision-based navigation methods are proposed for one-dimensional (1-D) positioning. With more LED traffic lights being deployed, their use as a transmitter for positioning has been proposed to obtain the distance between the traffic light and the vehicle using cameras [42, 43]. However, only the relative position of the vehicle is attained. Figure 2.8 shows the most recent outdoor VLP schematic using streetlight. Figure 2.8 shows the existing schematic of outdoor VLP schematic. The study proposes streetlights and cameras for vehicular positioning [44]. However, the aforementioned methods for outdoor VLP require a complex image processing procedure and an expensive high-speed camera to determine the position of the vehicle.

Having reviewed VLP, its existing and potential applications, the following section presents the review of VLP.

2.3 VLP algorithms

VLP can be categorised into active and passive positioning. Passive positioning does not require the target to carry any active tag or active device. Furthermore, there is no need to modify the lightning infrastructure [45]. In active positioning, the target device has a receiver(s) that estimates its position. For active localisation, image sensors or PDs at the target device are responsible for receiving signals from the transmitter and estimate its position based on the various algorithm discussed in the following section. The transmitted signals have the geographical location or the Identification of the LED,

Figure 2.8: *Existing outdoor VLP model [44].*

which enables the receiver to estimate its position. Note that this thesis considers both passive and active positioning.

The design in Figure 2.5 shows a typical indoor active VLP system configuration. Multiple transmitters, often LEDs, are used to transmit the signals. Time Division Multiplexing (TDM) or Frequency Division Multiplexing (FDM), as detailed in section 2.4 are used so that the receiver can separate signals from different sources. A target analyse/process the received signal from multiple sources and estimates its position [46].

Figure 2.9 summarises several positioning algorithms and techniques. By measuring the signal through RSS, AOA, TOA, TDOA or hybrid methods, a positioning method is applied to retrieve the receiver position ranging from triangulation/trilateration, fingerprinting, imaging, proximity or hybrid methods. Different studies use different peripherals ranging from inertial measurement unit (IMU), laser, RF, PDs and extra transmitters. The following section provides a brief review of these techniques. The analysis of the selected algorithm is presented in Chapter 3.

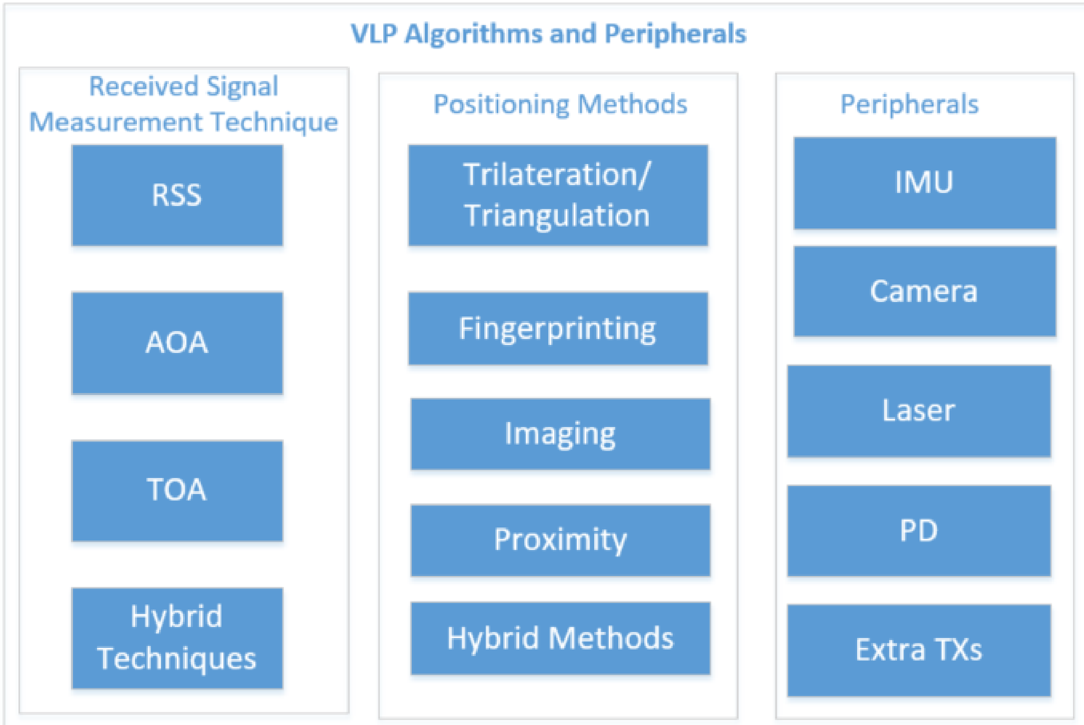

Figure 2.9: *VLP algorithms*

2.3.1 Received Signal Strength

RSS is the measurement of the power in the received signal [47]. The RSS algorithm in VLP is designed to attain the location of the target using the signal strength with the mathematical model given by [17]:

$$P_r = \begin{cases} \frac{(m+1)A_r}{2\pi d^2}\cos^m(\phi)T_s(\phi)g(\psi)\cos(\psi) 0 \leq \psi \leq \Psi_c \\ 0, \quad \psi > \Psi_c \end{cases}, \tag{2.1}$$

where m is the Lambertian emission order, A_r is the PDs physical area, ϕ is the irradiance angle $T_s(\psi)$ is the optical filter gain, ψ is the angle of incidence, $g(\psi)$ is the optical concentrator gain, d is the distance between the receiver and the transmitter, Ψ_c is the PDs field of view. RSS is combined with a positioning method (trilateration/triangulation) to localise the target. Note that the positioning methods are discussed later in Section 2.3.5.

In [48,49], RSS-based 2-D positioning systems were proposed for VLP using the light from three LED base stations on the ceiling. LEDs were modulated using quadrature phase-shift keying (QPSK) at non-identical frequencies. At the receiver end, each signal was processed distinguished. The distance between the receiver and each transmitter is attained in two steps. The first step taken was to estimate the rough distance without considering the effect of incidence and irradiance angle on the power. The effect of these two angles is ignored because of the absence of sensors such as a gyroscope or accelerometer, which can slow the estimation process. However, the signal strength is reduced, leading to an overestimation of the distance. The second step determines the maximum possible distance where the lighting coverage of the LED and height is known. The distance obtained after the second step is then subtracted from the distance in the first step to provide the final distance estimated. The localisation is then done using trilateration and the linear least squares (LLS) method. Using the aforementioned methods, an accuracy of 6cm was reported for a room of dimensions 60 cm$\times$60 cm $\times$85 cm.

The work in [50] uses three PD receivers in a circular form each 20 cm apart on a mobile device. The research assumed that locating the PD over a diameter of 40 cm is acceptable in the case of large autonomous machine applications. Note that such a large receiver separation may be restrictive for other applications. The distance from each receiver to the transmitter is first calculated using the RSS. The relative position of the PD is then determined by exploiting the known LEDs locations. The proposed model yielded an RMS error less than 1.5 m in a room dimension of $2 \times 2 \times 2$ m^3.

Optical symmetrical code (OOC) was utilised in [51] to differentiate different signals. Using RSS, the distance to the base station was calculated and the position of the receiver was determined using trilateration. In a 12 m $\times$35 m area, an average error of 8 cm was achieved in a simulation environment.

In [52], dual-tone multi-frequency (DTMF) was used to distinguish different base stations from the LED. DTMF is traditionally used in electronic banking systems, telephone dialling and voicemail. An algorithm was developed to calculate the path loss based on different frequencies corresponding to the RSS. The coordinates to the LED base stations were assumed to be pre-set on the mobile device. In a 2 m $\times$2 m area, an average error of 18 mm was achieved in a simulation environment.

A deep neural network (DNN) approach to VLP was proposed in [53]. The transmitted signals are multiplexed using FDM and the RSS information to a single receiver is fed to the DNN for training. The training was achieved based on Bayesian regulation with sparse training points. An RMS error of 4.58cm was achieved in a room of 1.8 m$\times$1.8 m$\times$2.1 m. A modified particle swarm optimisation (PSO) algorithm was proposed in [46, 54] for 3-D positioning. However, only 605 points were tested in a room of 3 m$\times$ 3 m $\times$4 m. An error of 3.9 mm is achieved with only 20 iterations.

A 2-D VLP system with multipath reflection was analysed in [55]. Using the RSS and trilateration, the distance between the LED base station and the mobile device was calculated. Simulation studies with a PD receiver resulted in an average RMS error of 4cm for LOS scenario and up to 80 cm with reflected light in a room of 6 m$\times$6 m$\times$3.5 m. ANN for indoor VLP was used in [56] to mitigate the effect of reflected light on VLP in 2-D VLP. Simulation studies demonstrated that an average error of 6.39 cm is achievable using multiple transmitters and a single PD in a room of 5 m$\times$5 m$\times$3 m.

The 3-D VLP based on ANN is investigated in [57]. The study assumes a receiver array of 19×19 and a 4×4 grid of LED each 1 m apart. The model yielded an RMS error of 0.4 mm in a 4 m$\times$ 4 m $\times$3 m room. The work in [58] demonstrated the feasibility of 3-D VLP using a two-layer ANN. The study works under the assumption that the room is divided into multiple trilateral positioning cells and the RSS was fed into the ANN. In a room of 0.9 m$\times$ 1 m $\times$0.4 m, the model yielded an RMS error of 1 cm. Though it's not an improved accuracy on the work reported in [57], it provides a more realistic study with less system structure. The reduction in the system structure is from three ANN with 16 nodes to a single ANN with 8 nodes for [57] and [58], respectively.

A VLC based vehicle positioning using LED street light and rolling shutter CMOS sensors was proposed in [44]. The vehicles were assumed to be equipped with cameras able to receive information on the position of the transmitters. The position of the vehicle was determined based on the geometric relationship between the LED and the cameras. A small scale experiment was conducted where the transmitters were 2.5 m high with longitudinal and lateral distances between any 2 LEDs equal to 0.6 m. The proposed system yielded an average and maximum error of 15 cm and 150 cm, respectively.

A passive VLP approach considering the effect of reflection, shadow and ambient light was investigated in [59]. The simulated system considered random/unpredictable target movement patterns in a room with an array of 60×60 LEDs on the ceiling and 25 receivers on the floor. It considered LOS and NLOS signal propagation paths as well as possible blockage due to shadowing. A min-max filter and a Kalman filter were adopted to track the target position resulting in an RMS error of less than 0.5 cm in a $10 \times 10 \times 3$ m^3 room.

In [60,61], an RSS-FDM approach to passive VLP is used to construct a 3-D human skeleton. By using five transmitters on the ceiling and 324 receivers on the floor, the model had a 10 degree mean angular error in a room of 3×3 m^2 and RMS error of 9.7 cm (95% of the case).

A RSS-TDM approach to VLP to detect occupancy of a room was proposed in [62]. The proposed system employed six transmitters and twenty-four receivers on the ceiling of a room with dimensions $7.5 \times 6 \times 2.74$ m^3. A median error of 0.89 m was achieved.

The work in [63] proposed a RSS-fingerprinting approach to passive VLP for object identification. The experimental model, with 14 light sensors on the wall in a room of 2×3.6 m^2, yielded an RMS error of 13 cm. The authors experimentally extended the work in [64] to detect human participants with an error of 84 cm in a 4.8×9.6 m^2 lab.

A study in [65] used the object impulse response to establish positioning. By using nine transceivers on the ceiling in a room of 5×5 m^2, the model yielded an RMS error of less than 10 cm.

2.3.2 Angle of Arrival

AOA is the measurement of the angle that the transmitted signal reaches the receiver. AOA calculations are done based on the angulation (triangulation) of the signals from different light sources [66]. Figure 2.10 shows the basic configuration of AOA where ϕ_1 and ϕ_2 is the irradiance angle of the first and second LED, respectively. With the

AOA obtained, the target's position is calculated using the point of intersection of the signals.

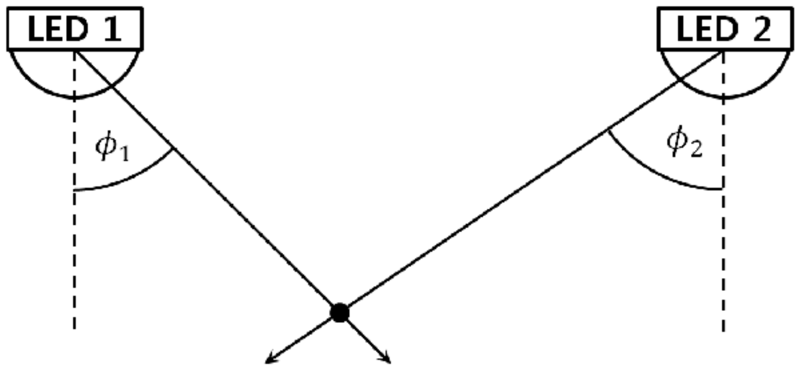

Figure 2.10: *AOA localization using 2 LEDs [18].*

AOA is very advantageous in VLP as compared to RF in LOS scenarios as the signal in VLP is mostly transmitted in LOS. Unlike other positioning techniques including TDOA and TOA, AOA does not require synchronisation between the transmitters. However, AOA calculations generally require extra sensors or peripherals, thus resulting in higher complexity in system structure and algorithms [66].

A PD array (two and above) can be used to obtain the AOA. The LED emission follows a Lambert cosine law. The change of AOA can therefore be predicted based on the measured or calculated power received by the PD. The signal's angle can be deduced from the difference between the power received at the current angle and the power received at a known angle.

The authors in [67] proposed an array of PDs to estimate the AOA as shown in Figure 2.11 where ψ is the incidence angle. The irradiance angle of the light was determined using a truncated-weighting algorithm, which is a weighted sum of angles of PDs in the PD array. The magnitude of each PD angle was determined by comparing the received power at each angle. Simulation studies resulted in distance errors of less than 30 cm.

In [68, 69], a simulation study was used to demonstrate the feasibility of using an accelerometer to calculate the AOA with a single PD. The PDs angle was changed in different directions, and the received power with respect to the direction was calculated for a given position of the transmitter. The PD's orientation was estimated with the help of the accelerometer. Two measurements were taken for each base station for each PD orientation. With the measurements taken (received power), the irradiance angle of the signal is calculated. The present location of the transmitter was sent using VLC to the receiver, where all the transmitters transmit at different times, thereby employing TDM. The position of the device was obtained after the successful acquisition of the three corresponding irradiance angles. The model yielded an average error of 25 cm while the receiver is not in motion.

Research conducted in [70] enhanced the work in [68, 69] by including a second PD.

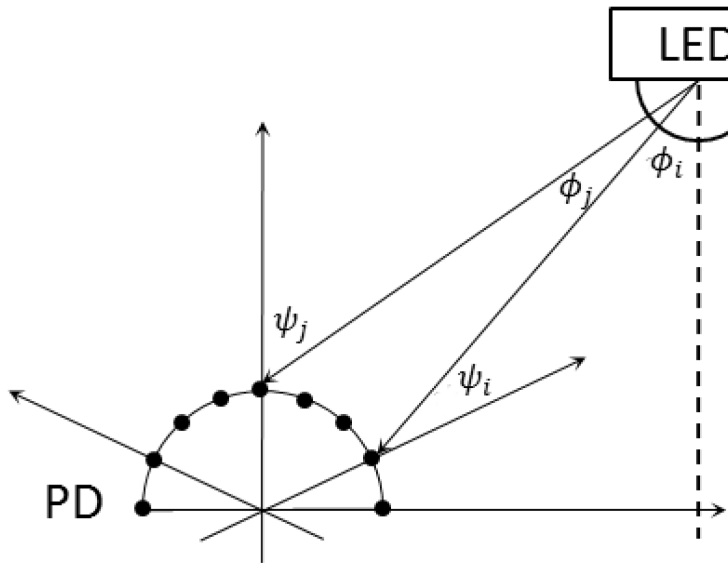

Figure 2.11: *Receiver setup for estimating AOA [18].*

When the PDs are combined with the accelerometer, the AOA is estimated without tilting the PD. The computational speed was improved, allowing the users to become mobile. The accuracy was also improved by mitigating the errors that were caused by the non-zero distance between multiple PDs. The simulation result showed an average position error of less than 6 cm even while the receiver was in motion at speed up to 1.3 m/s.

An approach to estimating AOA was proposed in [71] by using a group of three orthogonal PDs to receive signals from multiple LED base stations. The transmitter uses FDM with ranging frequencies between 2 kHz to 3 kHz. The PDs were placed at different angles, thus making them preferentially sensitive to the light incident to help with the angulation. The complexity of the mathematical expression was challenging to solve algebraically. Therefore the incidence angle was estimated using least angle regression (algorithm for fitting linear regression models to high-dimensional data [72]). In a simulation environment, a positioning error of 5 cm was attained.

To improve practicality, the work in [73] used a single PD to determine the AOA information. The PD is assumed to be perpendicular to the floor, thus assuming an identical incidence and irradiance angle. This also provides for a higher signal-to-noise ratio (SNR) due to the directionality of the transmitter and receiver. The multipath propagation of reflections was also considered, hence adding a path loss exponent to the equation. The receiver was assumed to know the maximum received power that was calculated beforehand. Hence, with the received power, the irradiance angle can be calculated. Each signal for a transmitter was modulated using Orthogonal frequency division multiplexing (OFDM).

The study in [74] proposed the use of a single receiver for AOA for vehicular positioning. The system uses vehicle tail lights or headlights as the transmitter, and a

PD-based receiver is placed on the vehicle. The underlying assumptions of the work were: a) the transmitter and receiver are perfectly synchronised for communication purposes, b) the transmitting and receiving vehicle can measure their real-time speed and global headings with on-board sensors, c) the transmitter is capable of transmitting the speed and global heading information through the VLC channel and d) the receivers measure the AOA of the transmission beam. The study demonstrates that the vehicles heading can be detected with a mean error of 11 cm.

2.3.3 Time of Arrival

TOA is propagation time-dependent. In the TOA approach, the transmitters send signals simultaneously to the receivers to calculate arrival time, then use this information to estimate the receiver position. This is the same approach used in GPS cases. The speed of light is multiplied by the propagation delay of the signal to calculate the distance. According to [75,76], to estimate the location in 2-D, the signal from at least three transmitters is required. As shown in Figure 2.12, transmitters A, B, and C have a corresponding distance of R_1, R_2 and R_3 to the device. The intersection of circles A, B and C is then utilised to estimate the receiver's position.

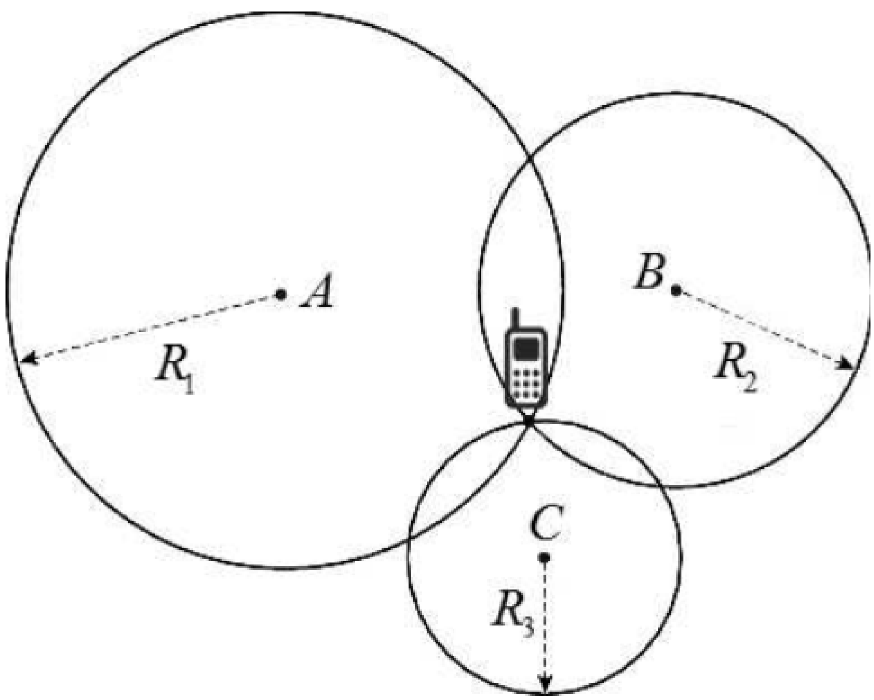

Figure 2.12: *Mobile phone TOA localization using 3 LEDs [18].*

For most TOA applications, the location of the device is determined using the LLS algorithm. This is a mathematical process that minimises the sum of the squares of the offsets for finding the best-fitting curve to a given set of points [15].

The authors in [77] investigated the TOA based VLP. By employing OFDM, each signal was transmitted to make it distinguishable to the receiver, where the transmitters and receiver are assumed to be synchronised. Using Cramer-Rao bound, the system showed a positioning error of less than 7cm. The work in [78] proposed the use of smartphones cameras to measure the modulated signals from the LEDs and TOF of sound waves from speakers placed in the room. The LED signal contains a time reference that is used to synchronise the receiver. Thereafter, multi-lateration is used to determine the receiver position. The model yielded an average error of 10 cm. The complex nature of TOA that comes from the need to perfectly synchronise the transmitter and receiver has led to limited studies in VLP. This lead to more research in TDOA, which is discussed in the following subsection.

2.3.4 Time Difference of Arrival

TDOA is a popular ranging technique that is more versatile than TOA [79]. This is because only the transmitters need to be synchronised. In the TDOA application, all the transmitters transmit the signal simultaneously. Due to the difference in distance between the transmitters to the receivers, the arrival times of all the signals will be non-identical. In the TDOA algorithm, the time difference of arrival is used to determine the position of the receiver. The distance calculated will then help estimate the position of the receiver. The speed of light is multiplied by the propagation delay of the signal to calculate the distance.

Hence, for each TDOA measurement whose distances to the pair of base stations have a constant difference, its respective hyperbola of possible positions can be determined as illustrated in Figure 2.13. To achieve 2-D positioning, the signal from at least three transmitters should be received by the PD. Figure 2.13 illustrates the distances $R3 - R1$, and $R2 - R1$ with respect to transmitter A, B, and C. These distances intersect at a certain point which is regarded as the estimated position of the receiver.

In [80], an indoor VLC localisation system based on TDOA was proposed for departmental stores, theatres, museums and restaurants. Four different transmitters were modulated using binary phase-shift keying (BPSK). The LLS algorithm was used to estimate the position of the receiver. In a simulation environment, the system had a positioning error of 0.14 m in a radius circle between 0.16 m and 0.2 m.

The authors in [75] proposed a TDOA based VLP where the PD has prior knowledge of the transmitter position. The signal transmitted from the LED does not convey any information. However, with the use of TDM, the receiver was able to distinguish between signals. Once all the signals are received, a special guessing mechanism is used to identify the signals, finding the device's location. In a simulation environment of 5 m×5 m×3 m, the system had a positioning error of 3 cm.

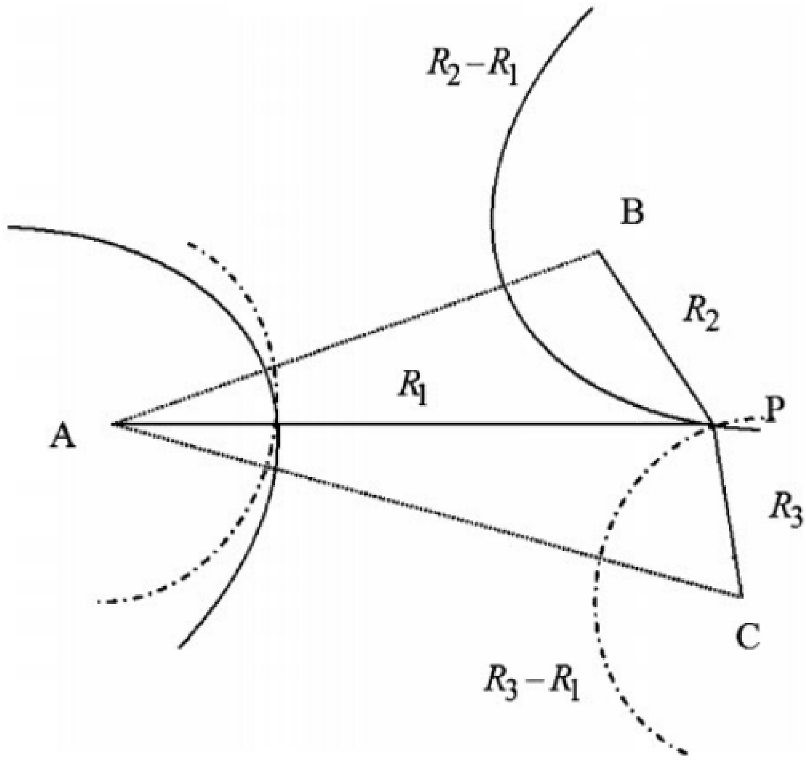

Figure 2.13: *TDOA based localisation [18].*

The authors in [81] used a sinusoidal signal instead of a square pulse as introduced in [75]. This is done to consider the rising and falling edge of the PD and LED for real-time implementation. In the simulation, the falling and rising times of the LEDs were taken into consideration to obtain the TDOA. The simulation results showed an average error of 68.2 cm in a room of 5 m $\times$5 m $\times$3 m.

In [82], a TDOA localisation for automobiles was proposed using the tail light of the vehicle as a transmitter. The LEDs transmit signals which are modulated at different frequencies to the car behind where PDs are placed in front of the car. The signals were then filtered at the receiver end using a band-pass filter. Thereafter, the phase difference of arrival at each receiver is determined. With the known modulated frequency, the speed of light and phase difference, the distance difference is then calculated. In a simulation environment, the system had a positioning error of 1 cm.

The work in [68] and [48] used a similar method of modulation and multiplexing. The first step taken was to modulate the signal from the transmitters at different frequencies. A band-pass filter was present at the receiver which to extract signals of different transmitters. The phase of each pair of signals was calculated by using Hilbert transform to distinguish the quadrature and in-phase components of every signal. The second step was to switch the modulated frequencies between each transmitter and calculate the phase difference based on it. With the distance from the transmitters and phase differences calculated, the receiver's location was then estimated using trilateration. In a simulation environment, the system had a positioning error of 1 cm.

The authors in [83] proposed to improve the research conducted in [48] by adding additive white Gaussian noise (AWGN) to the simulation and using statistical methods to predict the position of the receiver. The proposed method is shown to reduce error from 15.3 cm to 2 cm in a room of 5 m $\times$5 m $\times$3 m.

The authors in [84] proposed Darklight positioning, a positioning technique when the lighting system is not necessary. With the use of low power LEDs, the study proposed a TDM and pulse width modulation (PPM) scheme to measure the TDOA signal from five different transmitters. The three strongest received signals are selected and their respective distances (hyperbola) are defined. The intersection between the three hyperbolae is the target's position. In a room of 6 m $\times$6 m $\times$3 m, the model yielded an error of 5 cm.

The work in [85] modulated signals from different transmitters at different frequencies in a sinusoidal form. The phase difference was calculated by measuring the peak to peak amplitude of the sinusoidal light signal. The position can then be determined based on TDOA which is calculated based on the calculated phase difference, the speed of light and the known modulation frequency.

In most standard conditions, a TDOA based system requires three base stations or receivers to predict the estimated position accurately. The work in [42] proposed 2-D positioning using the minimum requirement of one traffic lighting transmitting a signal to two PDs at the vehicle's facial. This concept is detailed in Figure 2.14. During t_1, the transmitting signal collected by the two PDs and the TDOA Δt_1, is calculated alongside the corresponding hyperbola H_1 is obtained. During $t2$, when the vehicle is in a closer approximation to the traffic light, the second hyperbola H_2 is obtained, which is in response to TDOA Δt_2 being obtained. In the assumption that both periods t_1 and t_2 are known, the position of the traffic light in relation to the vehicle is obtained and calculated as the intersection between the two hyperbolas H_1 and H_2. The unconditionally absolute position of the vehicle can be calculated based on the relative and absolute position of the traffic light. The results of this proposed concept were provided in a simulation analysis that displays the system's accuracy depends on the difference in distance between the vehicle and the traffic light. The study also shows the accuracy is affected by the speed of the vehicle. The simulation shows a decrease in accuracy when the distance decreased, i.e. the positioning errors were extremely high when the distance was less than 5 m. However, when the distance increased to 50 m, the positioning errors reduce to 0.5 m. The positioning errors increase when the speed of the vehicle increases, which is to be expected. However, when the distance was larger than 20 m, the vehicle's speed had a minimum effect on the accuracy.

The preceding sub-sections have discussed the existing literature based on the received signal measurement technique. In the following sub-section, the positioning

Figure 2.14: *Two PDs to traffic light TDOA [42].*

methods will be discussed.

2.3.5 Positioning Methods

As seen in Figure 2.9, after measuring the signal using an appropriate technique, the signal goes through a positioning method that is explained in this section.

Trilateration

The most generic name given to positioning algorithms that use a geometric relationship to establish positioning is triangulation [1]. This technique is classified into angulation and lateration techniques. In the angulation technique, the angle relative to several points is measured (AOA). Then, the intersection points of direction lines are used to determine the position. Lateration methods exploit the distance between several points to estimate position. These distances can be calculated based on RSS, TDOA or TOA.

Fingerprinting

Fingerprinting, also called scene analysis, entails positioning techniques that match pre-measured location-related data with online measured data. This method exploits the irregularities in the distribution of transmitters in the presence of different barriers in the environment. For example, in a room with an uneven distribution of transmitters, the scatter of light and reflections off the wall and appliances will make the received power at different positions in the room different. Furthermore, the transmitted power in each transmitter is made different to ensure uneven distribution of received power. This method relies on these differences to establish positioning.

Imaging

Imaging is also known as vision/scene analysis is a method for positioning an object with multiple known image sensors. In this application, the geometric relationship is established using a pinhole camera. Using this method, complex positioning scenarios such as collinearity condition can be addressed [18].

Proximity

Proximity is the most straightforward positioning technique that outputs the proximity information of the transmitters but not their relative or absolute positions. In this technique, only a single transmitter is needed to provide the proximity of the transmitter. The transmitter transmits its identification code which is pre-installed and stored in a database. When a mobile device receives the signal, the corresponding information is looked up in the database to link it with its associated location. The position of the receiver is then provided based on an area of coverage.

2.4 Multiplexing Technique

As the majority of VLP techniques utilise multiple sources in the same space, multiplexing at the transmitter is required to enable signal separation at the receiver. Multiplexing is a fundamental technique as VLP can fail without it [18]. The commonly used multiplexing techniques in VLP are TDM and FDM.

2.4.1 Time Division Multiplexing

In the TDM approach, different transmitters transmit their respective signals at different points in time. The TDM has the advantage of a simple implementation as compared to other techniques. However, this is not efficient when there is a large number of transmitters. This is because it requires significant time to receive individual signals from all transmitters. Furthermore, TDM requires perfect time synchronisation of all the transmitters for positioning. However, the burden of synchronisation can be avoided by employing a random-access mechanism such as additive links on-line hawaii (ALOHA) [86]. Moreover, to use TDM in positioning, the number of transmitters need to be limited to avoid flickering.

2.4.2 Frequency Division Multiplexing

In FDM, the transmitters are modulated at different frequencies. This method introduces complexity in designing the de-multiplexer. However, many positioning systems employ FDM as it provides a platform for asynchronous positioning. A comparison of TDM and FDM on their application for indoor positioning is done in [86] which stated FDM base positioning systems perform better than TDM. A time synchronisation error as low as 10% makes TDM based designs perform poorly.

2.5 Analysis

Amongst the aforementioned algorithms, TOA is the most straightforward mechanism in terms of estimating the receiver location. Once the TOA has been obtained for each transmitter, the receiver's position can be calculated by the intersecting TOA circles. However, this method is known to produce high error magnitudes for the following reasons. First, the transmitter and the receiver need to be perfectly synchronised to measure the propagation time of the signal. This has been reported in [18] to provide issues even for indoor applications. Second, the accuracy of the measured propagation time between the transmitter and receiver is low. This is because the transmitter introduces a time delay to prepare the message to be sent. Third, the measured time accuracy relies on the response of the PD and clocks resolution. Due to these challenges, the accuracy of TOA in practical applications is low, thus limiting its applicability to VLP.

TDOA is more complex, in terms of mathematical formulation, compared to TOA. However, the application of TDOA based localisation only requires synchronisation on the transmitters side. This is more practical than synchronising both receivers and transmitters. However, TDOA requires a very precise time measurement. The accuracy of the time measurement is limited by the PD response time and the clock resolution. These limitations can result in errors in time measurement that will reduce the localisation accuracy.

AOA triangulation algorithms tend to yield the highest accuracy at the cost of complex implementation and set-up. It requires an accurate estimation mechanism and multiple receivers. For mobile devices, additional inertial sensors such as a 6-axis sensor or gyroscope are used to measure the AOA [48, 49]. This makes the practical realisation of this algorithm expensive. A major disadvantage of AOA triangulation is that the accuracy drops drastically when the distance from the receiver to the transmitter increases. This is because a small error in calculating the AOA results in a large positioning error.

The most investigated positioning algorithms in the literature are RSS-based due to their ease of implementation and asynchronous operation. The most popular algorithm with RSS is trilateration. In practice, the effects associated with incidence and irradiance angles are challenging to determine from the path loss model due to changes in the environment. Hence, the system works better when PDs are placed horizontally to the transmitter. Recent developments have shown that artificial intelligence (AI) methods can be used to enhance 2-D positioning accuracy in RSS based VLP ANN [56, 58] and DNN [53] as well as 3-D positioning [57]. This is achieved with more powerful and higher cost micro-controllers such as field-programmable gate array (FPGA) [87] at the receiver end, which is capable of handling the complex process of ANN. However, the aforementioned studies use a large ANN structure (3 ANNs) without optimisation. This has therefore been identified as a gap in the literature to study an optimised ANN structure for 2-D and 3-D VLP.

Most of the indoor VLP systems reviewed have not considered the NLOS path. However, [55, 56, 88] indicated that NLOS increases positioning error. It is found in [55] that, for a 2-D environment, there is a 90% increase in positioning error when NLOS is considered. The research in [56] proposed the use of ANN to reduce the effect of NLOS in VLP. The model improved the VLP performance with a positioning error of 0.065 m. However, all the aforementioned work only studied a 2-D VLP system. Therefore, this has been identified as a gap in the literature to study indoor 3-D VLP with a diffuse link and investigate methods to improve system performance. ANNs have been selected based on their demonstrated benefits and will be applied to 3-D VLP with NLOS. A singular research has been conducted in [84] for 2-D dark VLP using TDOA. This thesis also investigates the feasibility of applying an RSS-based approach for 3-D dark VLP.

Few studies have been conducted in the field of passive VLP. All these exploit RSS-based approaches as the receiver is not on the target. Most of the existing studies have considered the use of techniques such as shadowing (places with lower RSS due to signal blockage [59]) and numerous receivers [60–62]. Given the successful application of ANN for active positioning in the literature, this thesis will investigate its performance for passive VLP.

A significant amount of research has been done on indoor positioning applications. However, only a limited amount of work has considered the outdoor VLP system. It has been argued in [89] that alternative technology should coexist with GPS due to the limited accuracy of GPS in cities, tunnels and GPS dead zones. The introduction of VLP for autonomous vehicles is a promising area of research to improve positioning accuracy. The application intended for vehicles require the use of streetlights and traffic lights for localisation. In many instances, small sets of streetlights (3 to 5) are positioned along an almost straight line. This makes it challenging to apply traditional positioning techniques due to collinearity conditions. According to [18], achieving localisation with transmitters that are collinear is close to impossible using a single PD. The work in [44] proposed the use of cameras to solve the collinearity condition. Although a straight road with the streetlights located along a straight line are considered, the study assumes the use of a distributed transmitter, i.e. streetlights on both sides of the road. This means that the proposed model will not work when the streetlights are only on one side of the road. This thesis proposes a diversity technique with ML to address the collinearity condition and make VLP work when the streetlights are either on both or on a single side of the road.

ML algorithms can enhance VLP performance as shown in various studies in the literature. The performance of an ML algorithm is dependant on the optimisation of the network structure and the respective data set. Hence, this work optimises ML to enhance the VLP system performance and identify the best ML for this application. The study in [90] applied different ML algorithms such as GRU, RNN, MLP and LSTM for vehicle tracking using IMU sensors. These algorithms will also be investigated for outdoor vehicular VLP to select the most suitable neural network (NN) for the application. CMD has been shown to be well suited to both indoor and outdoor VLP. It has been investigated and experimentally studied to provide high accuracy without the need for extra hardware or processing power [91]. Therefore, this thesis adopts CMD as a benchmark for performance comparison for indoor and outdoor VLP.

This thesis considers the use of CMD as a benchmark for performance comparison. This algorithm has been investigated and experimentally studies to provide high accuracy without the need for extra hardware or processing power [91].

2.6 Summary

This chapter has reviewed VLP technologies. LEDs have become the technology of choice for transmitters due to their environmental friendliness, ruggedness, controllability, energy efficiency, fast switching and long lifetimes. The prominent receivers of VLP are cameras and PD. Though cameras are capable of capturing images in real-time, their application requires complex image processing technology (more processing power), and their high cost makes their realisation more difficult. PDs on the other hand, are cheaper and easier to deploy when compared to a camera and offer competing accuracies compared to camera-based VLP. The main VLP algorithms are RSS, AOA, TDOA and TOA, with positioning techniques ranging from triangulation, fingerprinting, imaging and proximity. One of the gaps identified in the literature is the need to account for the effect of NLOS in 3-D VLP. ANN has proven to help improve performance in NLOS link, thus making it the algorithm of choice. Given the limited research in indoor dark VLP and passive VLP, the application of ANN to improve the existing state-of-the-art is a novel area that this thesis will explore. A gap was also identified in outdoor VLP for vehicular application. This thesis will then investigate the feasibility of using PDs for vehicular VLP and critically evaluate the system's performance for different road and weather conditions.

Chapter 3

VLP System Modelling

Visible light positioning is a promising positioning technique delivering centimetre accuracy and widespread coverage for indoor and outdoor applications. VLP has emerged as an inexpensive, easy to configure and viable indoor and outdoor positioning technique. However, to make VLP a reality, certain challenges still need to be addressed. This includes the presence of multipath reflection (NLOS), weather conditions, system infrastructure and a suitable positioning algorithm. To do this, it is paramount to model and understand the characteristics of the optical channel. A summary of the methodology in this thesis is presented in Figure 3.1.

This chapter outlines the channel model for both indoor (active and passive[1]) and outdoor environments using LED luminaries as transmitters and PD as the receiver in Section 3.1. The remainder of this chapter is organised as follows: Section 3.2 describes the RSS estimation with respect to different noise and weather environments. Section 3.3 details the computation of neural networks, the different networks considered in this thesis and how a network can be over or under fitted when training. Section 3.4 describes the CMD algorithm and its cost function, which can be used to extend 2-D VLP to 3-D. The performance criteria are detailed in Section 3.5.

This chapter considers both indoor environment (see Figure 3.2) and outdoor environment (see Figure 3.3). Generally, a VLP system incorporates three components namely a transmitter, a channel and a receiver. In the proposed active VLP system with M transmitter and N receivers, the receiver determines its absolute position ($\widehat{x}_j$,$\widehat{y}_j$,$\widehat{z}_j$) based on spatially distributed light signals where $j = 1 \dots N$. As mentioned in section 2.3, the receiver should have a prior knowledge of the transmitter coordinates (i.e. $(x_{t,i}, y_{t,i}, z_{t,i})$) where $i = 1 \dots M$. This limited knowledge may also be transmitted using VLC. Moreover, only the receiver will have information about the estimated coordinates thus making it a one-sided positioning. This provides privacy and reduces the chances of exploitation by intruders.

To establish positioning, the existing lighting infrastructure needs to be modified to transmit the signal without voiding its primary purpose (illumination). In this thesis,

[1]We define active and passive positioning as positioning that takes place with and without user participation, respectively.

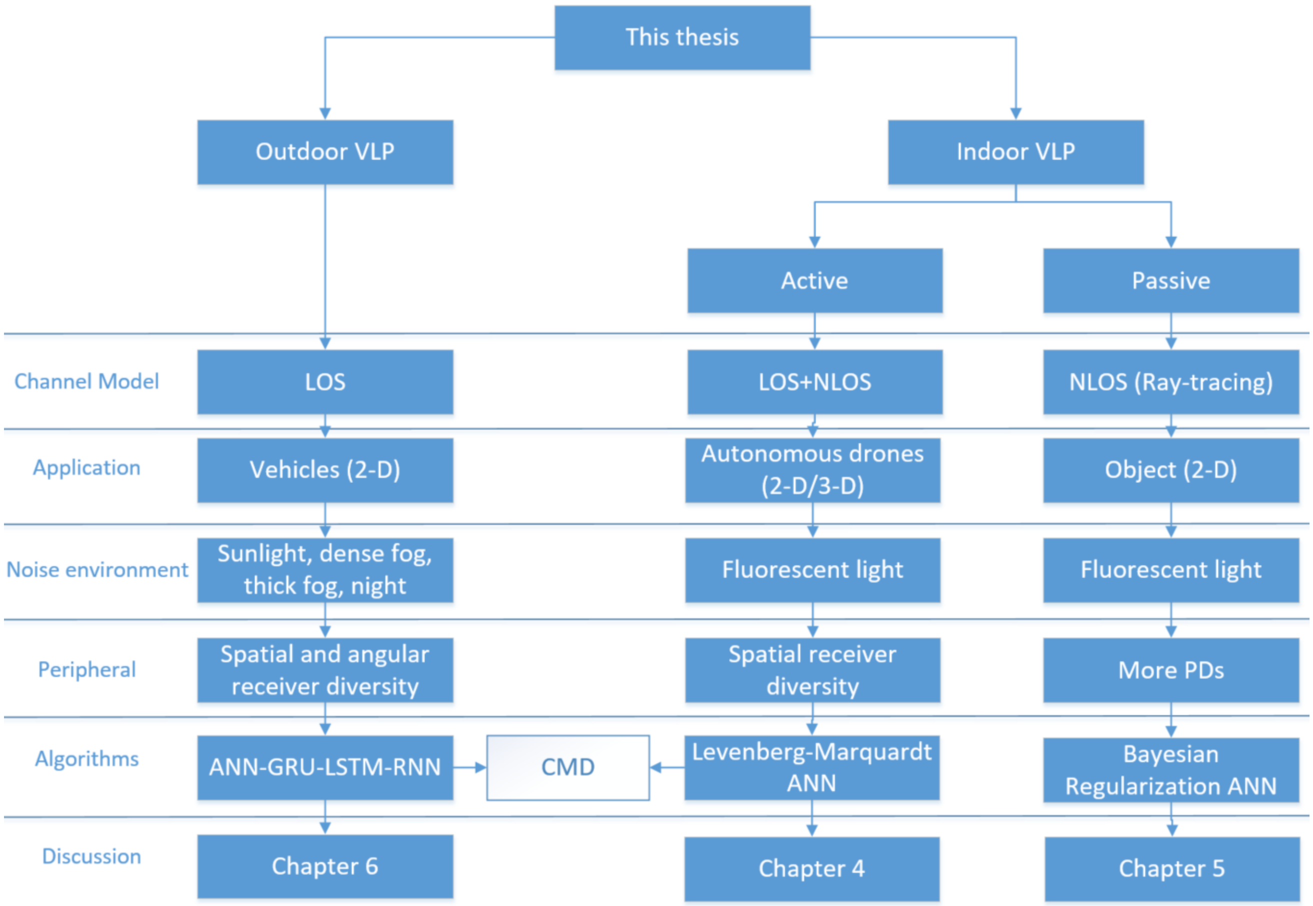

Figure 3.1: *Thesis methodology.*

LED driver is added to modulate the signal using TDM or FDM as outlined in Chapter 2.4. With each transmitter having a different time or frequency, the receiver can distinguish each signal using an appropriate filtering technique, thus the transmitters need not be synchronised. The PDs detect the transmitted signals and generate photocurrents, which are digitized. The resulting digital signals are filtered in RSS values to the transmitter and receiver. The channel links are discussed in the following sections.

3.1 Channel Model

As seen in Figure 2.4, there are several possible link configurations in VLP. This can be classified depending on the degree of directionality between the transmitter and receiver. To cover both active and passive positioning, both LOS and NLOS links will be considered.

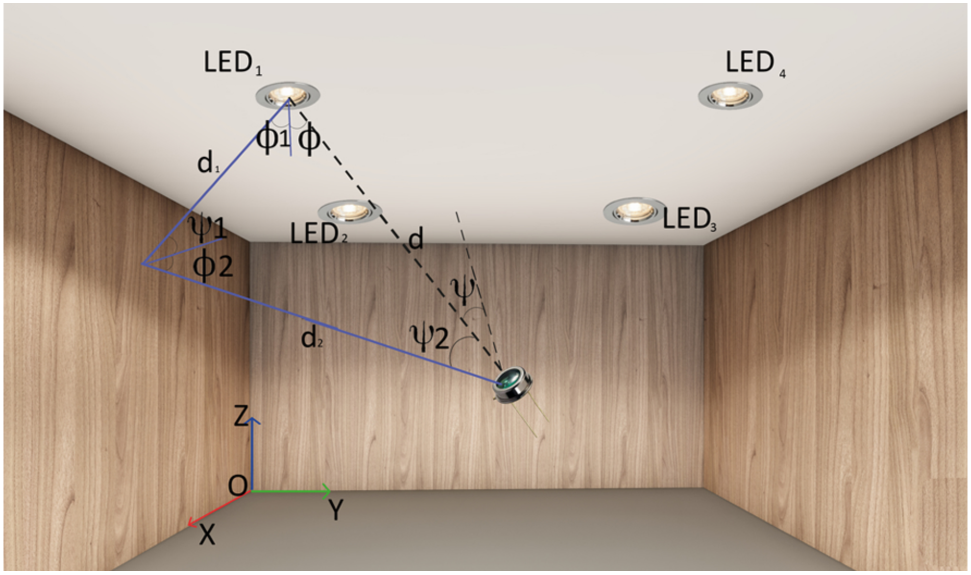

Figure 3.2: *Indoor localisation model for VLP*

3.1.1 Line of sight channel gain

The DC channel gain depends on the link distance, the channel configuration and the angle of incidence. This VLP application uses LED as transmitter and PD as receiver. Using a generalized Lambertian radiant intensity (R_0), the angular distribution is given by [17]:

$$R_0(\phi) = \begin{cases} \frac{(m+1)}{2\pi}\cos^m(\phi) & \text{for } \phi \in [-\pi/2, \pi/2] \\ 0 & \text{for } \geq \pi/2 \end{cases} \tag{3.1}$$

where $\phi = 0$ at maximum radiated power and m is the Lambertian emission order expressing directivity of the source beam, which is given by:

$$m = \frac{-\ln 2}{\ln(\cos\phi_{1/2})} \tag{3.2}$$

where $\phi_{1/2}$ represents the half-power angle of the LED. The radiant intensity at a given transmitted power P_t is given by:

$$S(\phi) = P_t\frac{(m+1)}{2\pi}\cos^m(\phi) \tag{3.3}$$

The radiation incidence angles ψ is collected by a photo-detector and is modelled as an active area which is given by:

$$A_{eff}(\psi) = \begin{cases} A_d\cos^m(\psi) & 0 \leq \psi \leq \pi/2 \\ 0 & \psi > \pi/2 \end{cases} \tag{3.4}$$

Though having a PD with a large area would provide for higher power reception, this will bring issues in practice, such as increased junction capacitance, receiver noise, manufacturing cost and reduced receiver bandwidth. Thus, a concentrator is introduced as a cost effective mechanism to increase the effect of the collection area . The optical concentrator gain with a refractive index n_c is given by [17]:

$$g(\psi) = \begin{cases} \frac{n_c^2}{\sin^2\psi} & 0 \leq \psi \leq \Psi_c \\ 0 & \psi > \Psi_c \end{cases} \tag{3.5}$$

where $\Psi \leq \pi/2$ is the FOV.

Base on the Etendue limit theorem, the collection area of the lens A_{coll} is directly related to the FOV of the receiver and its PD area is:

$$A_{coll}\sin\left(\frac{FOV}{2}\right) \leq A_d \tag{3.6}$$

It is clear from 3.6 that the concentrator gain is inversely proportional to FOV. Considering a link with a Lambertian source, a receiver with concentrator gain $g(\psi)$ and optical filter $T_s(\psi)$, the DC gain at an angle ϕ and distance d between the transmitter and receiver (see Figure 3.2) is given by [17]:

$$H_{los}(0)_i, j = \begin{cases} \frac{(m+1)A_r}{2\pi d_{i,j}^2}\cos^m(\phi)T_s(\phi)g(\psi)\cos(\psi) & 0 \leq \psi \leq \Psi_c \\ 0, & \psi > \Psi_c \end{cases} \tag{3.7}$$

Hence the received power for the LOS path is given as:

$$P_{r-los} = P_t H_{los}(0) \tag{3.8}$$

3.1.2 Non Line of Sight

In diffuse links and NLOS links, factors such as the orientation of transmitter and receiver, reflectivity of the walls, ceilings and objects within the room need to be considered, thus making it more complex to predict [88]. The received power is given as:

$$P_{r-nlos} = (H_{los}(0) + H_{nlos}(0))P_t \tag{3.9}$$

where H_{nlos} is calculated under the assumption that the reflective surface (wall) consist of several reflectors ΔA and a reflection coefficient of ρ and is given by:

$$H_{nlos}(0)_{i,j} = \begin{cases} \sum_{\text{wall}} \frac{(m+1)A_r\rho\Delta A}{2\pi^2 d_1^2 d_2^2}\cos^m(\phi_1)\cos(\psi_1)\cos(\phi_2)\cos(\psi_2)T_s(\phi_2)g(\psi_2) & 0 \leq \psi_2 \leq \Psi_c \\ 0, & \psi_2 > \Psi_c \end{cases} \tag{3.10}$$

where ψ_1 and ψ_2 are the angles of incidence, d_1 and d_2 are the reflected distances (see Figure 3.2), and ϕ_1 and ϕ_2 are angles of irradiance.

3.2 RSS Estimation

For the proposed VLP application, an environment with M (where $M > 1$) LED luminaires and $N \geq 1$ PDs based receiver is considered as shown in Figure 3.2 and Figure 3.3. The transmitters transmit TDM or FDM signals encoded with their unique position information as outlined in section 2.4. The LEDs can be dimmed to reduce its brightness using PWM scheme. The PWM signal consists of a periodic train of pulses with adjustable widths relative to varying values of D, thus resulting in a variation of the DC level of the waveform. By using PWM, LEDs can be dimmed to have a very-low average transmitted power. Furthermore, flickering can be avoided by adjusting the value of (D) with the respective frequency of the PWM signal. The period of the PWM signal $a(t)$ equals T_{PWM}, and for $0 \leq t \leq T_{PWM}, a(t)$ is given by:

$$a(t) = \begin{cases} 1 & 0 \leq t \leq \tau \\ 0 & T_1 < t \leq T_{PWM} \end{cases} \tag{3.11}$$

where τ is the duration of the PWM pulse.

The VLP in this study is based on RSS, which requires the estimation of the received power from the various transmitters. Hence, to estimate the received from the i^{th} transmitter to the j^{th} receiver, 3.9 can be modified as:

$$P_{r-i,j} = (H_{los}(0)_{i,j} + H_{nlos}(0)_{i,j})P_{t,i} \tag{3.12}$$

where $P_{t,i}$ is the average transmitted optical power of the respective LED.

3.2.1 Noise

The VLP system is affected by thermal and shot noises, which are generally modelled as AWGN [17]. The background light and the photo-current generated by the desired signal is known as the shot noise and its variance is calculated as [17]:

$$\omega^2_{shot,j} = 2qI_{bg}I_2B + 2qR_pP_{r-i,j}B \tag{3.13}$$

where I_{bg} represents the background current, I_2 is a noise bandwidth factor of the current, B represents the bandwidth, q is the electronic charge and R_p is the receiver responsivity. The thermal noise that arises from the amplifier at the receiver is given as [17]:

$$\omega^2_{thermal,j} = \frac{8\pi k T_k}{G}\eta A I_2 B^2 + \frac{16\pi^2 k T_k \Gamma}{g_m}\eta^2 A^2 I_3 B^3 \tag{3.14}$$

where k represents the Boltzmann's constant, T_k, G and η represent absolute temperature, open-loop gain and fixed capacitance of the PD. g_m and Γ represent FET trans-conductance and FET channel noise factor, respectively. In VLP, the value of I_{bg} differs across different noise environments and are provided in table 3.1 [92, 93]. The

Figure 3.3: *Outdoor localisation model for VLP*

Table 3.1: *Noise Parameters*

I_{bg}(A)	Noise environment
5100μ	Direct sunlight without optical filter
1000μ	Direct sunlight with an optical filter
190μ	Indirect sunlight with an optical filter
740μ	Indirect sunlight without optical filter
58μ	Incandescent light and fluorescent light with an optical filter
40μ	Fluorescent without optical filter

Table 3.2: *Simulation Parameters*

Parameter	Symbol	Value
Boltzmann's	k	1.38×10^{-23}(J/K)
Electronic charge	q	1.6×10^{-19}(C)
Absolute temperature	T_k	300(K)
Open-loop voltage gain	G	10
Noise bandwidth factor	I_2	0.562
FET trans-conductance	g_m	30 (ms)
FET channel noise factor	Γ	1.5
Fixed capacitance of the PD	η	112(pF/cm^2)

list of the values commonly used in the noise model parameters are shown in Table 3.2 [93].

Finally, the average SNR given as $\overline{SNR}$ can be calculated as:

$$\overline{SNR} = \frac{1}{MN}\sum_{i=1}^{M}\sum_{j=1}^{N}\frac{(P_{r-i,j}R_p)^2}{\omega^2_{shot,j} + \omega^2_{thermal,j}}, \tag{3.15}$$

3.2.2 Fog Model

Among the various atmospheric conditions that cause signal attenuation, fog is considered to contribute the most severe attenuation [94]. The atmospheric attenuation due to fog is related to the visibility V and wavelength λ. Using the empirical approach, the relationship between V and the fog attenuation given by Kruse model [17] is:

$$V(km) = \frac{10\log_{10}T_{th}}{\beta_\lambda}(\frac{\lambda}{\lambda_0})^{-w} \tag{3.16}$$

where β_λ is the atmospheric attenuation, T_{th} is 2% visual threshold, w is the particle size distribution coefficient and λ_0 is the solar band maximum spectrum, where $\lambda_0 = 550$ nm in this study. The fog attenuation is estimated using Kims model from the w value and visible - NIR wavelengths, which is a function and V and is defined as [94]:

$$w = \begin{cases} 1.6 \text{ for } V > 50\text{km} \\ 1.3 \text{ for } 6 < V < 50\text{km} \\ 0.16V + 0.34 \text{ for } 1 < V < 6\text{km} \\ V - 0.5 \text{ for } 0.5 < V < 1\text{km} \\ 0 \text{ for } V < 0.5\text{km} \end{cases} \tag{3.17}$$

Table 3.3 shows the visibility range under different weather conditions [17].

The atmospheric attenuation given by Beer-Lambert law as [95]:

Table 3.3: *Weather conditions and their visibility range values [94].*

Weather condition	Visibility range (m)
Dense fog	< 50
Thick fog	200
Moderate fog	500
Light fog	$770 - 1000$
Thin fog/heavy rain	$1900 - 2000$
Haze/medium rain	$2800 - 40000$
Clear/drizzle	$18000 - 20000$
Very clear	$23000 - 50000$

$$\beta_\lambda = \frac{\ln \frac{I_0}{I}}{d} [\mathrm{km}^{-1}] \tag{3.18}$$

where $I_0[\mathrm{W.m}^{-2}]$ is the optical intensity at zero distance ($d = 0$), I is the optical intensity at distance d.

3.3 Machine Learning Positioning algorithm

The novelty of this work is the combination of ML algorithms with receiver diversity and a realistic channel model to enhance positioning accuracy. The most prominent algorithm is MLP-ANN [56, 57, 96] which is examined at the first instance in this thesis. Thereafter, a variety of ML algorithms are considered to see their impact on performance. Hence in this section, the proposed ML algorithms are explained.

3.3.1 Computation of a neural network

ANNs are inspired from biological brains and consist of an arbitrary number of nodes, each representing a biological neuron. There is an arbitrary input and output data stream for each node. These can be considered as the neural fibre of the neural network. There is an activation function per node that enumerates a new value to be transmitted to adjacent neurons. This is similar to the electric transmission in the brain [97]. The node consists of an integration function that will produce a single value from the number of input values. This is fed to the activation function.

The common non-linear activation functions are Logistic Sigmoid and hyperbolic tangent activation function, also known as Log-sig or Sigmoid and Tan-sig or Tanh, respectively. As it can be seen in Figure 3.4, Logistic Sigmoid works on the probability of output being between 0 and 1, hyperbolic tangent operates between -1 and 1.

Figure 3.4: *Hyperbolic tangent v/s Logistic Sigmoid [97].*

3.3.2 Feed-forward neural networks

In a feed-forward neural network, information is considered to move in only one direction starting from the input to the output, see Fig 3.5. This interprets that in each training iteration, the activation signal will always progress and never revisit nodes that they have encountered before [98]. Moreover, each training data point is treated independently of other training data points. There are three types of feed-forward neural network namely single layer perceptron (SLP), MLP and "other feed-forward neural network". A SLP consists of a single input and output layer. Due to its single-layer structure, a SLP is only capable of learning linear problems. A MLP consists of one or more hidden layers between the input and the output layers. Unlike SLP, MLP can be used to solve non-linear problems. However, the weight-update procedure is more complicated. An effective way to solve this issue is by using a back-propagation algorithm which is detailed in the following section 3.3.3. Other feed-forward neural networks include CNN, RBFN, RNN, LSTM and GRU. These networks vary in the structure where some nodes with (with no children) are the designated outputs and some nodes (with no parents) are the designated inputs.

Figure 3.5: *MLP-ANN with one hidden layer [85].*

3.3.3 Artificial Neural Network (ANN)

In ML, propagation is widely used to train a feed-forward neural network. Unlike other naive fitting techniques in a neural network with direct computation of the gradient for each weight, back-propagation in ML efficiently evaluates the gradient of the loss function to the weights of the network for a single input-output example [97]. This makes it possible to employ gradient methods or variants, such as stochastic gradient descent efficiently, for training MLPs. In this work, the Levenberg-Marquardt supervised training algorithm is adopted to train a feed-forward back-propagation network. This algorithm requires less training time but more memory. Once the generalisation stops improving, the training stops automatically as indicated by an increase in the mean squared error (MSE) of the validation samples. This second-order training method has speed similar to the quasi-Newton methods, without the need to solve the Hessian matrix. In a typical feed-forward network where the performance function entails the form of a sum of squares, the Hessian matrix denoted as H can be calculated as [98]:

$$H = J^T J \tag{3.19}$$

where T represents transpose, the gradient g_r is

$$g_r = J^T e \tag{3.20}$$

In (3.19) and (3.20), J represents the Jacobian matrix. This holds the weights and the biases for the first error derivatives. e represents the vector of the network errors, hence, the Jacobian matrix can be computed. Thus, the Levenberg-Marquardt algorithm ($\mathbf{X}_{k+1}$) can be calculated as follows:

$$\mathbf{X}_{k+1} = \mathbf{X}_k - [\mathbf{J}^T\mathbf{J} + \mu\mathbf{I}]^{-1}\mathbf{J}^T e \tag{3.21}$$

where μ is a scalar close to zero and is a Newton-like update method that approximates the Hessian matrix. When μ attains a large magnitude, it becomes gradient descent with a small step size. The aim is to shift towards Newton's method quickly as it is more accurate and faster to converge to a minimum error. Hence, after each successful step, μ decreases and otherwise only increases when a tentative step increases the performance function.

A common issue in estimating the weights in a network is the over fitting of the neural network (discussed later in this section). The Bayesian regularisation approach is proposed in [99] to solve this issue. This algorithm (Bayesian regularisation) requires less memory but more time as compared to Levenberg-Marquardt algorithm. However, this can result in a better generalisation for noisy, small or difficult data sets. The training stops on adaptive weight regularization. This is when there in no longer an improve in generalisation. Therefore this technique was also considered in this thesis. The approach of Bayesian regularization occurs within the Levenberg-Marquardt algorithm. The Jacobian matrix ($\boldsymbol{jX}$) of the performance is calculated using back-propagation with respect to the bias and weight and bias variables x. Hence each variable is adjusted as [99]:

$$\boldsymbol{J = jX.jX} \tag{3.22}$$

$$\boldsymbol{je = jX.E} \tag{3.23}$$

$$\boldsymbol{dX = -(J + I.\mu)/je} \tag{3.24}$$

3.3.4 Simple Recurrent Neural Network (sRNN)

RNN differ from the MLP by their ability to learn relationships within sequences. They have feedback loops, which helps in connecting relationships learnt in the past. The connections are sometimes called memory. Such information learnt within the sequential dimension of the data are stored within the hidden state of the RNN which extends to the defined number of time steps and are mapped forward and continuously to the output. The unrolled architecture of the RNN is presented in Figure 3.6. The equation governing the operation of the sRNN are:

$$\boldsymbol{h_t} = \tanh(\boldsymbol{U_h h_{t-1} + W_x x_t + b_h}) \tag{3.25}$$

$$\boldsymbol{y_t = \sigma(W_0 h_t + b_o)} \tag{3.26}$$

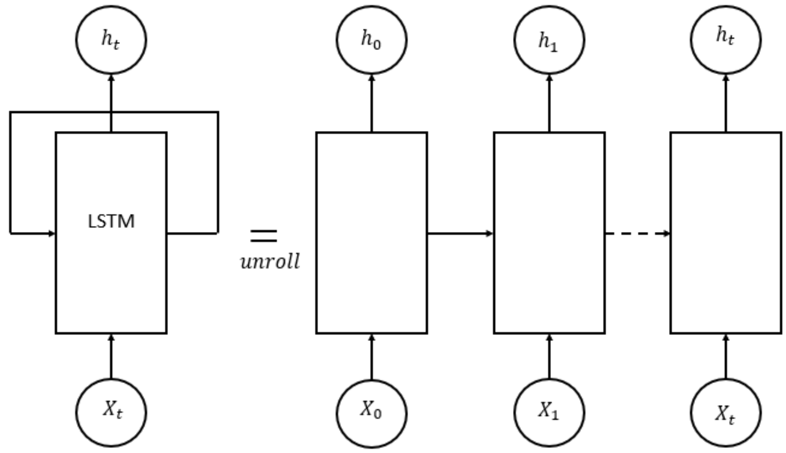

Figure 3.6: *Unrolled RNN architecture [90].*

where y_t is the output state, tanh is the hyperbolic tangent function, $\mathbf{U_h}$ is the hidden weight matrix, x_t is the input state, $\mathbf{b_h}$ is the hidden bias vector, $\mathbf{b_o}$ is the output bias vector, $\mathbf{h_{t-1}}$ is the previous state, $\mathbf{W_x}$ is the input matrix and $\mathbf{W_0}$ is the output weight matrix. The detailed operation of the sRNN is given in [90, 100].

3.3.5 Long Short-Term Memory (LSTM) neural network

LSTM's are a variant of the RNN. They were created to address the long-term dependency problems of the sRNN. Through the use of gated architectures: input gate, forget gate and output gate, LSTM can recall information from long periods of time. The cell structure of LSTM is presented in Figure 3.7. The gated operations of the LSTM are shown by the following equations:

$$forget\ gate : \boldsymbol{f_t} = \boldsymbol{\sigma}(\boldsymbol{W_f x_t} + \boldsymbol{U_f h_{t-1}} + \boldsymbol{b_f}) \tag{3.27}$$

$$input\ gate : \boldsymbol{i_t} = \boldsymbol{\sigma}(\boldsymbol{W_i x_t} + \boldsymbol{U_i h_{t-1}} + \boldsymbol{b_i}) \tag{3.28}$$

$$current\ memory\ state : \boldsymbol{\widehat{c}_t} = \tanh(\boldsymbol{W_c x_t} + \boldsymbol{U_c h_{t-1}} + \boldsymbol{b_c}) \tag{3.29}$$

$$cell\ state : \boldsymbol{c_t} = \boldsymbol{f_t} * \boldsymbol{c_{t-1}} + \boldsymbol{i_t} * \boldsymbol{\widehat{c}_t} \tag{3.30}$$

$$output\ gate : \boldsymbol{o_t} = \boldsymbol{\sigma}(\boldsymbol{W_o x_t} + \boldsymbol{U_o h_{t-1}} + \boldsymbol{b_l}) \tag{3.31}$$

$$final\ memory : \boldsymbol{h_t} = \boldsymbol{o_t} * \tanh(\boldsymbol{c_t}) \tag{3.32}$$

where $\mathbf{h_{t-1}}$ is the previous state and $*$ is the Hadamard product. $\mathbf{W_i}$, $\mathbf{W_f}$,$\mathbf{W_c}$ and $\mathbf{W_o}$ are the weight matrices of the input gate, forget gate, current memory state and output gate respectively, $\mathbf{U_i}$, $\mathbf{U_f}$, $\mathbf{U_c}$ and $\mathbf{U_o}$ are the hidden weight matrices of the input gate, forget gate, current memory state and output gate respectively, and $\mathbf{b_i}$, $\mathbf{b_f}$, $\mathbf{b_c}$ and $\mathbf{b_l}$ are the bias of the input gate, forget gate, current memory state and output gate respectively.

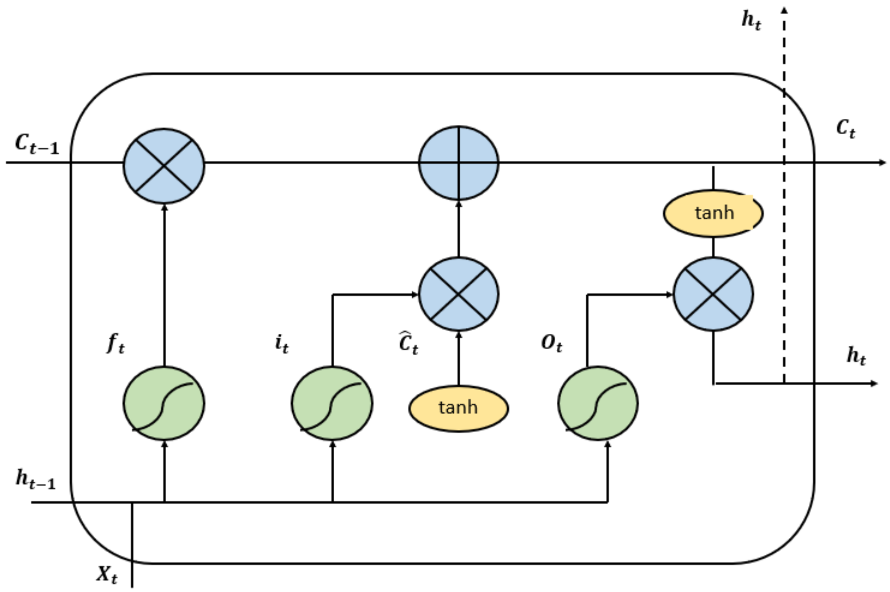

Figure 3.7: *LSTM cell structure [90].*

3.3.6 Gated Recurrent Unit (GRU) neural network

Cho et al in [101], introduced the GRU to address the vanishing gradient problem of the RNN giving it the ability to learn long term dependencies. Just like the LSTM, the GRU cellular operation is characterised by gated operations with its cell structure shown in Figure 3.8. However, the GRU has its hidden state and cell state merged to form a more computationally efficient model. The operations of the GRU are governed by the following equations:

$$\textit{update gate} : \boldsymbol{z_t} = \boldsymbol{\sigma}(\boldsymbol{W_z x_t} + \boldsymbol{U_z h_{t-1}} + \boldsymbol{b_z}) \tag{3.33}$$

$$\textit{reset gate} : \boldsymbol{r_t} = \boldsymbol{\sigma}(\boldsymbol{W_r x_t} + \boldsymbol{U_r h_{t-1}} + \boldsymbol{b_r}) \tag{3.34}$$

$$\textit{current memory state} : \ \widehat{\boldsymbol{h}}_{\boldsymbol{t}} = \tanh(\boldsymbol{W_h x_t} + \boldsymbol{r_t} * \boldsymbol{U_h h_{t-1}} + \boldsymbol{b_m}) \tag{3.35}$$

$$\textit{final memory} : \boldsymbol{h_t} = \boldsymbol{z_t} * \boldsymbol{h_{t-1}} + (\boldsymbol{1} - \boldsymbol{z_t}) * \widehat{\boldsymbol{h}}_{\boldsymbol{t}} \tag{3.36}$$

where $\mathbf{W_h}$, $\mathbf{W_r}$ and $\mathbf{W_z}$ are the weight matrices of the current memory state, reset gate and update gate respectively, $\mathbf{U_h}$, $\mathbf{U_r}$ and $\mathbf{U_z}$ are the hidden weight matrices of the current memory state, reset gate and update gate respectively, and $\mathbf{b_m}$, $\mathbf{b_r}$ and $\mathbf{b_z}$ are the bias of the current memory state, reset gate and update gate, respectively.

3.3.7 Over-fitting and under-fitting neural networks

A neural network is said to be over-fitted when it has either too many layers and nodes or when a data set is presented to the network too many times. This results in tiny

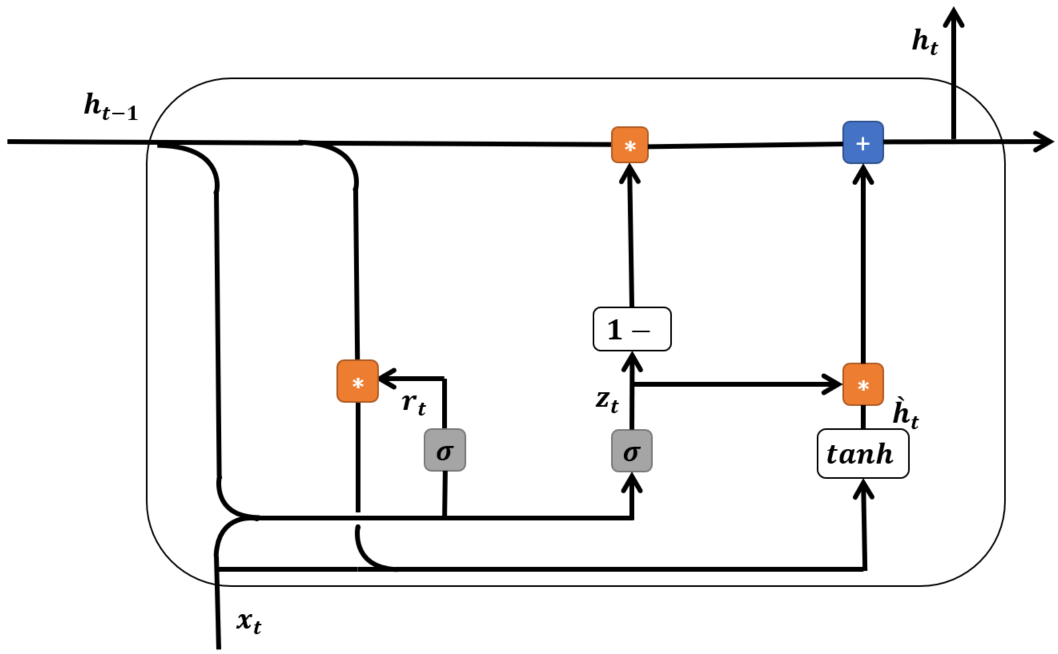

Figure 3.8: *Cell structure of GRU [90].*

training error and medium-large testing error. However, this can be spotted by plotting the test and training data errors. A graphical presentation is seen in Figure 3.9, the optimum number of iterations is the inflexion point, also known as the early stopping point. At the inflexion point, the network exhibits a god compromise between small testing as well as training errors. A neural network is under-fitted when the training does not reach the inflection point. This can be caused by low number of iterations, which result in a large training and testing errors. Hence, it is important to monitor the number of iterations, also known as epochs.

In summary, a degradation in descent is observed until the testing error stops decreasing and starts to increase. Thereafter, the training is stopped. This process is known as early stopping and is widely used in NN training.

3.4 Cayley Menger Determinant

Trilateration has been selected as a benchmark for VLP based on its effectiveness and wide use, see Chapter 2.3.5. A recent study in [15] uses trilateration based on CMD for positioning. The aforementioned work achieves high accuracy using LEDs and PDs without the need for extra hardware hence making it a better model for comparison. CMD is a trilateration based algorithm that extends the cost function for positioning using RSS as described in [15]. This enables 3-D positioning with the receivers knowledge of its height. Figure 3.10 illustrates the transmitter position labeled

Figure 3.9: *Illustration of error from training and test sets with increasing number of iterations [85].*

as r_1, r_2 and r_3, with r_4 being the unknown receiver location. Only three transmitter signals are required for the CMD algorithm. Hence, the three strongest signals are selected for further calculations.

The Cayley–Menger bi-determinant of two sequences of n points $[r_1, r_2, \ldots, r_n]$ and $[q_1, q_2, \ldots, q_n]$ is given as [102]:

$$D(r_1, \ldots, r_n, q_1, \ldots, q_n) = 2(\frac{-1}{2})^n \begin{vmatrix} 0 & 1 & 1 & 1 & 1 \\ 1 & D(r_1, q_1) & D(r_1, q_2) & \ldots & D(r_1, q_n) \\ 1 & D(r_2, q_1) & D(r_2, q_2) & \ldots & D(r_2, q_n) \\ \vdots & \vdots & \vdots & \ddots & \vdots \\ 1 & D(r_n, q_n) & D(r_n, q_n) & \ldots & D(r_n, q_n) \end{vmatrix} \tag{3.37}$$

where $D(r_i, q_j)$ is the squared distance between point r_i and q_j. The CMD occurs when there are two identical sequences of point i.e. $r_i = q_j$, then $D(r_1, \ldots, r_n, q_1, \ldots, q_n)$ is given as $D(r_1, \ldots, r_n)$. Hence, 3.37 can be written as:

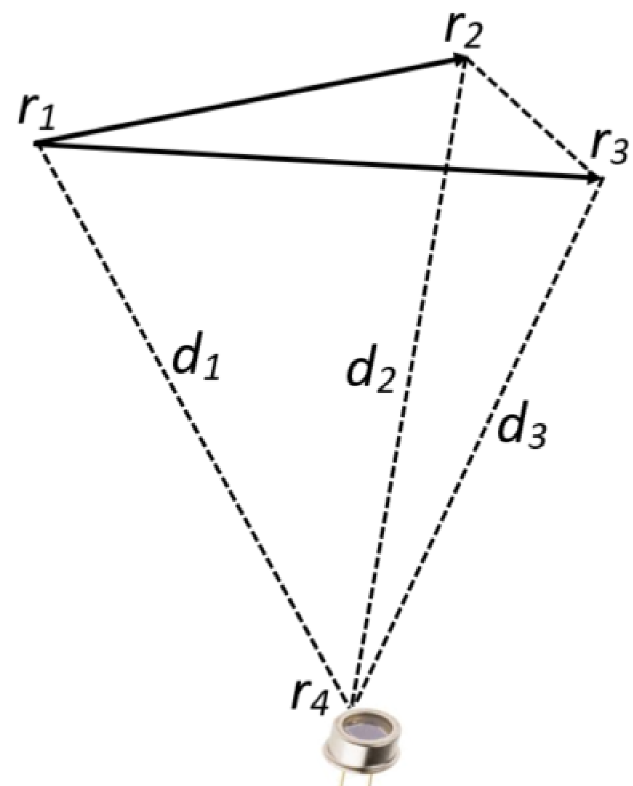

Figure 3.10: *The schematic diagram for the CMD trilateration problem and its parameters.*

$$D(r_1, r_2, r_3, r_4) = \frac{1}{8} \begin{vmatrix} 0 & 1 & 1 & 1 & 1 \\ 1 & 0 & D(r_1, r_2) & D(r_1, r_3) & D(r_1, r_4) \\ 1 & D(r_1, r_2) & 0 & D(r_2, r_3) & D(r_2, r_4) \\ 1 & D(r_1, r_3) & D(r_2, r_3) & 0 & D(r_3, r_4) \\ 1 & D(r_1, r_4) & D(r_2, r_4) & D(r_3, r_4) & 0 \end{vmatrix} \tag{3.38}$$

where r_4 is the unknown receiver location, $D(r_4, r_1), D(r_4, r_2)$ and $D(r_4, r_3)$ are the calculated distances $\widehat{d_1}, \widehat{d_2}$ and $\widehat{d_3}$. With transmitter coordinates (r_1, r_2, r_3), the receiver position r_4 can be calculated using [103]:

$$r_4 = r_1 + k_1 v_1 + k_2 v_2 \pm k_3 (v_1 v_2) \tag{3.39}$$

where $v_1 = r_2 - r_1$, $v_2 = r_3 - r_1$ and $\pm$ accounts for two mirror symmetric locations. However, given that the receiver cannot be above the ceiling, one of the possibilities is ignored. Thus, k_1, k_2 and k_3 are given by:

$$k_1 = -\frac{D(r_1, r_2, r_3; r_1, r_3, r_4)}{D(r_1, r_2, r_3)}, k_2 = \frac{D(r_1, r_2, r_3; r_1, r_2, r_4)}{D(r_1, r_2, r_3)}, k_3 = \frac{\sqrt{D(r_1, r_2, r_3, p4)}}{D(r_1, r_2, r_3)} \tag{3.40}$$

The predicted receiver coordinates $(\widehat{x}, \widehat{y}, \widehat{z})$ are then revealed as the CMD output for a given change in height δh. The most probable 3-D position of the receiver is the found at a minimum cost function $c(h)$ given as:

$$c(h) = \frac{1}{N} \sum_{i}^{N} = 1[\widehat{d}_i(h) - \sqrt{(\widehat{x}(h) - x_i)^2 + (\widehat{y}(h) - y_i)^2 + (\widehat{z}(h) - z_i)^2}]^2 \tag{3.41}$$

3.5 Performance criteria

In this thesis, five criteria to analyse the results of the proposed algorithms are adopted. These are RMS error, CDF and confidence interval (CI), percentage difference and percentage increase. The average RMS error evaluates the mean positioning error of all the sampled points. CDF analyses the distribution of error across the sampled points. CI computes the RMS value between the range of $s = 0$ to $s = 100\%$, where s is the confidence level. Percentage difference measures two differences between two values and percentage increase measures the increase (%) of performance from the previous one. The RMS error is defined as:

$$RMS\ error = \sqrt{(x - \widehat{x})^2 + (y - \widehat{y})^2 + (z - \widehat{z})^2} \tag{3.42}$$

where (x, y, z) is the actual receiver position and $(\widehat{x}, \widehat{y}, \widehat{z})$ is the estimated receiver position. In statistics and theory, CDF $F(x)$ is the likelihood that the value will be less than the threshold, which is given as:

$$F_X(x) = P(X \leq x) \tag{3.43}$$

where $F_X(x)$ is the function of x, X is the real value of the variable and P is the probability that X will have a value less than or greater than x. This is used in examining the distribution of data. Furthermore, an overlay can be made in a plot to analyse two distribution data. The confidence interval is the probability that a population parameter will fall between a set of values for a certain proportion of times. The CI criterion will be used in this thesis to determine the RMS error values attained 95% of the time. The CI of the error is given by:

$$CI = \bar{x} \pm w \frac{s}{\sqrt{n}} \tag{3.44}$$

where $\bar{x}$ is the sample mean, s is the sample standard deviation and n is the sample size. The percentage difference between two RMS error values can be calculated as:

$$Percentage\ Difference(\%) = \frac{|\Delta RMSerror|}{[\frac{\sum RMSerror}{2}]} \times 100 \tag{3.45}$$

The percentage increase between two RMS error values can be calculated as:

$$Percentage\ increase(\%) = \frac{RMSerror_2 - RMSerror_1}{RMSerror_1} \times 100 \tag{3.46}$$

Finally, the computational complexity of the neural network assessed by the number of multiplications each network has is given by:

$$O = O_n \times O_e(L_1 \times L_2 + L_2 \times L_3) \tag{3.47}$$

where O_n and O_e represent the number of training samples and epoch, respectively. L_1, L_2 and L_1 represents the first, second, and third hidden layer respectively.

3.6 Summary

This chapter introduced the generic system model for VLP that includes the channel model, noise model, fog model and positioning algorithms used for both indoor and outdoor purposes. For passive VLP, ray-tracing is used to model the channel. The positioning algorithms used in this thesis are ANN, RNN, GRU, LSTM and CMD. These algorithms are detailed for the application of VLP in this chapter. Finally, the method of analysing the results is shown as RMS error, CDF, CI, Percentage difference and Percentage increase.

Chapter 4

Indoor 3-D Visible Light Positioning

4.1 Introduction

This chapter presents a novel indoor 3-D VLP system using a realistic optical wireless channel model with receiver diversity. Recently, there has been an increase in demand for LBSss for indoor and underground parking, autonomous robot control, shopping centres and health applications. For several years, GPS has been one of the most successful means of tracking objects in outdoor environment. However, GPS signals suffer significant attenuation and multipath fading in urban cities and indoor environment, which results in large positioning errors [25]. There are several RF-based indoor positioning techniques such as Wi-Fi, Bluetooth, RFID but exhibit certain limitations as discussed in Chapter 1. The localisation accuracy of an RF system is in the decimetre range due to multipath propagation and interferences [27]. However, applications such as autonomous robots and drones require accuracy in the cm to mm range. In addition to conventional 2-D positioning, indoor applications such as indoor drone require 3-D positioning. VLP has shown to offer the high accuracy required by these applications and hence has been an active research topic for indoor positioning [18]. The suitability of VLP lies in its precision, ubiquity and cost-effectiveness. VLP is also free from electromagnetic interference but may suffer from ambient light interference.

The remainder of this chapter is organised as follows: Section 4.2 describe the related work. Section 4.3 present the indoor VLP system model. This modelling approach is then exploited in Section 4.4 to provide the data for the ANN design. Improvement to the baseline approach is then presented in Section 4.5, where the importance of receiver diversity, separation and FOV are demonstrated. The approach is then applied to 3D VLP in Section 4.6, where the impact of the channel model realism, in terms of LOS and NLOS link, on the result accuracy is demonstrated. The approach developed for 3-D VLP is then applied to 2-D VLP in Section 4.7. Following a critical evaluation of the VLP using ANN in Section 4.8, the best approach is applied to Dark VLP, with CMD used as a benchmark in Section 4.9. The chapter summary is then provided in Section 4.10.

4.2 Related Work

Most works on indoor VLP focused on 2-D localisation assuming a fixed receiver height which ignores the position error introduced by variation in the height [57,104]. Limited work has been reported in the application of VLP in 3-D. An AOA approach to 3-D VLP was investigated using an aperture-based receiver in [105]. Using multiple positioning algorithms such as triangulation, maximum likelihood and AOA, the system yielded an average RMS error of 0.1 m in a room of 5 m×5 m×2 m. An accelerometer in combination with LED was studied in [106] for 3-D positioning. The aforementioned work required the received power to be measured twice at different receiver orientations and a smartphone accelerometer was used to determine the receiver's orientation. Such work relies on the accuracy of the accelerometer, which is less accurate if the target device is affected by a significant amount of movement [107]. A hybrid indoor localisation method was proposed in [104] using AOA and RSS with multiple optical receivers. The study demonstrated that an RMS error of less than 0.06 m was achievable for a 2 m× 2 m× 2.5 m room. However, the proposed system required information on the angles of the receiver for the 3-D positioning. In [108], a 3-D VLP was proposed based on fingerprinting using K-means and random forest. However, the process of using the fingerprinting technique is considered labour intensive and time-consuming with respect to the size of the room [18]. A recent study in [109] considered the use of receiver tilt to establish a 3-D VLP using RSS. The mathematical analysis demonstrated that a RMS error of 0.0795 m was achievable for a 2.5 m× 2.5 m× 3 m room. Note that most of the aforementioned studies did not consider the effect of reflection on the accuracy of the positioning. A recent study in [88] considered the effect of NLOS link on VLP using geometric relationships. The simulated and experimental results demonstrated that the positioning error increased linearly with respect to the reflection coefficient of the walls. It was shown that by using irregular LED coordinated, resulting in a non-symmetric transmitter matrix, RMS errors up to 0.06843 m was achievable in a room of 6 m×6 m ×3 m. The LED arrangement does, however, reduce the practicality of the solution for real-life applications.

The adaptability and self-learning capability of AI has recently led to the development of several 2-D and 3-D positioning applications using AI [46, 53, 54, 57]. Among them, the work in [57] reported the best performance with RMS error of 4 mm. However, the work required a large transmitter and receiver array with 4×4 LEDs grid at the ceiling with 1 m spacing and a 19×19 receiver grid. Three ANNs (one for each dimension), each with 16 nodes in the input layer and 19 nodes in the output layer, were required to determine the 3-D position. This made the approach complex as well as impractical due to the large ANN structure and the requirement for a large number of transmitters and receivers arrays. A recent study in [58] demonstrated the feasibility of 3-D VLP using a two-layer ANN. It was assumed that the room was divided into multiple trilateral positioning cells and only considered receivers below 0.8 m in a room with a ceiling height of 2.7 m hence only containing 30% of the room. In addition, the effect of multipath propagation was not considered in the study as well as most of the study in the literature.

Therefore, this chapter considers 2-D and 3-D VLP using a realistic channel model that includes multipath reflections. An optimised two layers ANN is designed for positioning. The same approach is then adapted to dark VLP, with CMD used as a benchmark as it provides high performance without extra hardware or power requirement. All approaches presented in this chapter are also critically evaluated against solutions presented in the literature.

4.3 Indoor VLP System Model

For indoor application, a typical indoor room with M (where $M > 1$) LED luminaires and $N \geq 1$ PD based receiver is considered as shown in Figure 3.2. The transmitters transmit FDM analog signals encoded with the unique position information as outlined in section 2.4. The VLP in this study is based on RSS, which requires the estimation of the received power from the various transmitters. The received power $P_{r,i}$ from the i_{th} transmitter to the j_{th} receiver is given by 3.9. The transmitters are located at $(1.25, 1.25)$ m, $(3.75, 1.25)$ m, $(1.25, 3.75)$ m and $(3.75, 1.25)$ m on the ceiling (see Figure 4.1) to provide uniform illumination [17]. The simulations are all carried out on a laptop computer (Intel(R) Core(TM) i7-6820HQ CPU of 2.70 GHz clock rate, 16 GB RAM that runs 64-bit Windows 10 operating system).

When two receivers are placed in the middle of the room $(2.5, 2.5)$ m with a receiver spacing of 0.02 m, the received power and SNR values are presented in Figure 4.2. This shows a uniform received power and SNR across the two receivers from the four transmitters. However, this is not the case in all parts of the room as the distance between the transmitters and receivers changes. Figure 4.3 shows the received power distribution across the room with a peak value of 2 dB at the centre of the room and as low as -2 dB at the edges. These calculated received power values across the receiver(s) are fed into the NN as shown in the following section. This allows the ANN to exploit the differences in received power, compared to the expected received power in ideal conditions, to identify the location of the receivers. Note that the room is assumed to be empty without furniture.

4.4 ANN Design for Indoor Positioning

This section describes the proposed supervised feed-forward back propagation MLP ANN for 3-D localisation, as shown in Figure 4.4. This illustrates that the transmitted signal from i LEDs through the free space channel is received by j PDs. The study

Figure 4.1: *2-D View of Tx and Rx*

Figure 4.2: *Transmitter plot a) received power and b) SNR*

assumes that each transmitter transmits TDM or FDM as outlined in section 2.4. This is crucial to enable the receiver to distinguish the signals from each transmitter. The received signal from the transmitters (in this case, four transmitters) at various receivers given by 3.12 are first de-multiplexed and then fed to an ANN.

Figure 4.3: *Received power across the room*

4.4.1 ANN setup and tuning

This section describes the determination of the most appropriate network structure as well as the selection of hyper-parameters (ANN parameters) for the proposed supervised feed-forward back propagation MLP ANN for 3-D localisation. MLP-ANN with an input layer, a range of hidden layer(s) and an output layer is considered. The Levenberg-Marquardt algorithm is adopted to determine the weights of the network. The number of neurons in the input layer is equal to $M \times N$. The number of neurons in the hidden layer is varied from 8 to 40 (i.e. $5M \times N$). A maximum of $5M \times N$ nodes are considered to avoid the chances of over-fitting. The estimated RMS error for the various networks investigated is then calculated to evaluate the most appropriate network. The output layer has three neurons corresponding to the three coordinates to be estimated. A total of $60,025$ random 3-D positions within the room are sampled, 1500 randomly selected points are chosen for tuning the ANN with 70% of these points for training, 15% used for validation and 15% for testing.

The following subsection describes the determination of appropriate hyper-parameters

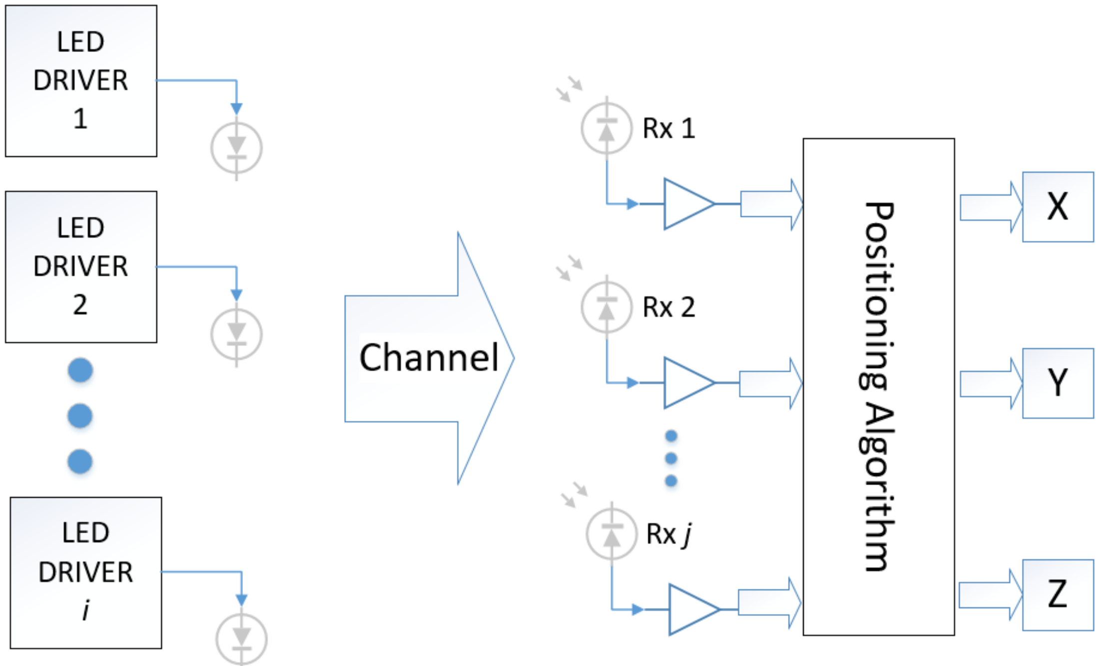

Figure 4.4: *Schematic of proposed VLP using ANN.*

to improve the network performance.

Hidden layers and nodes

By starting with a single hidden layer and $N = 2$ receivers, the number of layers and nodes are increased by a factor of one. Each layer is set to have an equal amount of neurons, as seen in Table 4.1. It is seen from the table that the ANN performs better with an increase in the number of nodes using a single hidden layer. However, when multiple layers are used, this behaviour changes. From 2 to 5 hidden layers, the best

Table 4.1: *RMS error (m) based on nodes and hidden layers*

RMS error (m)						
Number of hidden layers/Nodes	8	16	24	32	40	Time (s)
1	0.4219	0.1741	0.1128	0.0858	**0.0831**	1.7
2	0.1292	**0.0632**	0.0680	0.0740	0.0814	**1.1**
3	0.0968	**0.0657**	0.0675	0.0891	0.0775	3.9
4	0.0858	**0.0652**	0.0694	0.0824	0.0907	7.2
5	0.0757	**0.0651**	0.0756	0.0912	0.1022	11.7

performance is achieved at 16 nodes ($2M \times N$) in the hidden layer. The performance of the system deteriorates for nodes greater than 16 due to over-fitting. The best performance obtained when 2 hidden layers are used. A computational time analysis demonstrated that the shortest computational time was 1.1s for a network comprising 2 layers with 16 nodes. Hence, such a network was selected for VLP.

Activation function

Different combinations of activation functions are investigated to determine their impact on the overall performance. It was found that the log-sigmoid transfer function in both hidden layers yielded the best result. However, the difference in performance between the combinations is not significant (i.e. $< 5\%$).

Table 4.2: *RMS error at different activation function combination*

RMS error (m)		
	Log-sig	Tan-sig
Log-sig	0.0651	0.0678
Tan-sig	0.0663	0.0654

ANN performance optimisation

The performance of the proposed ANN is analysed with respect to MSE over 100 epochs as shown in Figure 4.5. The ANN was only able to achieve an MSE of 10^{-3} over 100 epochs. A drop in MSE is noticed from $1 - 70$ epochs. This performance then slightly improves until 100 epochs are reached. Hence, 100 epochs were selected as a good compromise between simulation time (0.8s), training accuracy and risk of over-fitting.

The impact of the number of training points is investigated. The RMS error of the VLP system is analysed when the ANN is trained using points ranging from 1 to 1500 with a step size of 50. As seen in Figure 4.6, the accuracy of the system visibly improves from 1 to 250 points. Thereafter, the performance does not significantly improve, with the percentage difference being $< 5\%$ from 500 to 1500.

Hence, a network with eight input nodes ($M \times N$), two hidden layers with sixteen nodes ($2(M \times N)$) in each hidden layer and log-sigmoid transfer function, and three nodes in the output layer is used for indoor VLP. Having identified the most appropriate tuning for the ANN hyper-parameter, the next section focuses on the impact of the VLP system parameters.

Figure 4.5: *MSE of ANN training against the number of training epochs.*

4.5 System optimisation

This section details the VLP parameters optimisation process that was used to set up the proposed positioning system in a typical home/office/industrial environment. This ranges from the number of receivers (receiver diversity), receiver separation and receiver field of view.

4.5.1 Receiver diversity

A CDF analysis for 3-D VLP using the proposed ANN is performed to determine the impact of receiver diversity. Diversity orders of 1 to 4 for the LOS link are considered. The receivers are located in a rectangular grid with a separation of 0.02 m. As demonstrated in Figure 4.7, there is a significant improvement in VLP using receiver diversity. For example, the RMS error using a single receiver is 0.037 m and 0.57 m at 0.95 CDF for 2-D and 3-D, respectively. This value reduces to less than 0.033 m and 0.28 m for 2-D and 3-D, respectively, when two or more receivers are used. It is noted

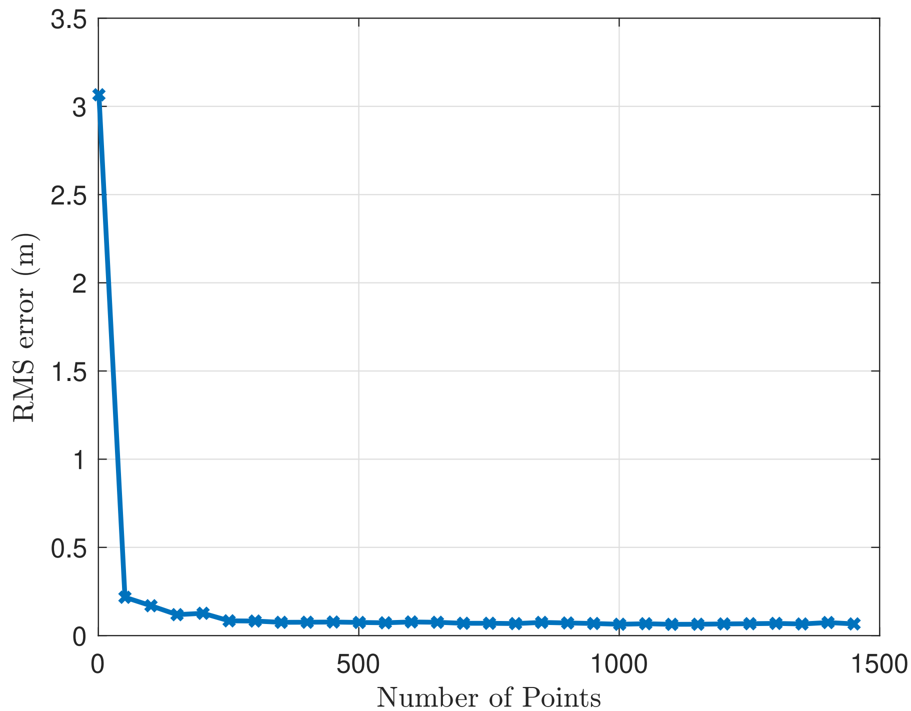

Figure 4.6: *ANN training performance with respect to number of points used for training.*

that increasing the number of receivers beyond two does not improve the performance significantly. For example, the RMS error values at 0.95 CDF (and average RMS errors) are 0.22(0.0124) m, 0.022(0.0122) m and 0.21(0.0136) m for diversity order of $2, 3$ and 4, respectively. There is a marginal error improvement when the number of receivers is increased from N=1 to N=2. The performance of the system improves with an increase in the number of receivers, however, at the cost of longer training time and ANN size. Hence, only two receivers are considered in the rest of the studies as this provides the best trade-off between complexity, computational requirements and system performance. Note that from 3.47 and Figure 4.8 it is that the complexity of the neural network increases linearly with the number of receivers. This increases the input vector, which in turn increases the number of weights in the hidden layers, respectively. Hence, it is deduced that the more the number of receiver, the more computationally complex the NN becomes, assuming the number of transmitters is kept constant.

4.5.2 Receiver separation

In this section, the separation between the PDs is investigated as it plays a vital role in VLP (i.e. the distance between two receivers can also affect the positioning

Figure 4.7: *RMS error versus the CDF for 3-D VLP with diversity order of $N = [1, 4]$ receivers for LOS link.*

accuracy). Both functionality and practicality of the system are considered. Hence, the separation between the receiver elements for the diversity order of two is optimised. Due to the size of the PD, a minimum distance of 0.02 m is considered. A maximum receiver spacing of 0.2 m is considered to maintain a safe PD separation that can be applied on mobile phones and autonomous drones. Figure 4.9 shows the positioning RMS error against the CDF for the various receiver separations. For example, at 0.95 CDF, the 3-D position accuracy improves from 0.11 m to 0.10 m when the receiver separation is increased from 0.02 m to 0.05 m, respectively. Increasing the receiver separation beyond 0.05 m provides some improvements. This illustrates that increasing the receiver separation improves the accuracy of the model. The average RMS errors for the receiver separation of 0.02m, 0.05 m, 0.1 m and 0.2 m are 0.012 m, 0.012 m, 0.011 m and 0.01 m, respectively. The error is seen to reduce with respect to increasing the receiver separation because the receivers take advantage of a very low probability of simultaneous dropouts with larger distances between them. Hence, in the following discussion, only the diversity receiver with a separation of 0.2 m is considered.

Figure 4.8: *Computational complexity as a function of receiver.*

4.5.3 Receiver FOV

The performance of 3-D VLP also depends on the FOV of the receiver. Determining the optimum FOV helps to ensure that the position of the receiver will be determined effectively to minimise the occurrence of dead-zone [110]. Figure 4.10 shows the CDF of 3-D VLP against the receiver FOV of 40° to 90°. To differentiate the performance improvement due to FOV from signal strength gain (i.e an increase in SNR), the optical gain at all the FOVs are considered unity. Note that the optical gain and FOV are related and the maximum gain for a given FOV is governed by Etendue [111]. Figure 4.10 shows that increasing the receivers FOV from 40° to 60° offers a significant performance improvement. However, FOVs beyond 60° degrade the performance. Though increasing the FOV reduces the dead-zone area in the room, the receiver is prone to receiving higher noise, thus reducing the SNR and performance of the system (see section 4.9 on the effect of SNR in VLP). Hence, in the rest of the study, a receiver FOV of 60° is selected as this provides near the optimum performance.

Figure 4.9: *RMS error versus the CDF for 3-D VLP with diversity order of two and different receiver separation distance.*

4.6 3-D VLP using ANN

The performance of the proposed 3-D VLP system using receiver diversity is evaluated using the parameters identified as being the most suitable. This section investigates the performance of the proposed ANN structure with and without the nLOS link in VLP.

4.6.1 Positioning using LOS link

Using the optimum parameters obtained for the 3-D VLP ANN, the performance of 3-D VLP using receiver diversity and ANN is simulated considering the LOS link and results are shown in Figure 4.11. Figure 4.11(a) shows the positioning errors in x, y and z-axis separately. It can be observed that each axis contributes almost equally to the overall error. Figure 4.11(b) shows the CDF of the estimation error at various height ranges, separated into the region of $[0, 1]$ m, $[1, 2]$ m and $[2, 2.5]$ m. Below a 2 m height, the average errors are found to be of similar magnitudes, equal to 0.0119

Figure 4.10: *CDF of 3D VLP as a function of receiver FOV.*

m and 0.0091 m for $[0, 1]$ m and $[1, 2]$ m, respectively. However, the position error in the height range of 2 m to 2.5 m is higher than the height of less than 2 m with an average error of 0.0198 m. Figure 4.11 (c) to (e) shows the average RMS error distributions across the room over the height of $[0, 1]$m, $[1, 2]$m and $[2, 2.5]$ m. There is an interesting pattern found in the error distribution. The highest position estimation error occurs across the diagonal where the signal strength from two transmitters to the receivers are identical. There is a higher estimation error at the edge of the room, and the highest error occurs at the corner of the room. Throughout the room, the estimation error is higher for heights above 2 m than it is for height below 2 m. At the height of 2 m, due to the limited divergence angle of the LEDs and limited FOV of the receiver, the received signal strength from one or more LEDs is very weak, leading to higher estimation error. To reduce the estimation error above this height, the number of transmitters needs to be increased.

4.6.2 Positioning using LOS and nLOS link

As mentioned in the previous section, the multipath propagation also affects the position estimation especially close to the wall where the reflected signal strength is at

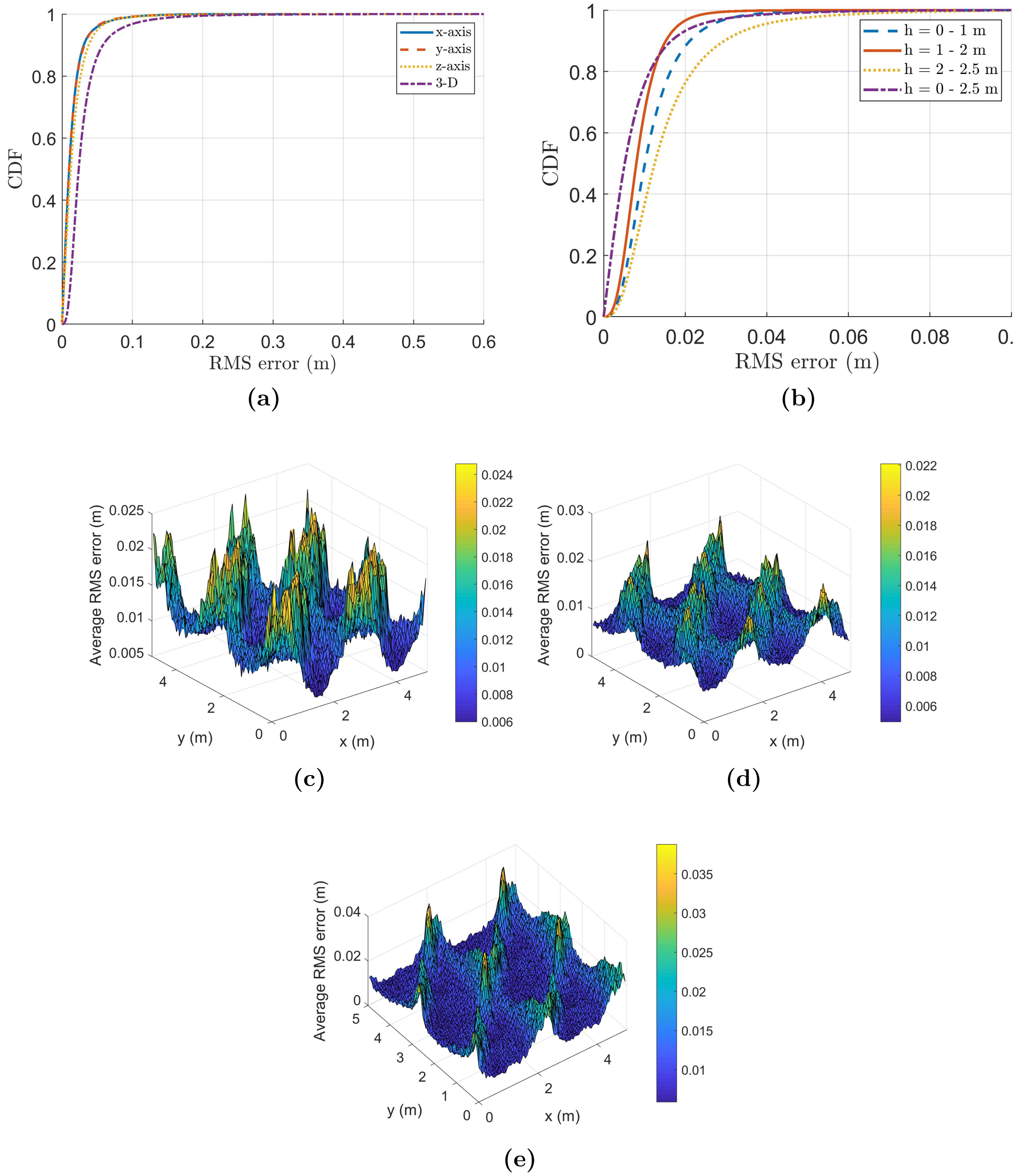

Figure 4.11: *CDF versus RMS error for 3-D VLP using receiver diversity for a LOS link: (a) error across the three different axes, (b) error across various height (c) average RMS distribution across the room averaged over the height of 0 m to 1 m (d) average RMS distribution across the room averaged over the height of 1 m to 2 m and (e) average RMS distribution across the room averaged over the height of 2 m to 2.5 m*

the highest. The performance of receiver diversity in VLP is evaluated considering a) LOS path only and b) LOS and nLOS propagation path for one and two receivers with the results presented in Figure 4.12. Figure 4.12 clearly shows that multipath

RMS error (m)

Figure 4.12: *CDF of 3D LOS vs non-LOS*

propagation reduces the accuracy in the position estimation for a single receiver. The RMS error value at CDF of 0.95 increases from 0.037 m for a LOS link to 0.094 m for a nLOS, using a single receiver. However, diversity receiver significantly improves the performance for both LOS and nLOS links with an RMS error of 0.0198 m and 0.021 m, respectively. Therefore, the diversity receiver scheme reduces the effect of NLOS by 77.7%.

The RMS error is sampled at 2500 random locations in the room and is analysed using a histogram, as shown in Figure 4.13. The error pattern follows a gamma distribution. It is seen that the RMS error with the most occurrence (461) is 0.015 m. All the RMS error instances fall below 0.08 m. A CI analysis is done to determine the upper bounds of the RMS error at 95% CI in a 3-D environment. This analysis is done over 2500 random locations with 100 different data set collected. Given n is 100 and w is 95%, the CI plot is shown in Figure 4.22. It can be seen that the estimated value falls under 0.07 m and 0.0003 m. Few points on the boundaries are seen to go beyond 0.1 m, with all points below 0.15 m. A combined standard deviation of 0.0072 m is

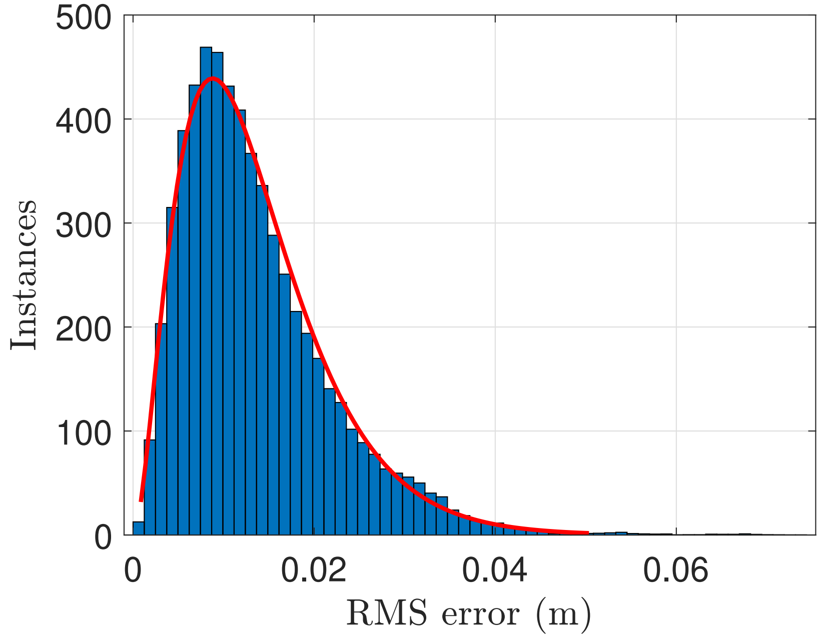

Figure 4.13: *Histogram of RMS error across the room in 3-D VLP.*

noted over the hundred data sets. This shows that the results in both Figure 4.13 and Figure 4.14 follow the same pattern.

4.7 2-D VLP using ANN

In this section, the performance of the proposed system in a 2-D environment is discussed.

The CDF of the RMS error for 2D VLP considering the LOS and non-LOS link using receiver diversity and ANN and receiver diversity is shown in Figure 4.15(a). There is a reduction in performance between the LOS and nLOS link for a single receiver with RMS error values of 0.033 m and 0.066 m, respectively at the CDF of 0.95. The average errors for LOS and nLOS links with two receivers are 0.0103 m and 0.0133 m, respectively. This has a respective standard deviation of 0.0066 m and 0.0085 m. The RMS error distributions in Figure 4.15(b) and (c) shows that receiver diversity reduces error close to the walls yielding to a lower average and RMS errors.

4.8 Comparative Study

A comparative study of the proposed technique is performed with other states of the art 3-D-VLP techniques. The findings are summarised in Table 4.3. Note that some of the work in the literature considered small room dimensions (e.g. [108], [58]), which

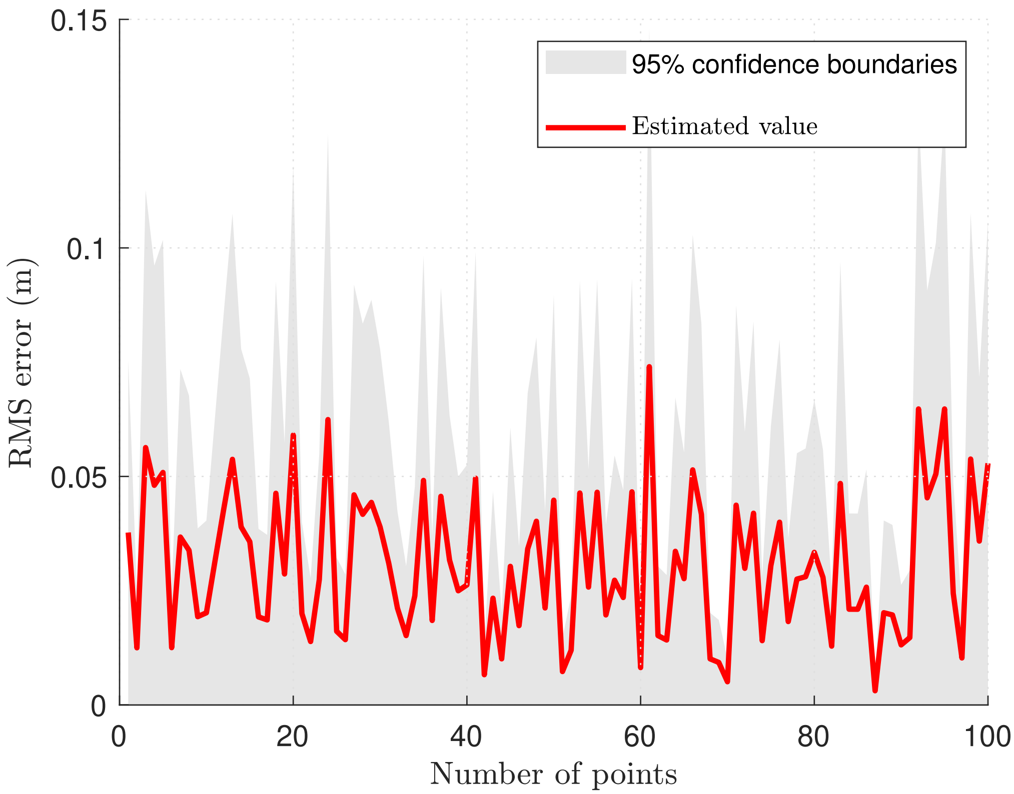

Figure 4.14: *CI analysis over 100 positions across the room in 3-D VLP.*

tends to improve the accuracy. The best performance is achieved in [57]. However, such a solution may be challenging to deploy as it requires a large number of transmitters (16) and receivers (361). Most of the existing work does not include the nLOS link. However, as reported in [88], the inclusion of nLOS increases the RMS error up to 0.06843 m. Therefore, whilst the work in [112] yielded an average RMS error of 0.01 m, including nLOS link and a larger room volume would likely increase the stated error. By comparison, simulating the system using the identical condition to that presented in [112], results in an average RMS error of 0.007 m, compared to 0.01 m in [112]. Based on these results, the proposed solution is practical and offers the best 3-D positioning results among the algorithms studied whilst accounting for LOS and nLOS.

Having demonstrated the benefits of ANN-based VLP, the following section applies the approach to dark VLP where the LED lights appear to be 'OFF' to the human eye [114, 115].

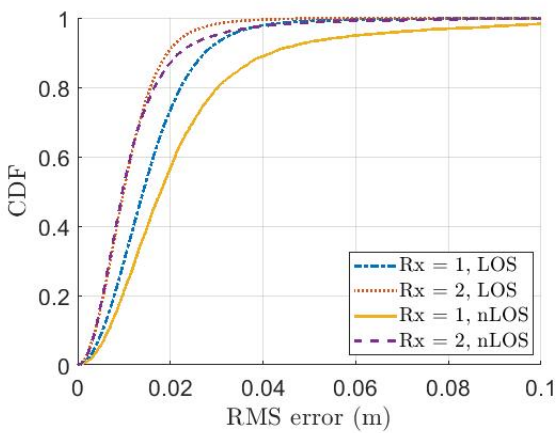

(a)

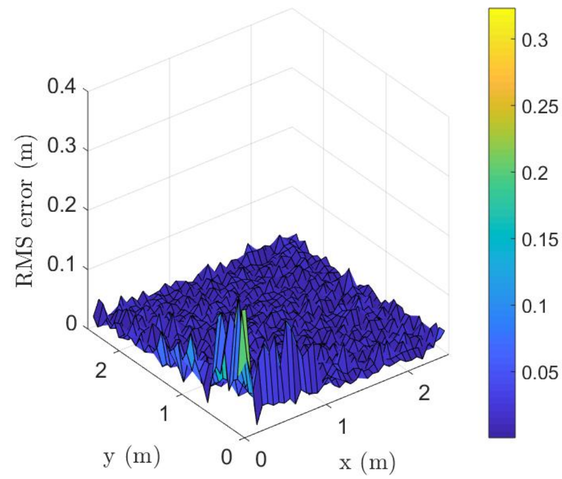

(b)

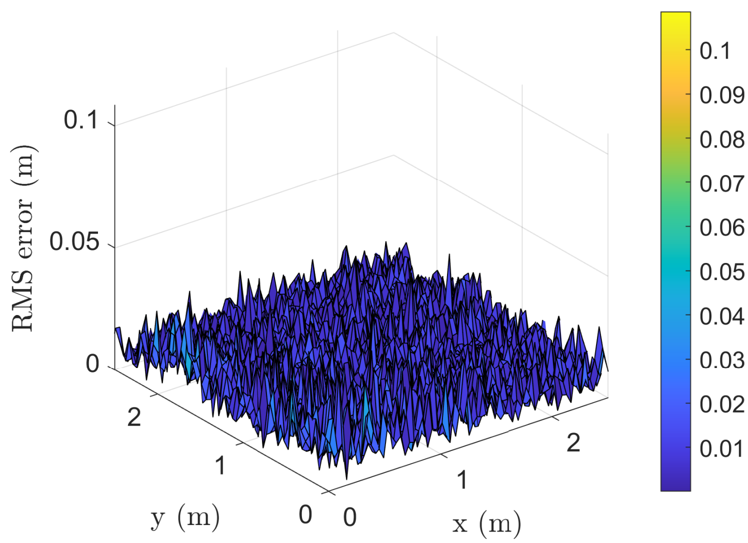

(c)

Figure 4.15: *CDF versus RMS error for 2D VLP using ANN and receiver diversity: a) CDF of RMS error for LOS and non-LOS link with 1 and 2 receivers. b) RMS error distribution for an nLOS link in a quarter of the room with 1 receiver and c) RMS error distribution for the nLOS link in a quarter of the room with 2 receivers.*

Table 4.3: *Comparative study of the proposed system with published work.*

Paper	Method	Channel model	Transmitter	Receiver	Room dimension(m)	RMS error (m)
[57]	Three ANN	LOS	4×4	19×19	$4 \times 4 \times 3$	0.0004
[105]	AOA	LOS	4	1	$5 \times 5 \times 2$	0.1
[108]	Fingerprinting	LOS	4	1	$2 \times 2 \times 5$	0.0445
[88]	Geometrical relationship	LOS+nLOS	4	1	$6 \times 6 \times 3$	0.06843
[54]	Genetic algorithm	LOS	4	1	$3 \times 3 \times 4$	0.021
[58]	2-layer ANN	LOS	4	1	$0.9 \times 1 \times 0.4$	0.009
[113]	Trilateration	LOS	4	1	$5 \times 5 \times 5$	0.091
[112]	Differential evolution algorithm	LOS	4	1	$4 \times 4 \times 3$	0.01
This work	ANN with receiver diversity	LOS+nLOS	4	2	$5 \times 5 \times 5$	0.021

4.9 Dark VLP

In dark VLC or Darklight, the communication data rate is encoded into ultra-short signals imperceptible by human eyes. Darklight is mostly applicable where natural light illuminates the room, thus requiring no additional illumination during the day or late at night. It has been shown in [114, 115] that at duty cycle D of 6.25%, 92% of the participants (aged 22 to 60) perceived the LED to be 'OFF' under indirect viewing conditions. Under direct viewing conditions, the value of D drops to 0.0071% with 80% of the participants perceiving it to be 'OFF'. This thesis will therefore consider these two duty cycles as the best and worst-case scenarios. The application of Darklight is extended in [84] for positioning. The study proposed a TDOA approach to VLP, thereby locating devices in a 2-D environment. In a room of $6 \times 6 \times 3$ m^3, the model yielded an RMS error of 5 cm. The method used in the aforementioned study requires perfect synchronisation between the transmitters, hence making it difficult in a practical environment [18]. Furthermore, the effect of nLOS is ignored in the channel model.

This section describes the proposed dark RSS-based VLP, a positioning technique that allows localisation when the LEDs emit very low luminance, which practically appears as 'OFF' to human eyes. The use of RSS for positioning as compared to TDOA in the literature means the transmitters do not need to be synchronised.

In this study, a dark room with no ambient noise is assumed. No windows and furniture are also considered; hence any possible reflection originates from the walls. Each transmitter is assumed to transmit PWM signals to attain a really low transmitted power.

The respective PWM signals ($a(t)$) used in this section are presented in Figure 4.16 where Figure 4.16 (a) represents $D = 0.0071\%$ and Figure 4.16 (b) represents $D = 6.25\%$.

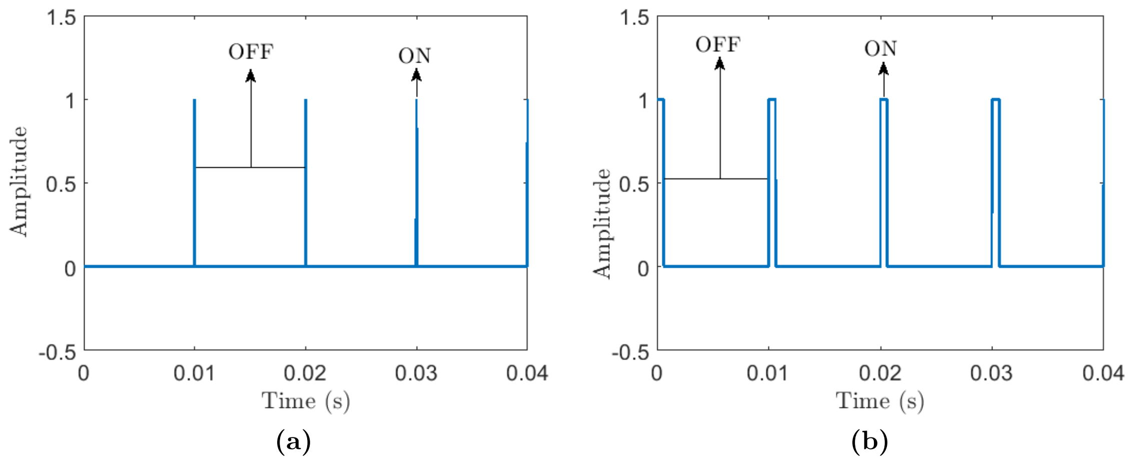

Figure 4.16: *PWM signal with varying duty cycle of a)* $D = 0.0071\%$ *and b)* $D = 6.25\%$.

First, CMD is used as a benchmark for dark RSS-based VLP. Thereafter, the optimised ANN model presented in Section 4.4.1 is adopted for dark VLP using the same system architecture.

4.9.1 2-D dark VLP

CMD

Assuming a fixed height of $h = 0$, VLP is studied. Figure 4.17 (a) shows the 2-D RMS error distribution across the room using receiver diversity at $D = 6.25\%$ using CMD.

The model yields an average RMS error of 0.0943 m. Due to low SNR values at $D = 0.007\%$, the CMD algorithm fails to yield any results. It has been found that for this algorithm to work, a minimum duty cycle of $D = 0.17$ is needed, resulting in an RMS error of 0.71 m. The corresponding RMS error distribution is shown in Figure 4.17 (b). To improve system performance and chances of attaining positioning at low SNRs, ANN is introduced.

ANN

The performance of the ANN model for 2-D positioning was first compared to the CMD algorithm for $D = 6.25\%$. Figure 4.18 shows the RMS error across the room for ANN-

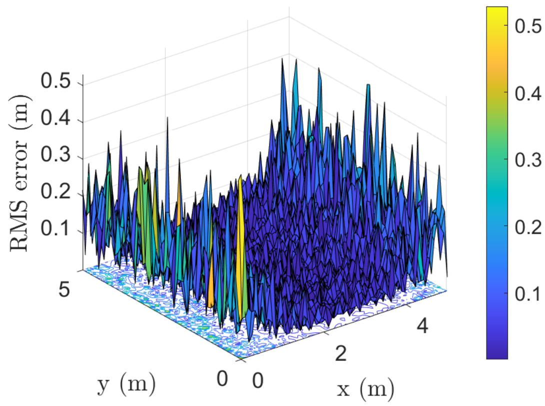

(a)

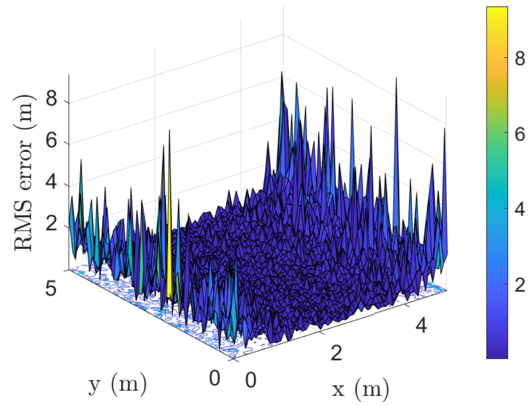

(b)

Figure 4.17: *2-D RMS error analysis across the room using CMD at a) $D = 6.25\%$ and b) $D = 0.17\%$.*

based dark VLP. The ANN provide improve VLP with an average RMS error of 0.02 m. Furthermore, positioning errors in the corners of the room were significantly reduced, hence demonstrating the effectiveness of ANN to reduce multipath propagation in VLP.

4.9.2 3-D dark VLP

Increasing the dimensions to 3-D reduces the performance of both CMD and ANN positioning as shown in Figure 4.19 (b). At a duty cycle $D = 0.0071\%$, the accuracy of the ANN model from 2-D to 3-D reduces to an average RMS error and RMS error at 0.95 CDF of 0.28 m and 0.57 m, respectively. At a duty cycle of 6.25%, the ANN model yielded an average RMS error and RMS error at 0.95 CDF of 0.06 m and 0.10 m, respectively. At a similar duty cycle of 6.25%, the CMD model yielded an average RMS error and RMS error at 0.95 CDF of 0.194m to 0.34 m, respectively. From these results, it is understood that the performance of the system increases at higher duty cycles. Note that there is a 69% increase in performance between CMD and ANN. This thus makes ANN more viable for dark VLP.

The effect of SNR on 3-D dark VLP is analysed to understand its relationship to duty cycle and performance. It can be seen in Figure 4.20 that increasing the SNR values reduces the RMS error. The system's accuracy improves until an SNR value of 35 dB is achieved. Thereafter, the gradient of the RMS error reduces with no significant increase per rising values of SNR with respect to D. The corresponding value of D at 35 dB is $D = 3\%$, which offers the best trade-off between duty cycle and performance. Hence at $D = 3\%$, the system yields an RMS error of 0.064 m in a 3-D environment. Figure 4.20 reveals relationship between duty cycle and SNR, and their impact on RMS error. The dotted line show the dark VLP range, which correspond to a duty cycle

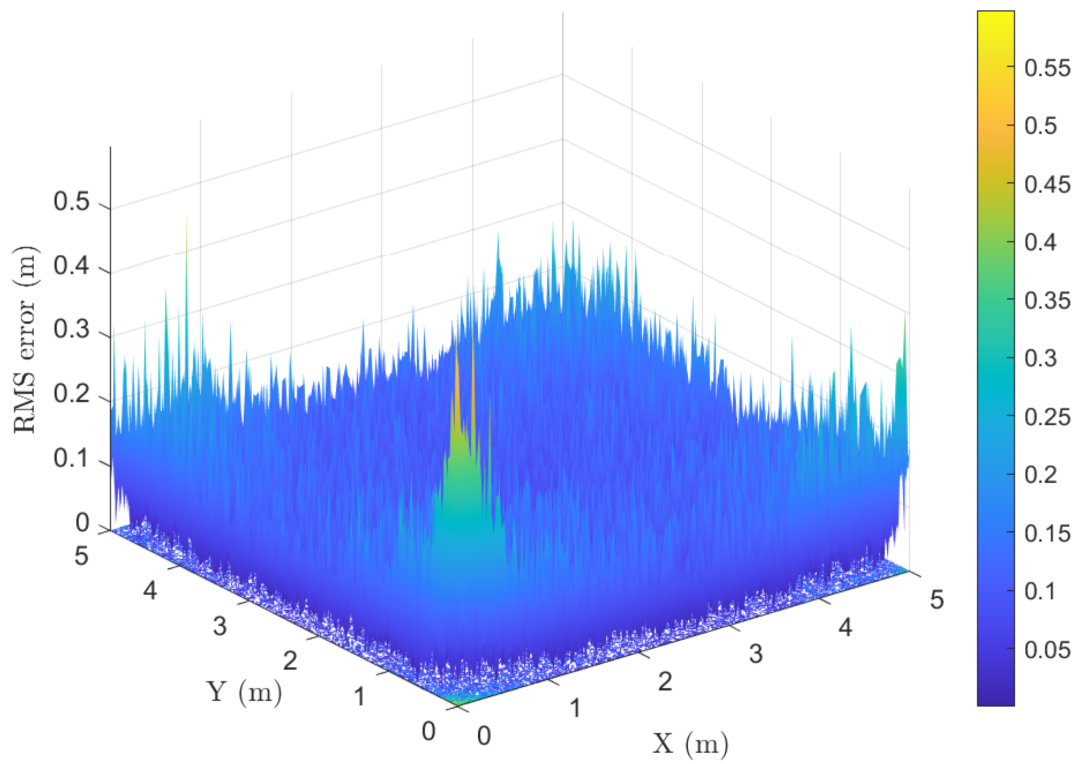

Figure 4.18: *2-D RMS error analysis across the room using ANN.*

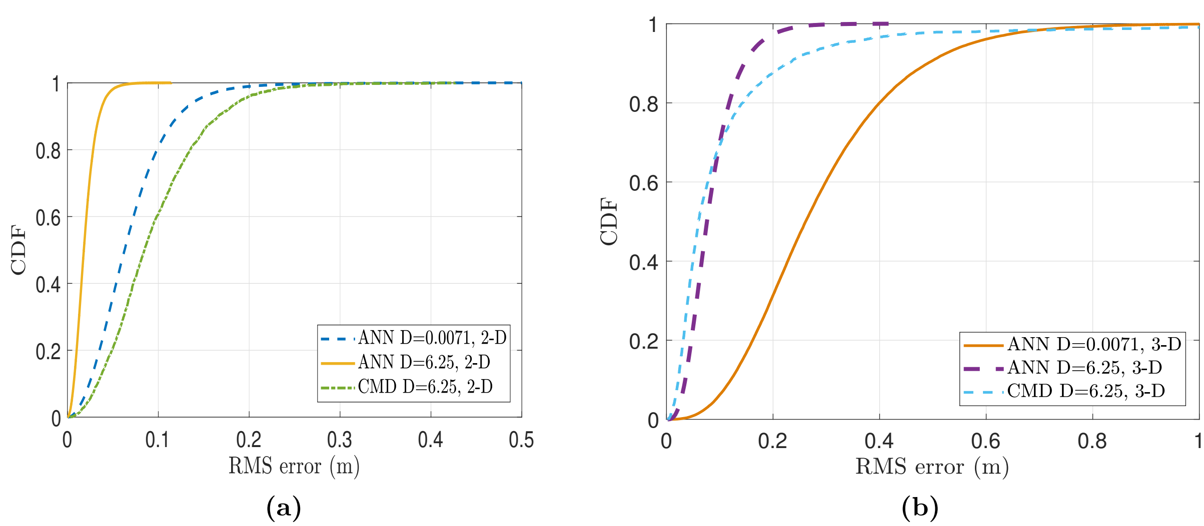

Figure 4.19: *CDF of VLP using CMD and ANN in a) 2-D and b) 3-D.*

between 0.0071% and 6.25%. Increasing the duty cycle increases the SNR from 9 dB to 41 dB and reduced the RMS error ranges from 0.1 m to 1.02 m.

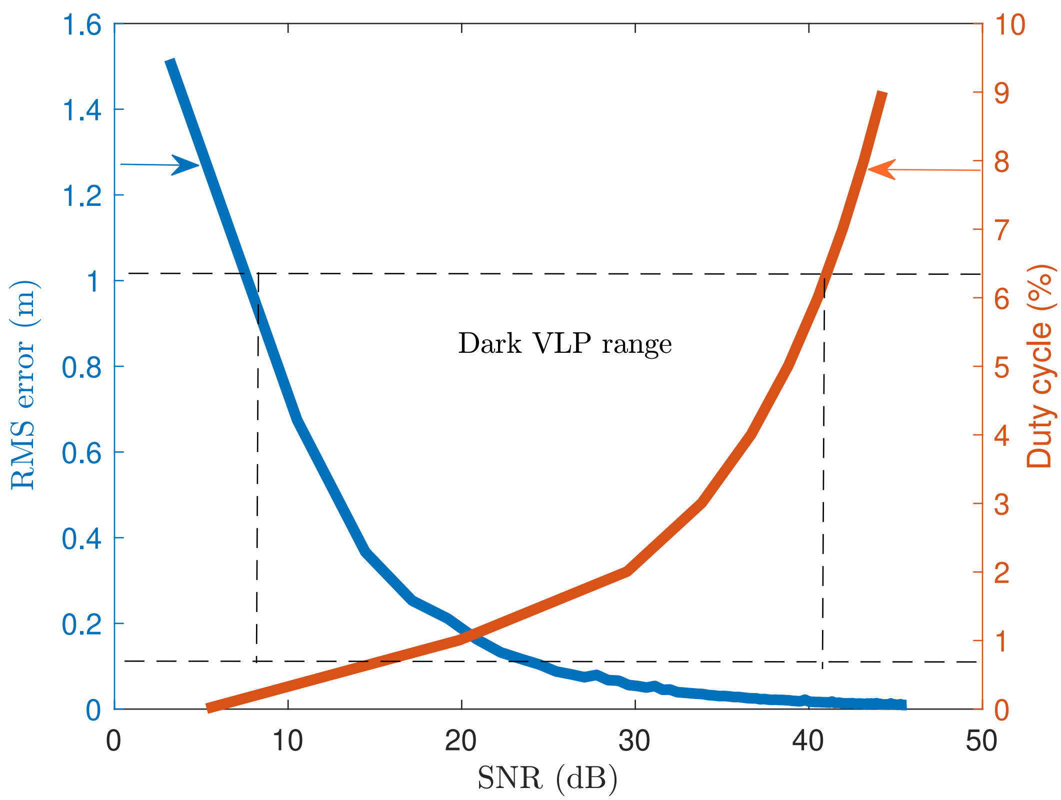

Figure 4.20: *Average SNR analysis at different duty cycle D.*

4.9.3 Analysis

Using the optimum simulation parameters, the RMS error sampled at 2500 random locations is analysed using a histogram, as shown in Figure 4.21. The error pattern follows a gamma distribution. It is seen that the RMS error with the most occurrence (278) is 0.03 m. Only in 24 instances, the RMS error is seen to go beyond 0.1m with a single occurrence at 0.14 m.

A CI analysis determines the upper bounds of the RMS error at 95% CI for $D = 3\%$. This analysis is done over 2500 random locations with 100 different data set collected. Figure 4.22 shows the CI plot for $n = 100$ and $w = 95\%$. It can be seen that the estimated value falls between 0.01 m and 0.08 m. Few points on the boundaries are seen to go beyond 0.1 m with a point above 0.15 m. A combined standard deviation of 0.0185 m is noted over the hundred data sets. This shows that the results in both Figure 4.21 and Figure 4.22 follow the same pattern even after 99 more simulations.

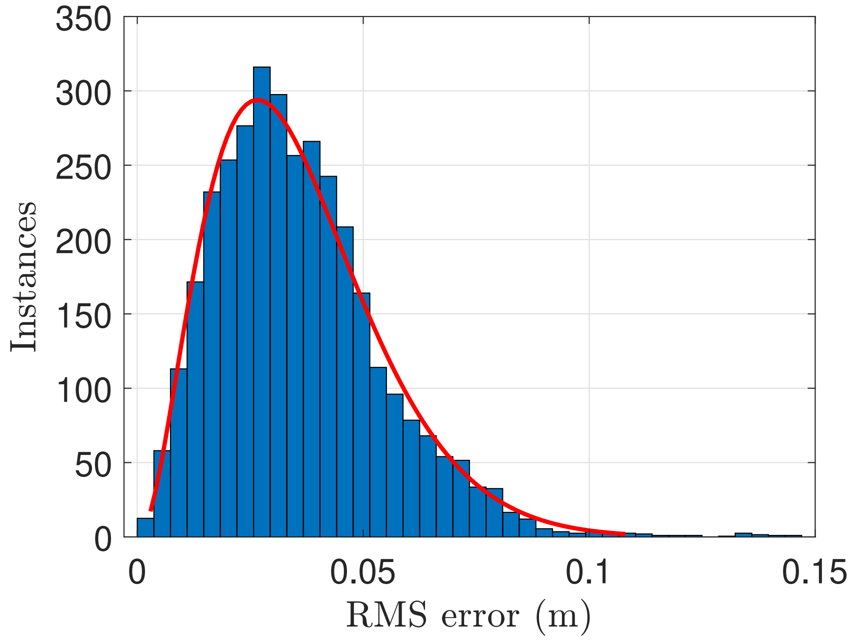

Figure 4.21: *Histogram of RMS error across the room in 3-D dark VLP.*

Finally, the RSS-based ANN model developed is compared to the TDOA model presented in [84] using the same room and simulation parameters with $D = 0.014$. The approach proposed in this thesis outperforms that in [84] by 52% with the RMS error reduced from 0.05 m to 0.024 m.

4.10 Summary

This chapter has introduced a realistic 3-D ANN-based VLP using receiver diversity for indoor applications. The channel model adopted considered the effect of not only LOS but also nLOS, which has been ignored in most of the literature to date despite being known to have an impact on VLP. By designing an ANN model to best fit the scenario, the ANN was trained using 1500 sampled RSS points across the room. To ensure reliable performance, the system architecture was optimised to determine the most appropriate combination between the number of receivers, the receivers' separation and the receivers' FOV. The model's performance was analysed using LOS only and compared to LOS and NLOS. Simulation results demonstrated that ignoring NLOS leads to a percentage increase of 87% compared to LOS in the case of a single receiver. This statistical analysis shows that the impact of nLOS is too significant to be ignored by researchers in VLP. However, the introduction of receiver diversity and optimisation of the system architecture has been shown to reduce the difference in performance to 5.8% between LOS and NLOS. A comparative study is conducted, which shows in a tabular manner that the proposed model in this work outperforms most in the

Figure 4.22: *CI analysis over 100 positions across the room in 3-D dark VLP.*

literature either by performance, structural complexity or both. Having demonstrated the benefits of the proposed ANN approach, the latter is applied to dark VLP in both 2-D and 3-D environments. This is achieved by employing PWM to dim the light. By dimming the lights at a really low duty cycle, the light appears to be off to the human eye. The PWM duty cycles used are 0.007% and 6.25. It is shown that the ANN outperforms CMD by at least 70% and is capable of achieving an RMS error of 0.28 m and 0.08 m, respectively.

In this chapter, it is verified that ANN can be used to actively determine the position of a receiver in a 3-D environment. However, certain positioning applications do not require users to actively participate in the positioning process. To cover all scenarios, consideration is given to passive VLP in the following chapter, where users do not need to participate in the positioning process.

Chapter 5

Passive Indoor Visible Light Positioning

5.1 Introduction

VLP for indoor application has been particularly interesting as it offers security and privacy benefits as the light emitted will be confined to a given room. Indoor VLP can be active or passive. In active localisation methods, a receiver is required in the target device. Using this method, accuracy in the range of cm-mm can be achieved depending on the size of the room. In passive positioning, the target has no tag or device [116]. Passive positioning has been proposed in [117, 118], where the researchers used passive infrared sensor (PIR) to detect the presence of a person in a room. Research has been conducted in the field of passive VLP for different applications such as intruder tracking [59], civilian monitoring or object detection [60–65] and track-pad and keyboard application [119].

As seen in Figure 5.1, the study of passive VLP in this thesis relies on the reflected light from the room. To model a passive VLP channel, reflection of the light from the walls, object and furniture's are required. Due to the complex nature of such channel model, researchers have proposed to place the receivers on the floor [59, 60], the walls [63] or the ceiling [65]. The latter uses the sum of the reflected rays, labelled as object impulse response (OIR), for positioning. To reduce the complexity of the channel model, only first-order reflection is considered. However, such assumption underestimates the positioning error by ignoring the impact of the higher (second) order reflection [55].

An adequate channel model needs to be developed to study passive VLP in indoor environments. Hence, in this chapter, a ray-tracing technique is adopted to model the indoor passive VLP channel. Similar to the positioning technique in chapter 4, the ANN will use the RSS information from the ray-trace for positioning.

The remainder of this chapter is organised as follows. Section 5.2 describes the proposed passive VLP channel model. Section 5.3 presents the ANN optimisation

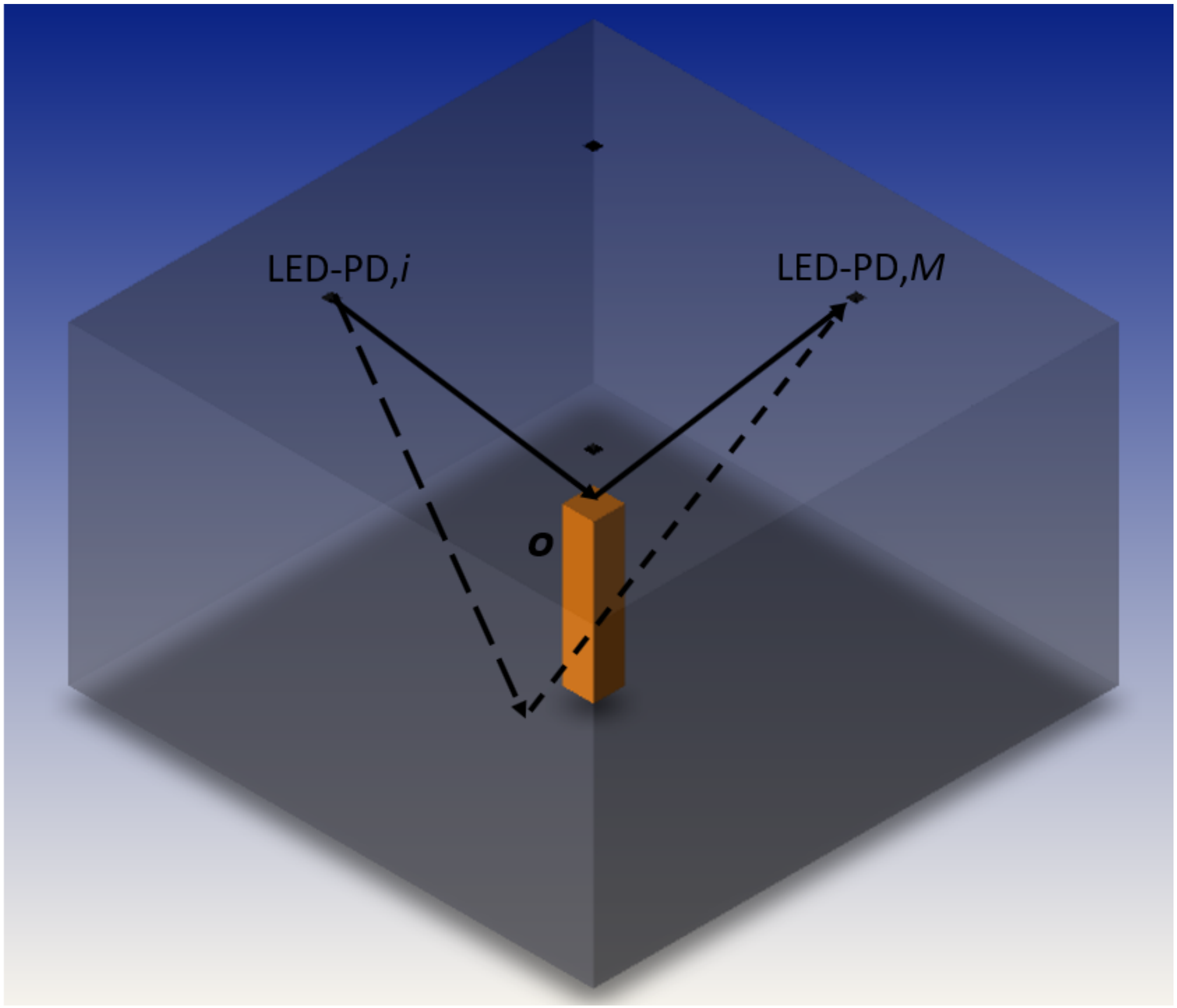

Figure 5.1: *Indoor passive VLP shaded model.*

process for passive VLP. Section 5.4 investigates the ANN performance and the effect of object size and reflectivity. Finally, a summary of the chapter is provided in section 5.5

5.2 Indoor Passive VLP System

This section describes the passive VLP parameters used in this study to establish a typical home or office positioning. The composition of the system is first defined for every element. The system consists of four elements, namely the room, transmitter, receiver and object.

Room

The room is a cuboid room with dimensions of 5 m×5 m×3 m, as seen in Figure 5.1. The inner body of the room is modelled as a reflector, which consists of four walls with reflection coefficient of $\rho_{wall} = 0.85$, one floor with reflection coefficient of $\rho_{floor} = 0.7$ and a ceiling.

Transmitter

The transmitters used in this research are regular LED bulbs that follow the Lambertian radiation pattern of a BXRE-50C3001-D-24 LED. Let M denote the number of transmitters. M LEDs are placed at the height of h from the ground vertically facing down, where h is the room's height (3 m). The transmitters are initially evenly distributed across the ceiling of the room. Each transmitter has b rays that follow the Lambertian emission order, where $b = 5 \times 10^6$ is considered for this study. The chosen value of b is close to the max number of rays the selected LED can emit with a transmitter power of 10 W. The number of reflection from each transmitter is limited to three as proposed in [120], thus considering up to 3rd order reflection.

Receiver

The receivers in this study are PD. Let N denote the number of receivers. N receivers are placed next to the transmitters (unless stated otherwise) on the ceiling. The distance between the transmitter and receiver is arbitrarily set at 2 cm. This is more realistic than the literature which assumes that the transmitters and receivers can have the same coordinate [65]. Note that, whilst the transmitter-receiver (transceiver)s are shown together in Figure 5.1, they can be arbitrarily distributed across the room to provide flexibility and reduce deployment cost. Moreover, where the receivers are placed on the wall, each receiver is placed at the height of 1.5 m. Their spatial distribution is made equal to the spatial distribution of the transmitters on the ceiling.

Object

The object considered in this study (adapted from [65]) is a cuboid with dimensions of 0.3 m ×0.3 m ×1.6 m placed in the room. The outer surface of the object is modelled as a reflector, which consist four sides with reflection coefficient of $\rho_{side} = 0.6$ and one top with reflection coefficient of $\rho_{top} = 0.5$.

A ray-tracing technique is adopted to examine the received power on the ceiling of the room as shown in Figure 5.2. To examine the received power pattern across the ceiling, a grid of 50×50 receivers are placed on the ceiling. It can be seen that the received power is higher at the position of the object. This is due to the object having a reflective surface and a height higher than the floor, thus reflecting a higher signal back to the PD. The received power is then fed into an ANN for training.

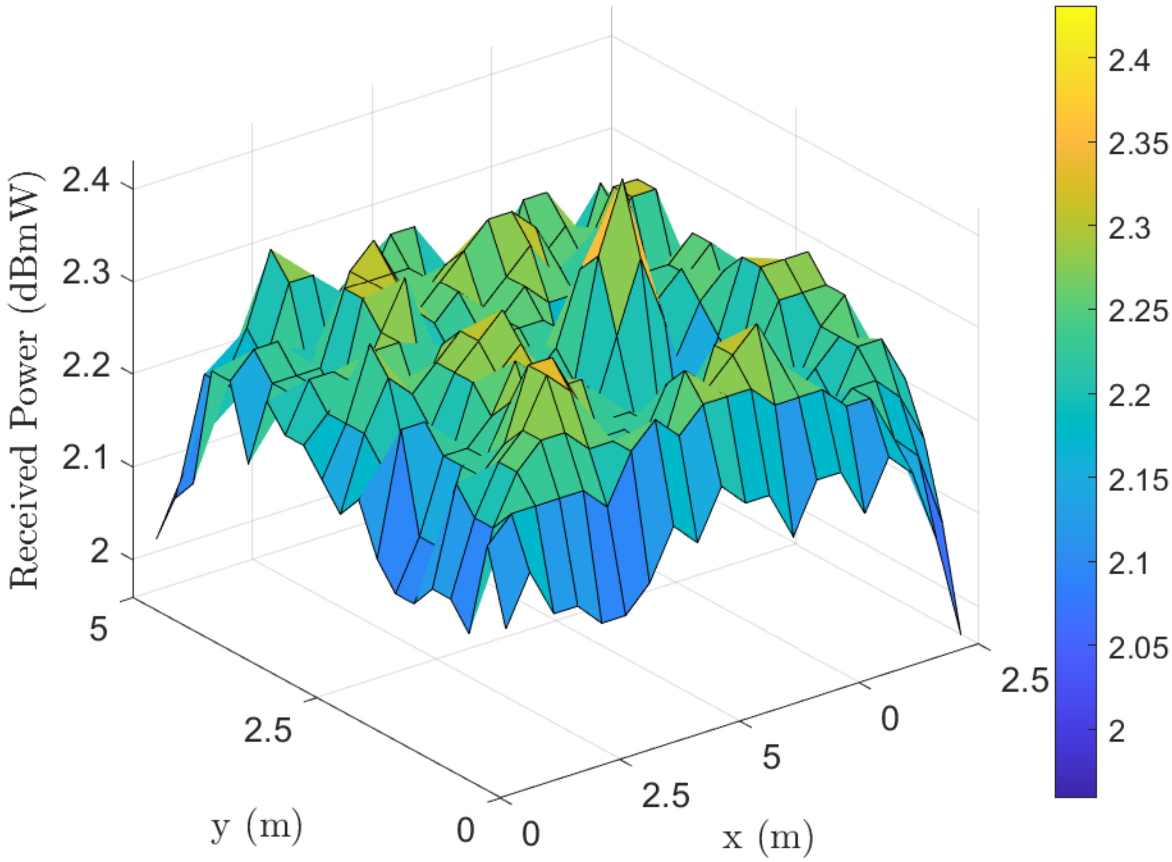

Figure 5.2: *Received power across the room with the object in the middle of the room.*

5.3 ANN design for Passive Positioning

This section describes the proposed supervised MLP ANN for passive localisation. The received signal from the receivers is fed into the ANN for training.

Though a similar MLP ANN architecture proposed in chapter 4 for active indoor positioning is considered, the structure is modified to fit this application best and yield the best performance. The number of neurons in the input layer equals $M \times N$. Similarly, the number of neurons in the hidden layers are made a multiple of $M \times N$ and are varied from $1 \times (M \times N)$ to $5 \times (M \times N)$. The network's output is set at 2 nodes, corresponding to the x and y coordinate of the object (O).

5.3.1 ANN Optimisation Process

This section describes the ANN parameter selection procedure for passive VLP. A total of 2500 random positions across the room are considered with 70% of the points for training, 15% for validation and 15% for testing. Bayesian regularisation is adopted due to the complex nature of the data. This algorithm requires more time when compared to Levernberg Marquardt but can result in good generalisation for difficult, small or noisy data sets. By starting with four transmitters and four receivers (similar setup in chapter 4) and with a single hidden layer, the RMS error and the computational time is monitored for the entire simulation, as shown in Table 5.1. It is observed that the best

Table 5.1: *RMS error* (m) *based on nodes and hidden layers*

RMS error (m)						
Number of hidden layers/Nodes	16	32	48	64	20	Time (s)
1	1.3861	1.3808	1.3818	1.3854	1.3979	94.1
2	0.8878	0.8701	0.7419	0.7451	0.7556	984.42
3	0.7911	0.7118	0.7410	0.7825	0.8444	2675.62
4	0.8137	0.7380	0.8206	1.1459	1.2720	7498.67
5	0.8018	0.7408	0.9074	1.1894	1.2778	9788.26

performing ANN is attained with $2(M \times N)$ or $3(M \times N) = 32$ nodes, irrespective of the number of hidden layers, with the best overall error obtained with 3 hidden layers and 32 nodes. Increasing the number of neurons beyond that decreases the performance of the ANN as well as increases training time and system complexity. The training and generalisability of the neural network is illustrated in Figure 5.3. The MSEs for training, validation and testing reduce in a similar manner until 40 epoch. However, whist validation keeps decreasing until epoch 98, the testing MSE remains almost constant. This shows that for a network containing 4 transmitters and 4 receivers, i.e. 16 inputs and 2 outputs 40 epochs is the minimum number of epochs required. In this work, this network was trained for 98 epoch, which provides the optimum results.

The outcome of this investigation was to adopt a network containing $3(M \times N)$ nodes for all other ANN MLP used for passive positioning and presented in the next section. Note that the number of epochs was increased for networks involving more transmitters and receivers to ensure good performance without over-training.

5.4 Passive VLP using ANN

This section analyses the performance of the proposed passive VLP system for a different number of transceivers and receivers. The transceiver design adopted is similar to that in [65]. However, this thesis investigates the impact of transceiver positions on the accuracy of passive VLP (see Table 5.2).

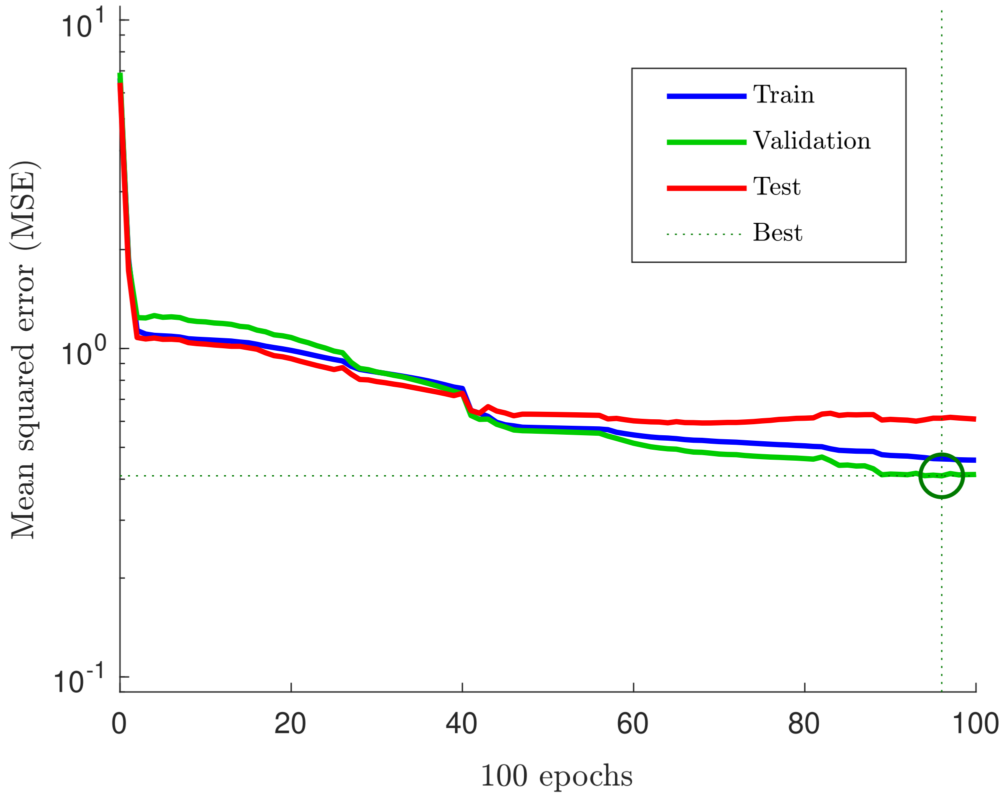

Figure 5.3: *ANN training performance for passive VLP over 102 epochs.*

Table 5.2: *Different transceiver scenarios in the room*

Case	Transmitter	Receiver	Receiver location
I	4	4	ceiling
II	4	4	wall
III	4	8	Wall + ceiling
IV	9	9	ceiling
V	9	12	wall
VI	9	21	wall + ceiling

The ANNs structures are designed and trained for each case from I to IV using the approach in section 5.3.1. Note that the same data containing 2500 data points were used for training. The accuracy of the trained ANN is then evaluated to detect 625 different object positions. The inputs used by the ANN are the received signal strength for each LED computed using ray tracing. Figure 5.4 (a) shows the RMS error distribution across the room. The model yielded an RMS error of 0.8191 m. A number of setups were investigated (Case I to VI) to improve the positioning accuracy of the system depending on the localisation of the receivers. Figure 5.4 (b) shows the

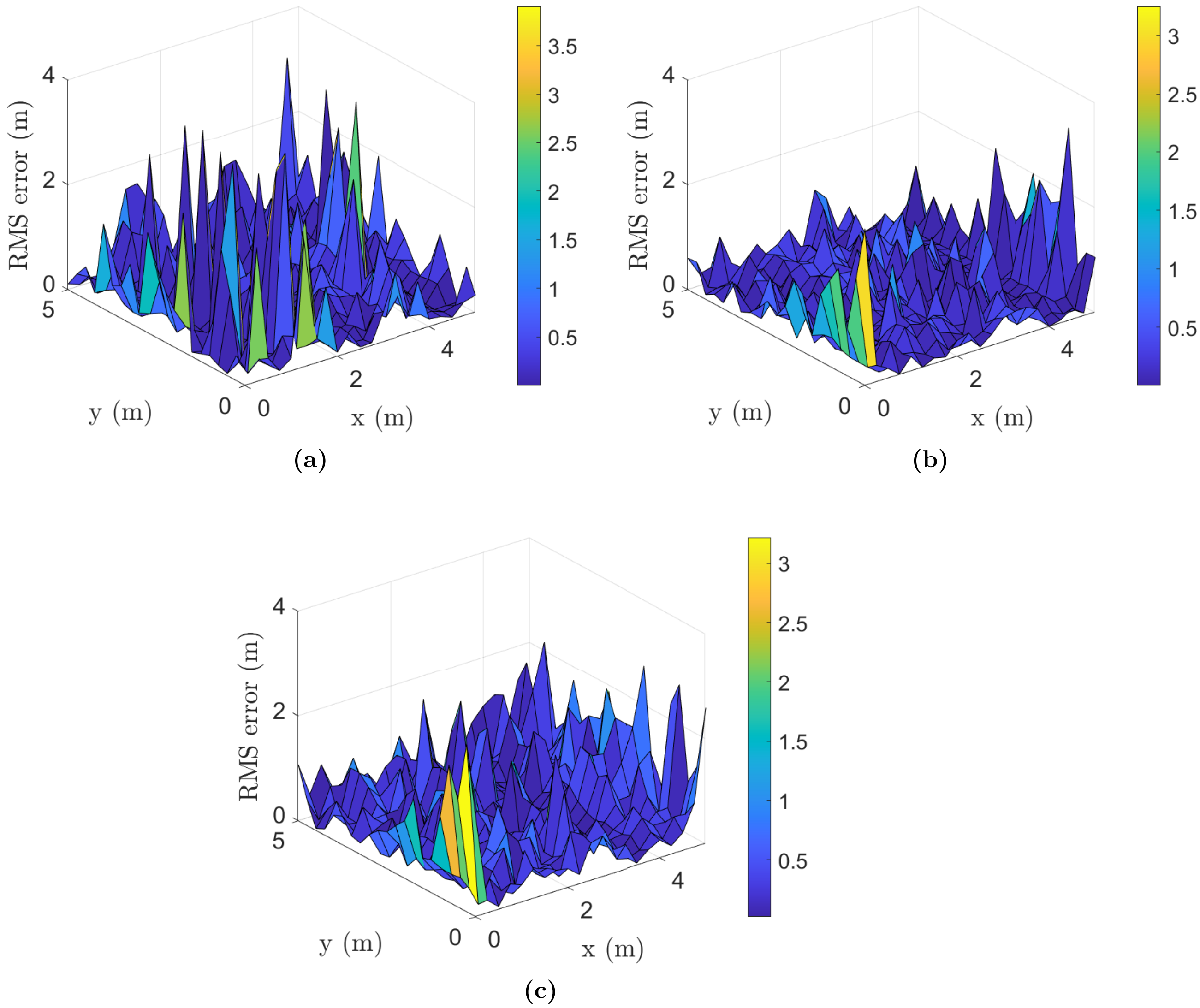

Figure 5.4: *RMS error for passive VLP using 4 transmitter when the receivers are located: a) on the ceiling b) on the wall and c) on the ceiling and wall.*

RMS error across the room when the receivers are placed on the wall. By changing the receiver position, the model yielded an RMS error of 0.6 m. Locating the transmitters on the ceiling and the walls (case III), with four transmitters on the wall and four on the ceiling, yielded an RMS error of 0.55 m. The respective RMS error distribution is shown in Figure 5.4 (c).

Changing the receiver position has only a slight impact on the overall accuracy. The next step was to change the number of transmitters in the room to see their impact on passive VLP. By considering the receivers on the ceiling and increasing the transceivers

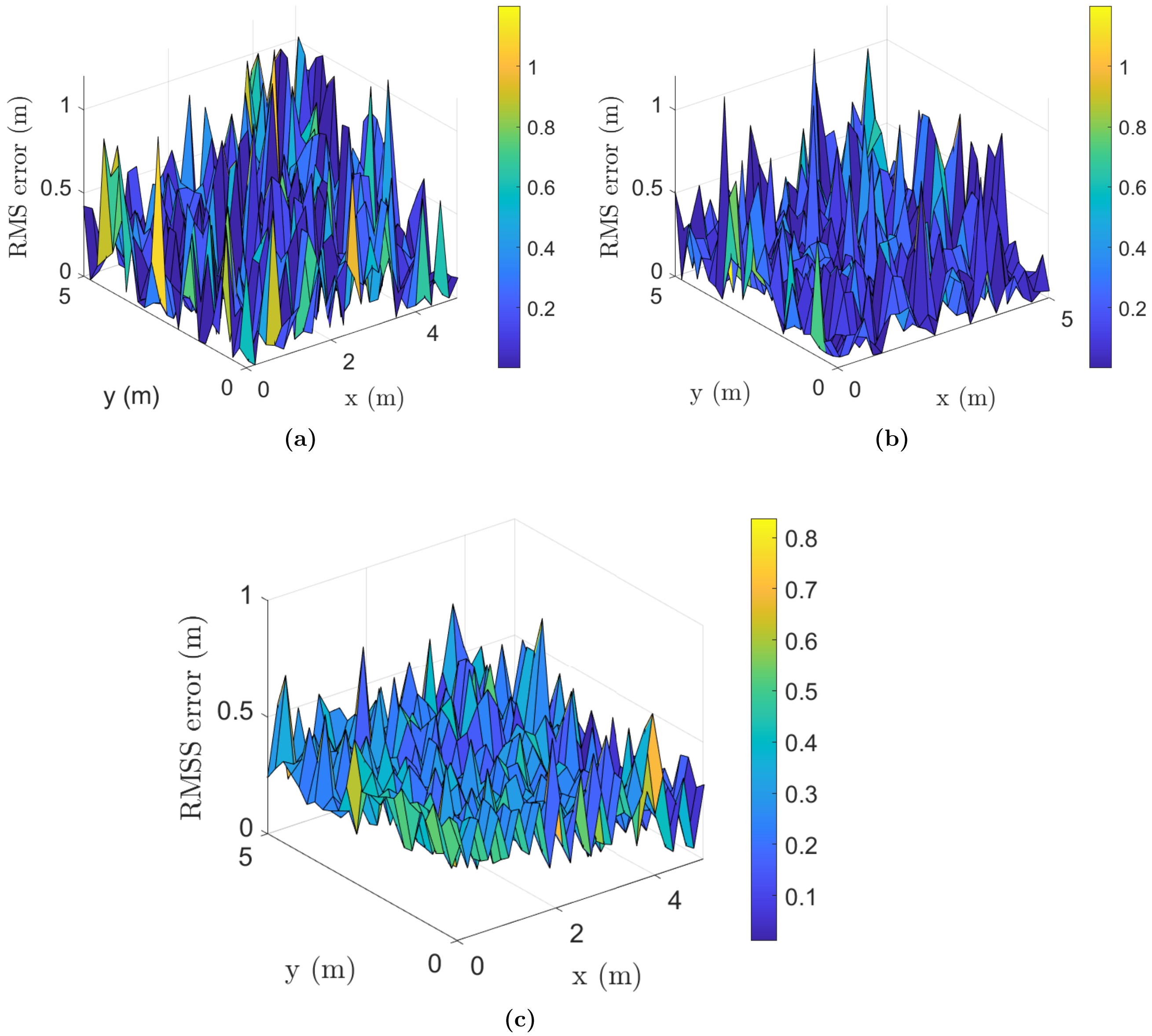

Figure 5.5: *RMS error for passive VLP using* 9 *transmitters when the receivers are located: a) on the ceiling, b) on the wall, and c) on the ceiling and wall.*

from 4 to 9 (case IV), the RMS error across the room reduces as seen in Figure 5.5 (a). With 9 transceivers, the model yielded an RMS error of 0.36 m.

Subsequently, the receiver position is changed from the ceiling to the wall as outlined in case V. The performance of the model is further improved with an RMS error of 0.27m with the RMS error distribution shown in Figure 5.5 (b). Finally, the receivers are located on the wall and the ceiling as outlined in case VI. Figure 5.5 (c) shows the

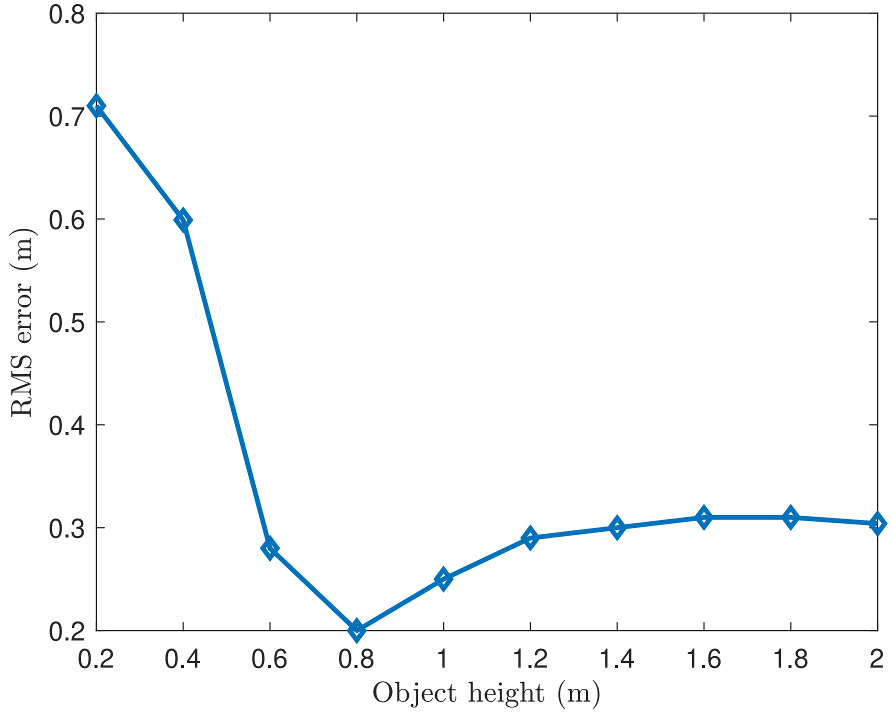

Figure 5.6: *RMS error at different object height.*

RMS error distribution across the room for this scenario. The model yielded a further accuracy improvement with an average RMS error of 0.23 m. It can therefore be concluded that the number of transmitters and receivers used is more important than the location of the receivers, even though both can improve the positioning accuracy.

5.4.1 Effect of Object Size

A favourable transmitter-receiver setup is achieved in the preceding section with 9 transmitters and 21 receivers (case VI) to locate an object of dimensions 0.3 m $\times$0.3 m $\times$1.6 m. In this section, the performance of the system is analysed by varying the object size. First, the height of the object is changed from 0.2 m to 2 m with a step size of 0.2 m whilst maintaining the same length and width, i.e. 0.3 m $\times$0.3 m, see Figure 5.6. The smaller the object, the larger the error. The optimal object height is 0.8 m with an RMS error of 0.2 m. However, good performance is achieved for object heights in the range 0.6 m to 2.0 m with an average RMS error of 0.3 m. This shows that even though the object's height directly affects the performance of the system, acceptable performance can be achieved as long as the object has a sufficient height, i.e. 0.6 m in this case.

Next, the object's length and width were changed with the height remaining constant (1.6m). Both dimensions are considered to have the same length. Therefore, the

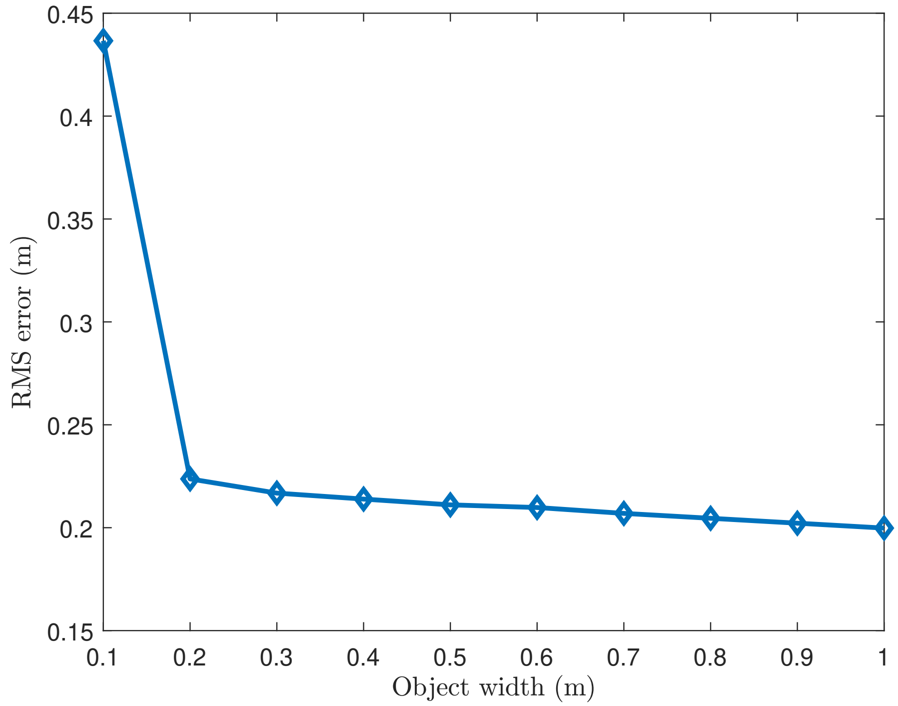

Figure 5.7: *RMS error at different object widths.*

length and width of the object are varied from 0.1 m to 1 m with a step size of 0.1 m, as shown in Figure 5.7.

It is found that good positioning accuracy could be achieved for object length and width superior to 0.2 m. More voluminous objects do not significantly improve the positioning accuracy, with RMS errors in the range of 0.2 m to 0.22 m. These results show that an object with a volume of $0.6 \times 0.2 \times 0.2$ m^3 reflects a suitable amount of light that the PD can detect. These good quality signals create good data that are easier to learn by the ANN. Smaller or shorter objects reflect fewer rays, thus resulting in a higher average RMS error.

Having analysed the effect of object size on the system's performance, the following subsection explores the effect a reflective surface has on VLP.

5.4.2 Effect of Object Reflectivity

The object's reflectivity is investigated to observe its effect on passive positioning. In this study, all the surfaces of the object are assumed to have the same reflection coefficient, i.e. $\rho_{side} = \rho_{side} = \rho_{all}$. The reflective coefficients investigated range from the object having little to no reflection at all ($\rho_{all} = 0$) to mirrors reflecting 100% of light ($\rho_{all} = 1$), with a third option where 50% of the light rays ($\rho_{all} = 0.5$) are reflected. Even without any reflection, it is still possible to detect an object position, but with

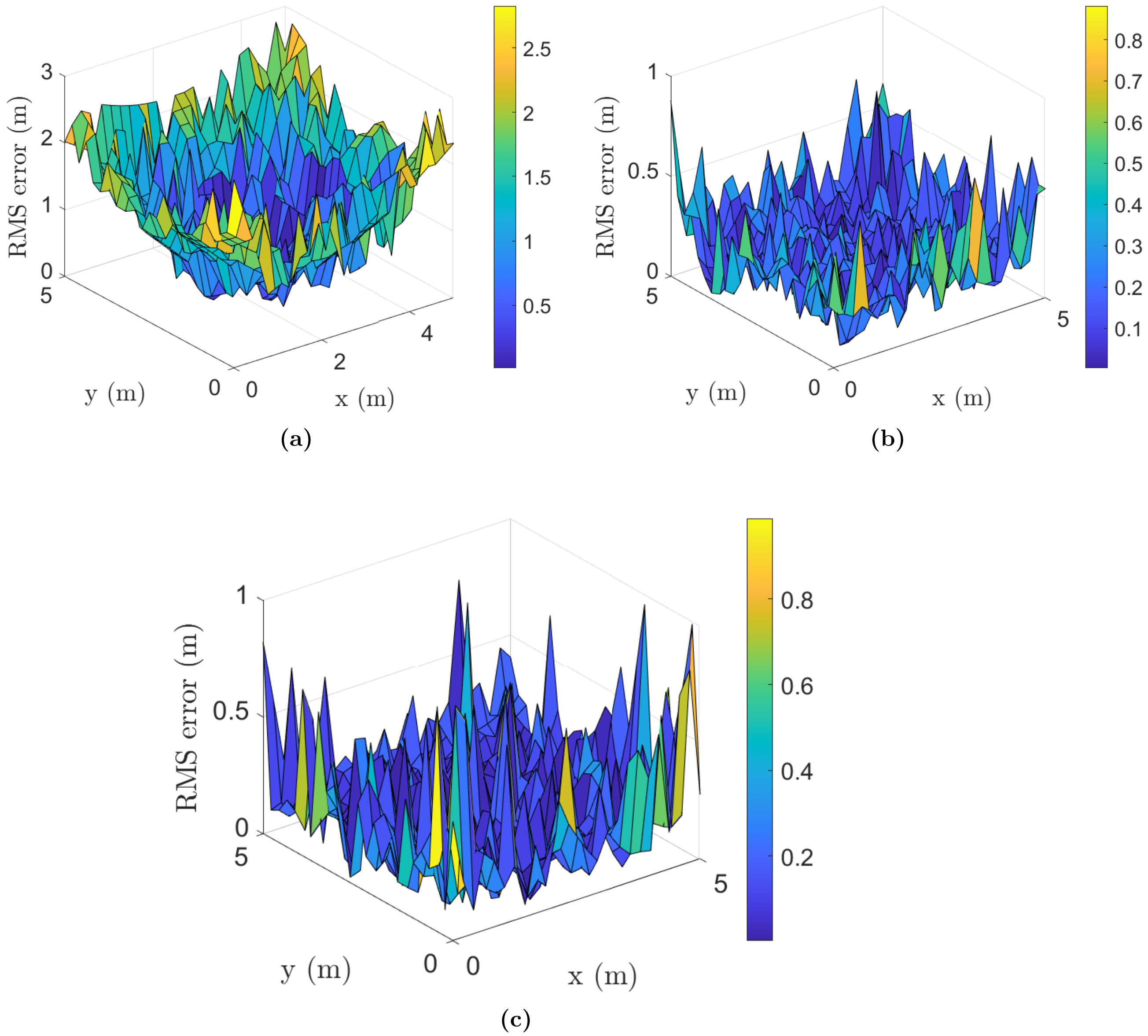

Figure 5.8: *RMS error for passive VLP at a) $\rho_{all} = 0$ b) $\rho_{all} = 0.5$ and c) $\rho_{all} = 1$.*

a low accuracy of 1.1 m. There is no significant difference in positioning accuracy for reflectivity above 50%, with an accuracy of the order of 0.2 m. The positioning error and reflection coefficient have a negative correlation; i.e. increasing the reflection coefficient reduces the RMS error. The respective RMS error distribution is seen in Figure 5.8.

$\rho_{all} = 0$ offers unfavourable performance as it is hard to relate the change in RSS caused by the wall and floor with respect to the object's position. However, a uniquely

Table 5.3: *Comparative study of the proposed system with published work.*

Paper	Method	Tx	Rx	Location	Room dimension	Performance	Environment
[119]	RSS,on-off	1	2	beside LED	9×7 cm^2	median 0.07 m	experimental
[60]	RSS,FDM	5	324	floor	3×3 m^2	10 degree mean angular error	experimental
[61]	RSS,FDM	20	20	floor	3.6×4.8 m^2	10 degree mean angular error	experimental
[62]	On-off, TDM	6	24	ceiling	7.5×6 m^2	0.89 m	experimental
[63]	shadow based RSS	NA	14	wall	2×3.6 m^2	0.021 m	experimental
[64]	shadow based RSS	NA	14	wall	4.8×9.6 m^2	0.84 m	experimental
[65]	IR	9	9	ceiling	$5 \times 5 \times 3$ m^3	0.1 m	theoretical simulation
This work	RSS,ANN	9	21	wall and ceiling	$5 \times 5 \times 3$ m^3	0.23 m	simulation

similar pattern is noticed across all reflection coefficients. Better system performance is noted in the middle of the room, with most peak errors at walls and edges. Note that even though $\rho_{all} = 1$ offers the lowest RMS error, more peaks are observed at the edge as compared to $\rho_{all} = 0.5$.

The passive VLP comparison between the work proposed in this thesis and that of the literature is summarised in Table 5.3. Unsurprisingly, experimental studies exhibit higher errors than simulation studies due to the inherent realism of the system. Simulation studies use a range of approximations to model light reflection on the object. The research in [65] is the closest to that presented in this chapter with the same room dimension, object size, and reflective coefficient of the room and the object. However, the main difference relies on the channel model and the positioning algorithm. In [65], the channel model only considers the 1st order reflection. This means that any ray of light that hits the wall's surface, than to the object to bounce back to the PD, is ignored. However, the work in [55] shows that the impact of 2nd order reflection is significant for VLP. Hence, this chapter also considers the 3rd order reflection as proposed in [120] for VLP. The ANN-based model approach proposed in this thesis provided an average RMS error of 0.23 m with 9 transmitters and 21 receivers and compared to 0.1 m in [65] with 9 transmitters and 9 receivers. The rationale for using a realistic channel model with up to 3rd order reflection is to reduce the gap in error between simulation and practical results.

5.5 Summary

This chapter introduced a passive VLP using ANN. By employing a ray-tracing technique, the passive VLP channel model was accurately modeled, thereby taking up to 3rd order reflection into consideration. Six different transmitter-receiver systems were considered to investigate their relationship with passive VLP performance. Unsurprisingly, the higher the number of transmitters and receivers, the better the positioning accuracy. In this work, the best performance is attained using 9 transmitters and 21 receivers, located both on the wall and on the ceiling, resulting in an average RMS error of 0.23 m. The best performance was attained at an object height of 0.8 m with a length and width above 0.2 m. Finally, it was demonstrated that the reflection coefficient of the surface of the target object is negatively correlated with the positioning accuracy.

Chapter 6

Outdoor Visible Light Positioning

Autonomous vehicles are expected to benefit ITS through improved efficiency, reduced traffic congestion and increased road safety. The practical realisation of these expected benefits requires autonomous vehicles to have precise localisation, perception (to identify their surroundings and the presence of obstacles), control functionalities and efficient communication [121]. Vehicles need precise localisation, often at centimetre accuracy for safety requirements [43]. Widely used outdoor localisation techniques such as GPS and differential GPS (dGPS) used by autonomous vehicles rely on satellites transmitting position information using the RF spectrum. The localisation accuracies of these technologies are in the meter range and worsen in adverse conditions [122,123]. Although recent developments of dGPS for autonomous vehicles provide decimeter-level accuracy [124], these signals do not extend to tunnels, underground areas and suffer significant path-loss and multi-path propagation in urban roads. Hence, there is a need for alternative localisation techniques to either complement or replace GPS (in the case of GPS failure) to improve the current localisation availability and accuracy for safety requirements and also to facilitate indoor navigation for smart parking. The popularity and wide availability of SSL such as LEDs for outdoor illumination, traffic signalling and variable message signs provide a unique platform to utilise them for high-speed communication and accurate localisation [125]. The current energy-saving schemes funded by the European Commission aiming to replace existing street lighting solutions with LED street lamps is attractive for outdoor positioning systems due to their ubiquity, especially in tunnels and underground roads [126].

Several studies have already proved that VLP system can provide accuracy in the centimetre range for indoor positioning. However, the use of VLP for outdoor positioning, especially for autonomous vehicle applications, is still under development. Outdoor localisation for vehicular applications is challenging due to the unavailability of a distributed light network. Streetlights are generally in a straight line. Techniques such as triangulation or similar algorithms form a reference plane equation for each transmitter. However, the transmitters must not be collinear for the algorithms to compute any valid output. Hence, these algorithms cannot be used, and most of the outdoor localisation strategies estimate the relative position or separation between vehicles (using the traffic light with head and tail light of vehicles), which is only adequate for vehicle collision avoidance.

The aim of this Chapter is to demonstrate the possibility of vehicle position irrespective of the alignment of the light. The remainder of this chapter is composed as follows. The following section reviews related work to identify the research gap and justify the approach adopted in this Chapter. Section 6.3 describes the systems for the two use cases considered. The first use case is positioning using outdoor streetlight. The second use case is positioning using traffic light(s). Section 6.4 presents the initial ANN design and tuning. Section 6.5 exploit the ANN to investigate the impact of angular and spatial receiver diversity and separation to determine a good setup for outdoor VLP. Section 6.6 evaluates the effectiveness of a range of ML algorithms. Section 6.7 describes the benchmark algorithm, namely CMD with spatial and angular diversity. Section 6.8 presents the best ML algorithm and evaluate its robustness against different solar illumination, weather conditions and road scenarios. Section 6.9 presents a traffic light based VLP using ANN.

6.1 Related work

A PD-based VLP was proposed in [74] for vehicular application. By mounting a PD on the vehicle as the receiver and using the headlights or taillights as the transmitter, the AOA information can be calculated. The study employs VLC, where each transmitter can transmit its actual speed. The speed information together with the AOA can then be used for vehicle collision avoidance. A camera-based navigation system based on traffic lights was proposed in [41] where cameras are used to take images within 1 s interval. They analyse images by taking three shots before the traffic light turns from red to green. The study has shown the ability of monitoring vehicles but has not shown the feasibility of pinpointing the exact location of a vehicle. In [127], a VLP technique using car tail light and tunnel lighting infrastructure is proposed. Image processing was adopted to extract information from a camera placed in front of the vehicle. However, the study assumes the constant availability of a neighbouring vehicle several meters ahead, continuously sending its updated position information.

Bai et al in [42] proposed a VLP based on a LED traffic light and PD. The traffic light conveys the position information to two photodiodes placed on the vehicle through a VLC link. The received information together with the TDOA of the signal is then used to estimate the location of the PDs mounted on the vehicle. The use of TDOArequires a perfect synchronisation between the transmitters (traffic light), which may be difficult in a heterogeneous environment. Furthermore, the best results were obtained with receivers located 2 m meters apart, which makes it not practical for a range of vehicles. The system yielded an RMS error of 5 m and 3.4 m for single and dual traffic lights, respectively. The feasibility of using streetlights for positioning using two rolling shutter CMOS sensors was shown in [44]. However, the streetlight setup adopted in the study, i.e. two-sided streetlight in a single two-lane road, provides distributed transmitter setup, hence, voiding the collinearity condition, as it can exploit trilateration. The performance of the system was affected by the blooming effect, which causes the LED images to be less clear in real-life applications. The streetlight location and design are heterogeneous. However, the aforementioned algorithms require a specific streetlight setup and are not compatible with non distributed streetlights. Hence, for VLP to work universally in all the streets, a method must be developed which works in the worst-case scenario where the streetlights are located in a linear array on only one side of the road. This thesis proposes a method combining spatial and angular receiver diversity with a supervised ANN to accurately estimate vehicles positions irrespective of the relative locations of the streetlights.

6.2 Outdoor VLP System Model

The proposed VLP system architecture is shown in Figure 6.1. Streetlights are installed on the side of the road and used as transmitters. It is assumed that each transmitter transmits TDM or FDM signals as outlined in section 2.4. The vehicles are assumed to travel on a tarmac road with a gradient close to zero. Therefore, the vehicle's movement along the x and y axis is significantly larger than the displacement along the z-axis. Consequently, this work focuses on 2-D localisation and considers only two degrees of movement along the x-axis and y-axis,. The proposed architecture of the receiver system with spatial and angular diversity is shown in Figure 6.1. The receiver system consists of multiple PDs, pointed in different directions. The tilting angles are independent for each PD and optimised for vehicular VLP in Section 6.5.3.

For outdoor application, a road with M (where $M > 1$) LED luminaires and $N \geq 1$ PD-based receiver is considered as shown in Figure 6.1. The transmitters are positioned collinearly of each other. Each transmitter/streetlight stands at 7 m high and are separated by 30 m from each other. This results in transmitter coordinates equal to $(0, 0)$ m, $(30, 0)$ m and $(60, 0)$ m and a road dimension of 60 m $\times$5 m. The power distribution across the road is shown in Figure 6.2. Less power reduction is noticed across the y-axis due to shorter link distances to the transmitters. In a situation where there is high signal reception, the signal from the three streetlights are received adequately, the PDs are capable of receiving up to 5 dB. This then worsens to SNR values of -10 dB when the signal received from the third street light is low. This scenario could happen at a sample receiver coordinates of $[35, 2.5]$ m; see Figure 6.3 which shows the respective SNR value for each transmitter-receiver link at the aforementioned coordinates. As expected, there is more signal received from the second transmitter (TX_2) located at $(30, 0)$ m. The signal from the first transmitter (TX_1) is the lowest, thus revealing the farthest transmitter from the receivers. It is observed from the simulation results that the PD is not capable of detecting a signal from TX_1 beyond $[35, 2.5]$ m. However, it could detect a signal if there were a fourth transmitter at $[90, 0]$ m. The rest of the simulation parameters can be found in chapter 3.

Figure 6.1: *Street light localisation model for VLP*

6.3 ANN Design for Outdoor Positioning

This section describes the proposed supervised feed-forward back propagation MLP ANN for outdoor 2-D VLP as illustrated in Figure 4.4. The different transmitters can be distinguished at the receiver end by employing TDM or FDM. The received signal from the transmitters (in this case, three transmitters) at various receivers given by 3.12 is first de-multiplexed and then fed to the ANN. For simplicity, the nLOS component is ignored for this application.

6.3.1 ANN setup and tuning

In this subsection, a base MLP-ANN is developed to establish positioning. The ANN structure developed in Chapters 4 and 5 is adopted as it has proved to work efficiently for VLP. However, the performance of the MLP-ANN is tuned for the system considered. Increasing the number of neurons tends to offer better performance at the cost of longer training time, larger training set, higher memory requirement and system complexity.

Figure 6.2: *Received power across the road that peaks at the same x coordinate than that of the transmitters located at $(0, 0)$ m, $(30, 0)$ m and $(60, 0)$ m.*

Hidden layers and nodes

To simplify the optimisation problem, the number of neurons in the hidden layers are made equal and is taken as a multiple of the diversity order (i.e. $M \times N$). By considering a two-layer ANN, the number of neurons in the hidden layer are varied from 6 to 36 (i.e. $6M \times N$), where $M = 3$ and $N = 2$. The RMS error for various number of neurons is calculated as seen in Figure 6.4. There is a large decrease in RMS error when the number of neurons is increased from 6 to 18. Thereafter, no significant drop in RMS error is noticed. Therefore, an MLP with 18 (i.e. $3(M \times N)$) neurons is adopted in the rest of this section. Note that this architecture will be further optimised once the optimum VLP system parameters are obtained.

Activation function

The impact of the activation functions is then investigated. It can be seen from Table 6.1 that the best performance is attained when both hidden layers use the log-sigmoid transfer function. Also, the worst performance is measured when the hidden layers

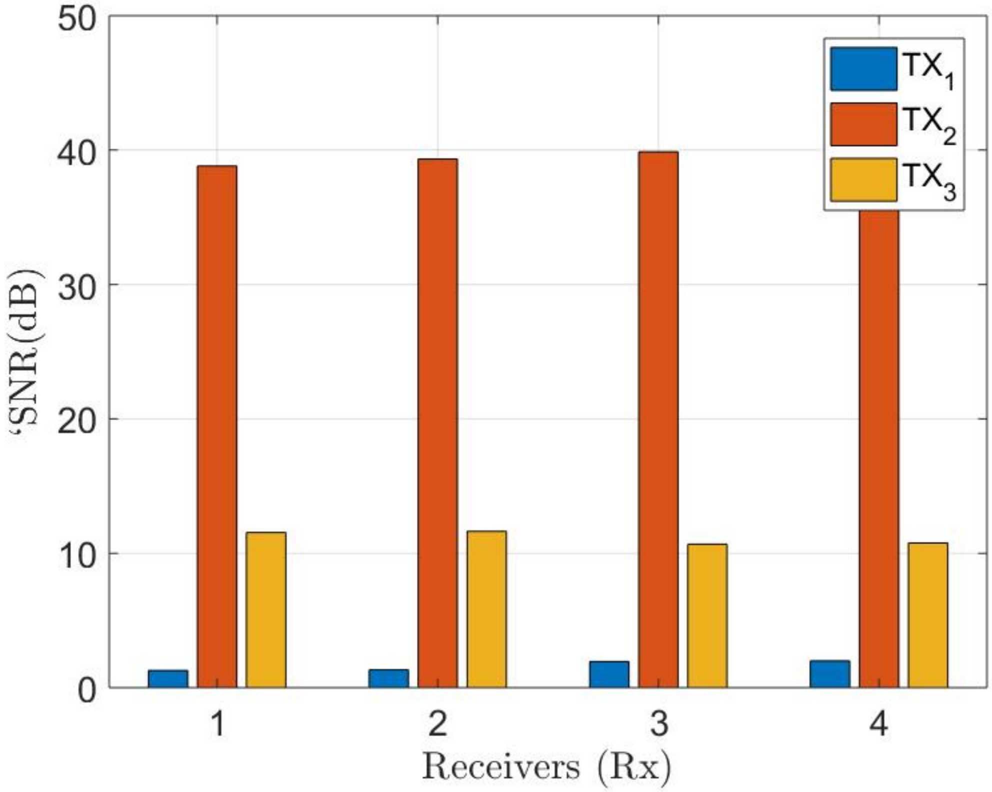

Figure 6.3: *SNR of across four receivers facing upwards positioned at [35,2,5]m.*

Table 6.1: *RMS error at different activation function combination*

RMS error (m)		
	Log-sig	Tan-sig
Log-sig	0.3210	0.3757
Tan-sig	0.3553	0.4399

have a tan-sigmoid transfer function. Using both transfer functions in the hidden layer slightly deteriorates the performance. Therefore, the log-sigmoid transfer function is adopted.

6.4 Outdoor VLP system setup

In this section, the VLP system architecture is optimised using the base ANN model. Several steps are taken to optimise the model ranging from the number of receivers (receiver diversity), receiver tilt angle (angular diversity) and receiver spacing (spatial diversity). First, the optimum number of receivers needed in the model is investigated

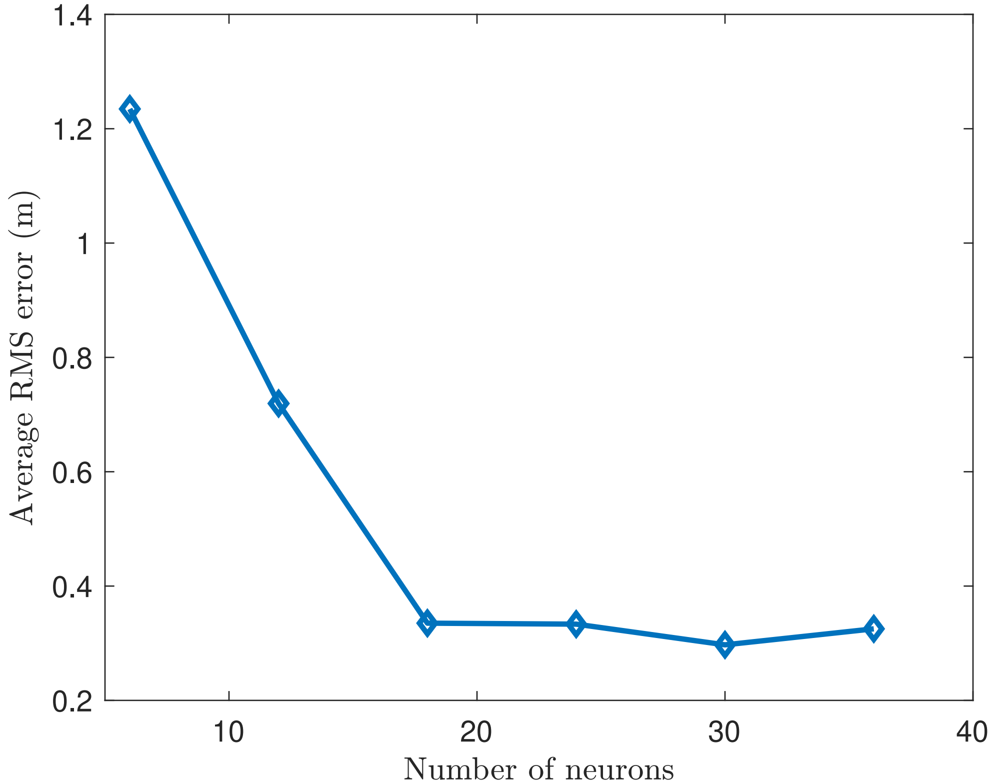

Figure 6.4: *RMS error versus the number of neurons.*

to demonstrate the need for receiver diversity in VLP. The following simulation assumes an environment with direct sunlight without an optical filter, thus considering the maximum noise as seen in Table 3.1. The noise parameters are provided in Table 3.1 and the rest of the simulation parameters are provided in Table 6.2.

6.4.1 Receiver diversity

Figure 6.5 shows the relationship between the RMS error and the number of receivers. Here, all the receivers are facing upwards. Note that the RMS error reduces as the number of receivers is increased. There is a significant performance improvement when the number of receivers increases from 1 to 4 with a percentage decrease of 35%, 10% and 26% for one to two, two to three and three to four, respectively. This is due to the direct proportionality between the number of receivers and the gain of the system. Though selecting a higher number of receivers will improve system performance, this will come at the cost of higher system complexity and longer training time. Moreover, increasing from four to five and five to six receivers only offers a 7% and 5% decrease in RMS error. Hence, four receivers are selected in the rest of the study as it offers the best trade-off between performance and complexity.

Table 6.2: *Parameters used for simulation*

Parameter	**Value**
Road parameters $[L \times W]$ (m)	60×5
Number of transmitters (M)	3
Transmitter height (m)	7
Transmitter spacing (m)	30
Transmitter power P_t (W)	90
Transmitter semi-angle (degree)	60
No. of receiver (N)	$[1 - 6]$
Receiver area, A (mm^2)	1
Optical filter gain	1
Noise bandwidth, B (MHz)	1
Noise bandwidth factor (I_2)	0.562
FET channel noise factor Γ	1.5
Fixed capacitance of PD (pF/cm^2)	112
Noise bandwidth factor (I_3)	0.0868

6.4.2 Receiver separation

The impact of receiver separation on VLP is also investigated to select a favourable receiver spacing on the vehicle. Only receiver separations from 0.02 m to 0.4 m are considered due to their practicality for real applications. Figure 6.6 shows the CDF of the RMS error for various receiver separations. The receiver separations investigated are 0.02 m, 0.04 m, 0.1 m, 0.2 m, and 0.4 m. At 0.95 CDF, the average RMS errors are 2.5 m, 1.86 m, 1.83 m, 1.3 m and 0.8 m, respectively. Figure 6.6 illustrates that increasing the receiver spacing increases the accuracy of the system. It is noticed that only a receiver separation of 0.4m (out of the chosen values) provide an RMS error below 1 m at 0.95 CDF. Hence, the separation between the receivers of 0.4 m is selected for further simulations.

6.4.3 Angular Diversity

Angular diversity is considered in this application to improve system performance through better signal reception. The first two PDs are facing the direction of travel (forward-facing), and the last two PDs are facing away from the direction of travel (rear-facing). The PDs are considered to have two degrees of freedom, namely $\angle x$ and $\angle y$ as illustrated in Figure 6.1. $\angle x$ represents the rotation across the x axis, that is, tipping the receivers towards or away from the direction of travel. $\angle y$ represents the rotation across the y axis, that is, tilting the receiver towards or away from the streetlight. $\angle z$ is the rotation of the PD across the z-axis. This is ignored as it does not introduce any difference to signal reception due to the circular nature of the PD. However, this could change on non-circular PDs. Starting with the forward-facing PDs,

Figure 6.5: *CDF of VLP as a function of number of receiver.*

their angles are changed from 0° to 90° and the back facing PDs from 90° to 180° with a step size of 10°. The $\angle y$ is kept constant for all the PDs, so they face towards the streetlights.

Figure 6.7 (a) shows the RMS error with respect to receiver angles. The forward-facing receivers are first considered. A rise in the error is first noticed when the receiver angles are tilted from 0° to 20° (note that the rear-facing receivers and $\angle y$ are kept at 90°). The accuracy of the system is seen to improve between 30° to 60° with optimum being at 40°. In the case of the rear-facing receivers, the RMS error reduces when the angle changes from 90° to 140° with 130° being the optimum angle. It was found that the RMS error decreases when $\angle y$ is tilted from 0° to 50°, where it reaches a minimum. The RMS error is seen to increase beyond after that. The selected receiver orientations are therefore $\angle x = 40°$ and $\angle y = 50°$ for forward-facing, and $\angle x = 130°$ and $\angle y = 50°$ for rear-facing receivers. Having optimised the number of receivers and their respective angles, a CDF analysis is conducted and presented in Figure 6.7 (b) to see their respective impact on the system's performance. This is initiated by analysing

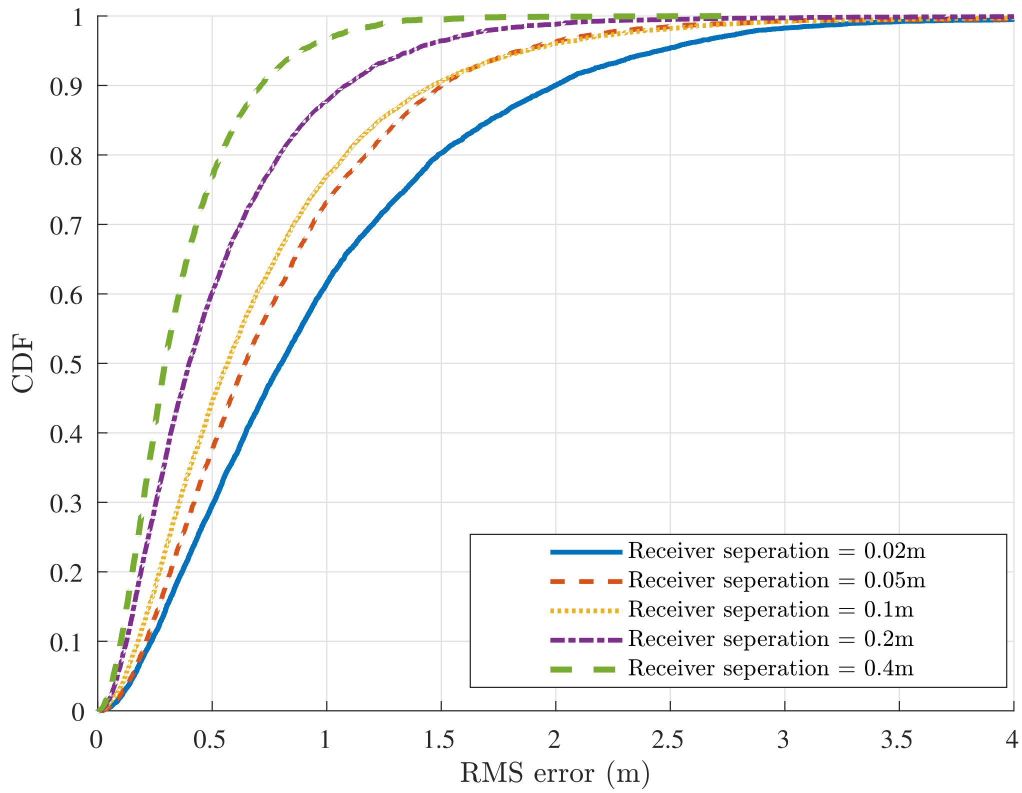

Figure 6.6: *CDF analysis at different receiver separation.*

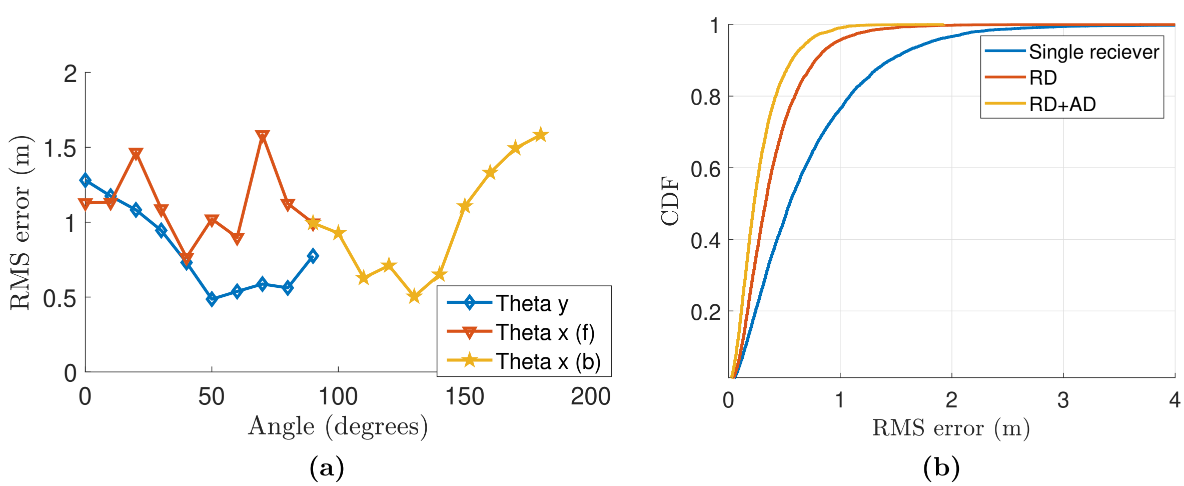

Figure 6.7: *a) Average RMS error at different receiver tilt angle and b) CDF analysis of the impact of receiver and angular diversities*

the system using a single receiver with the optimum simulation parameters. At 0.95 CDF, an RMS error of 1.8 m is noted for a single receiver. The value is seen to drop to 1 m when receiver diversity is applied. Furthermore, when angular diversity is included, an RMS error of 0.7 m is noted at 0.95 CDF. This reduction in RMS error shows that the proposed concepts can help provide improved performance for positioning systems in outdoor applications.

6.4.4 Receiver FOV

The model's performance is studied using different receiver FOV. This is attained by conducting a CDF analysis at different receiver FOV. The optical gains at all the FOVs are considered as unity to differentiate the performance improvement due to FOV. Figure 6.8 shows the CDF analysis ranging from 40° to 90° with a step size of 10. The system performance increases with an increase in FOV from 40° to 60°. However, no significant improvement is noted beyond 60°. In practice, though higher receiver FOV increases the chance of signal reception across the road, this also means more noise will be captured, thus reducing the accuracy of the system. Based on this study, a receiver FOV of 60° is selected for the rest of the simulation as it offers the best trade-off in terms of SNR.

6.5 ML algorithms

In this section, a comparative analysis between different ML algorithms is performed to determine the most suitable NN for outdoor VLP. The NNs considered are GRU, LSTM, sRNN and MLP-ANN (see Chapter 3.3). A total of $60,025$ 2-D positions from the same data set were considered in the simulation studies. A subset of 1500 positions was selected randomly to tune the NN. 70% of these positions were used for training, 15% for validation and 15% for testing. Each NN has a loss function of MSE. This is the method used to appraise the performance of the NN. However, the RMS values are shown for consistency with results in this thesis, as seen in Table 6.3. The aforementioned table shows all the parameters used to optimise the NN and the optimum hyper-parameters attained by the NN. Similarly to the approach in section 6.3, the number of neurons/weights is increased by one from 12 to 60 ($M \times N$ to $5(M \times N)$) with two hidden layers in the NN. Using GRU, the optimum performance was obtained at 16 neurons in the hidden layer with an average RMS error of 0.26 m. LSTM and RNN attained MSE minimum at 32 nodes with an average RMS error of 0.26 m and 0.29 m, respectively. MLP attained the MSE minimum for 36 nodes with an average RMS error of 0.22 m. From Table 6.3, it is observed that MLP performs the best; hence it is utilised for further analysis.

Next, the performance of the CMD and the MLP-ANN algorithms are evaluated using the optimum outdoor VLP structure. The simulation assumes an outdoor environment and thus considers the effect of sunlight in all the simulations unless stated

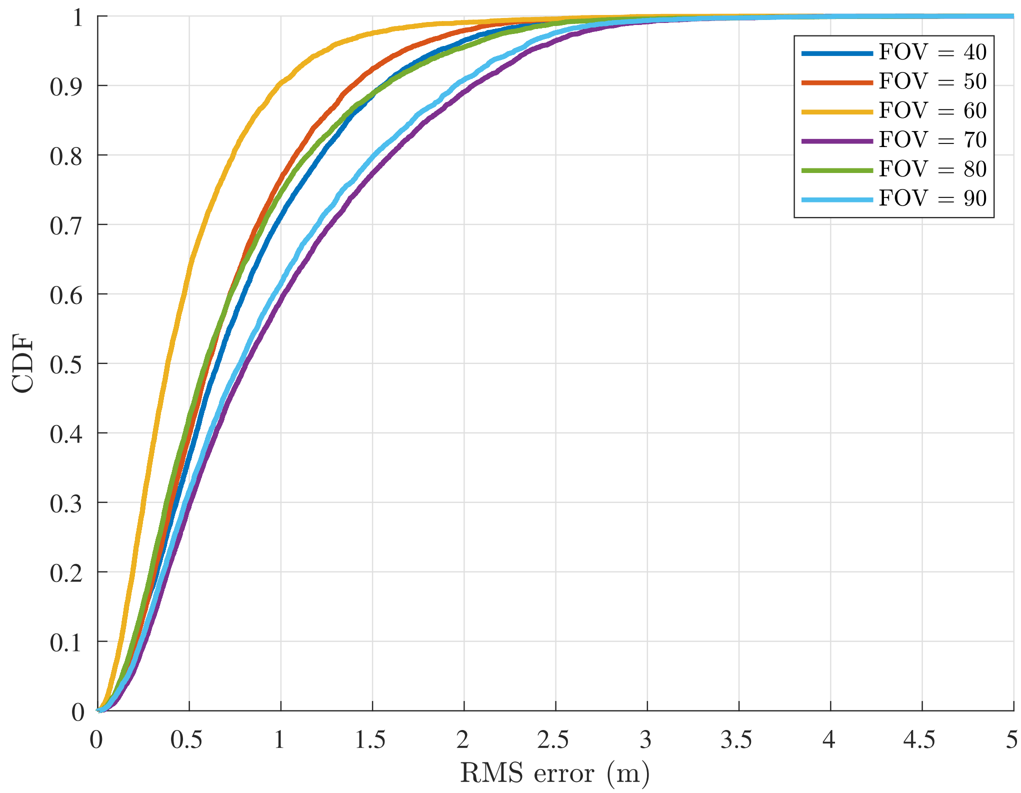

Figure 6.8: *CDF of VLP as a function of receiver FOV.*

Table 6.3: *Hyper-parameters of the machine learning algorithms*

Training Parameters	**GRU**	**LSTM**	**sRNN**	**MLP**
Number of weights per hidden layer	16	32	32	36
Learning rate	0.01	0.01	0.009	0.1
Number of hidden layers	2	2	2	2
Activation function (hidden layers)	tanh			
Kernel initialiser	Glorot Uniform			
Recurrent initialiser	orthogonal			
optimiser	Adam			LM
Loss function	Mean squared error			
Time step time step	1			-
Batch size	64	32	32	0.1
Dropout rate	-			0.25
Recurrent dropout rate	0.15	0.15	0.5	-
RMS error (m)	0.26	0.26	0.29	0.22

otherwise. In this study, streetlights are assumed to be turned on all the time. Considering the standardised illumination level of LED streetlights, the proposed VLP system is evaluated using RMS error, CI and CDF. The main parameters used for the simulation are shown in chapter 3.

6.6 CMD with Spacial and Angular Diversity

In this section, CMD is used to estimate the positioning error. Note that the simulation parameters used for this study are adopted from the optimised ANN model. Moreover, using a single receiver, it is impossible to estimate the positioning error due to the collinear arrangements of the streetlights. Hence, multiple receivers with spacial and angular diversity scheme are adopted as shown in Figure 6.1. Figure 6.9 shows the RMS error distribution across the road using 4 receivers. It can be seen that the localisation error is high at certain parts of the road reaching RMS error values of 12.1 m. The RMS error is seen to increase at the part of the road where the signal from the third streetlight is not received adequately and reduces as the received signal ratio between the three transmitters' increases. From the simulation, it is noticed that the system is more accurate in the x-axis than the y-axis, which yielded an average RMS error of 0.95 m and 6.77 m, respectively. This variation in error magnitude is highly influenced by the collinearity of the transmitter. This high RMS error is not helpful for the target application such as autonomous driving. Therefore, ANN is introduced to reduce the positioning error and improve accuracy.

6.7 MLP-ANN with Angular and Receiver Diversity

The performance of the proposed VLP system is first analysed during the day where sunlight is present. The model is simulated on a laptop computer (Intel(R) Core(TM) i7-6820HQ CPU of 2.70 GHz clock rate, 16 GB RAM, and runs 64-bit Windows 10 operating system) with a computational time of 75.9ms. Each analysis is done over 65554 test points. The RMS error analysis across the road is shown in Figure 6.10. The RMS error in x-axis is shown in Figure 6.10 (a). Given that the streetlights are on one side of the street (axis-$y = 0$), a rise in RMS error is noticed on the other side of the road due to lower signal reception. In the x-axis, an average RMS error of 0.02 m is recorded. It is noticed that the average RMS error in the y-axis is 0.17 m, see Figure 9 (b). Hence, the results show that the RMS error is higher in the y-axis than the x-axis. Notice that, unlike the CMD analysis, the RMS error is more evenly distributed across the road due to the learning abilities of the NN.

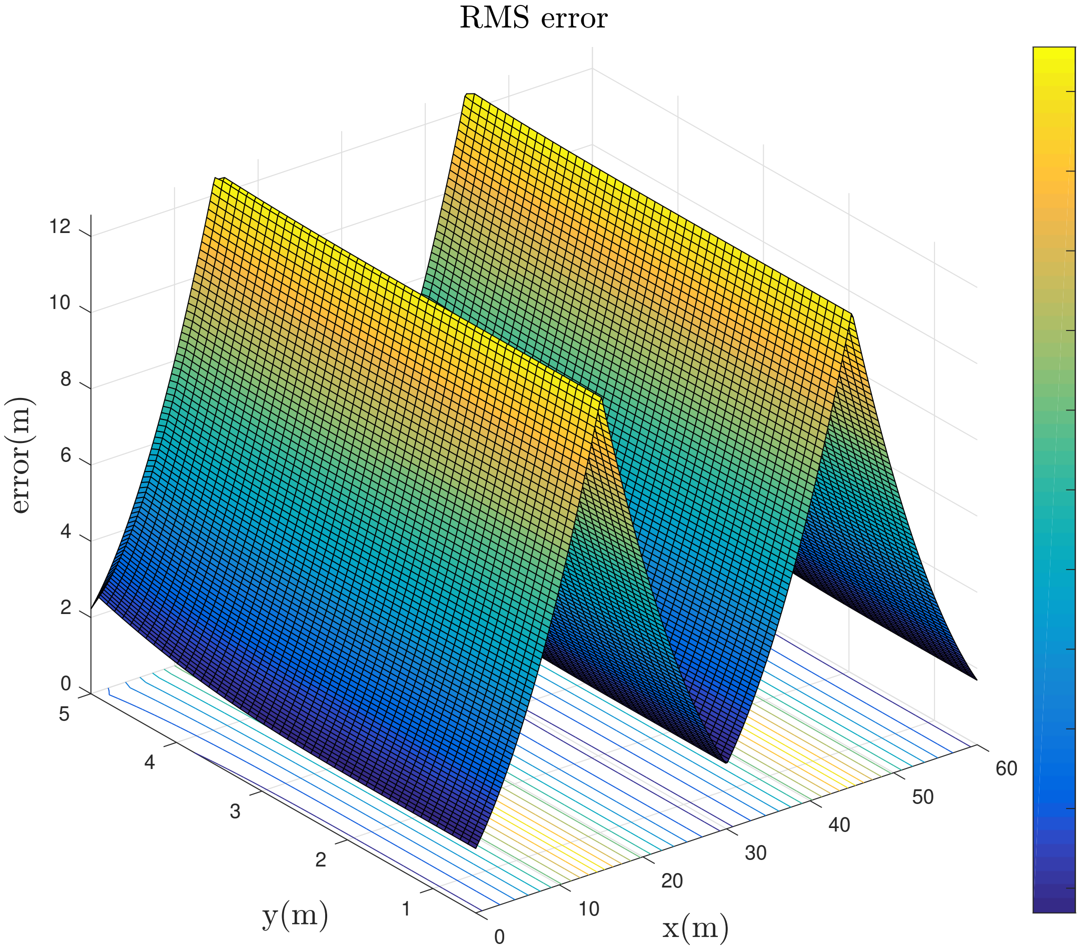

Figure 6.9: *RMS error across the road using CMD*

6.7.1 Day and Night

The performance of the system is analysed at night and compared during the day. During the night, ambient noise from the sun is absent. Figure 6.11 shows the RMS error distribution across the road during the day and night. An average RMS error at night is lower than the average RMS error at day due to reduced ambient light noise. The resulting average SNR across the road is 41 dB and 58 dB for day and night, respectively. The RMS errors are 0.22 m and 0.14 m during the day and night, respectively. This shows a percentage decrease of 36% between the day and night.

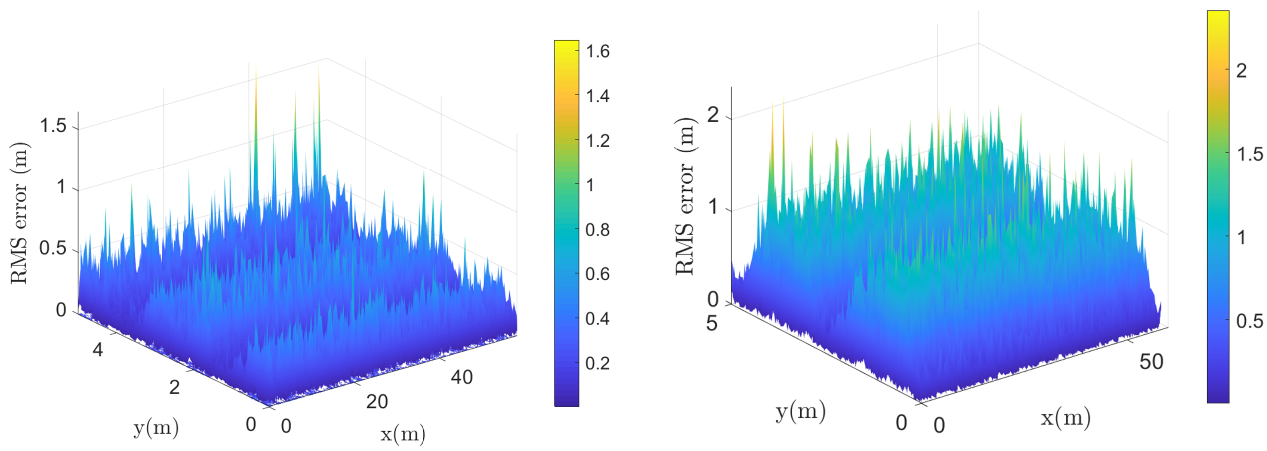

(a) **(b)**

Figure 6.10: *RMS error across the road: a) x-axis and b) y-axis*

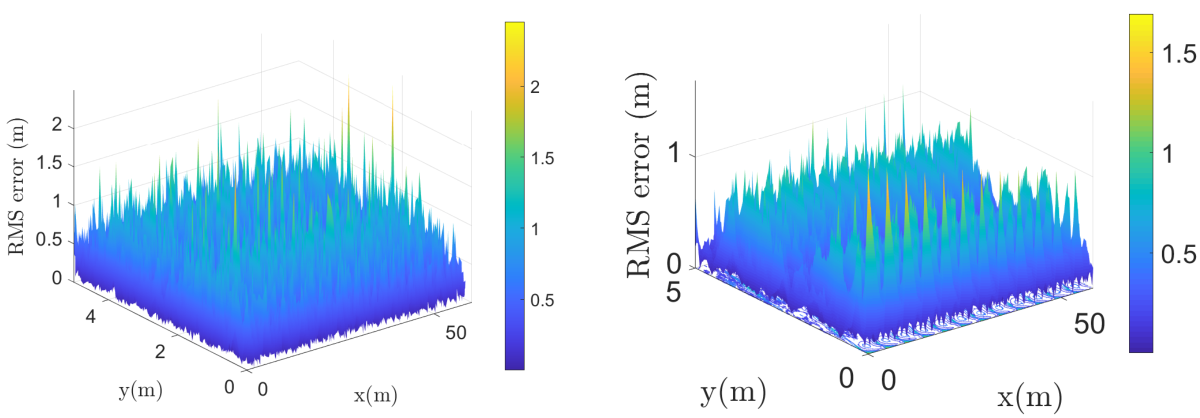

(a) **(b)**

Figure 6.11: *RMS error across the road: a) during the day and b) during the night*

6.7.2 Different weather conditions

In this section, the system's performance is analysed over the various weather conditions, and results are presented in Figure 6.12. Four representative weather conditions are selected, which are a) sunny day time under when the shot noise due to the sunlight is the strongest, b) night when there is very low ambient noise, c) think fog with visibility of 200 m and d) dense fog with visibility of 50 m when signal attenuation is very severe. The resulting average SNRs across the road for these conditions are 41 dB, 58 dB, 43 dB and 36.9 dB. Figure 6.12 illustrates the CDF analysis of the respective weather conditions, which reveals the best performance is obtained at night with clear weather when the noise is the minimum, followed by thick fog, sunny day time under the sun and dense fog with average RMS errors (RMS error at 0.95 CDF) of 0.14 m (0.49 m), 0.19 m (0.70 m), 0.22 m (0.72 m) and 0.29 m (0.98 m), respectively. As expected, the best performance is obtained at night when the received signal strength is the highest and the noise level is the lowest. The worst performance is obtained at the dense fog condition when the RSS is lowed due to attenuation of 78.2 dB/km. Though the RSS is higher during the sunny day than the thick fog condition with an attenuation of 39.1 dB/km, the performance is better at thick fog condition. This is because, in this condition, the absence of the shot noise due to sunlight outweighs the attenuation due to fog. Figure 6.13 shows the respective RMS error analysis at

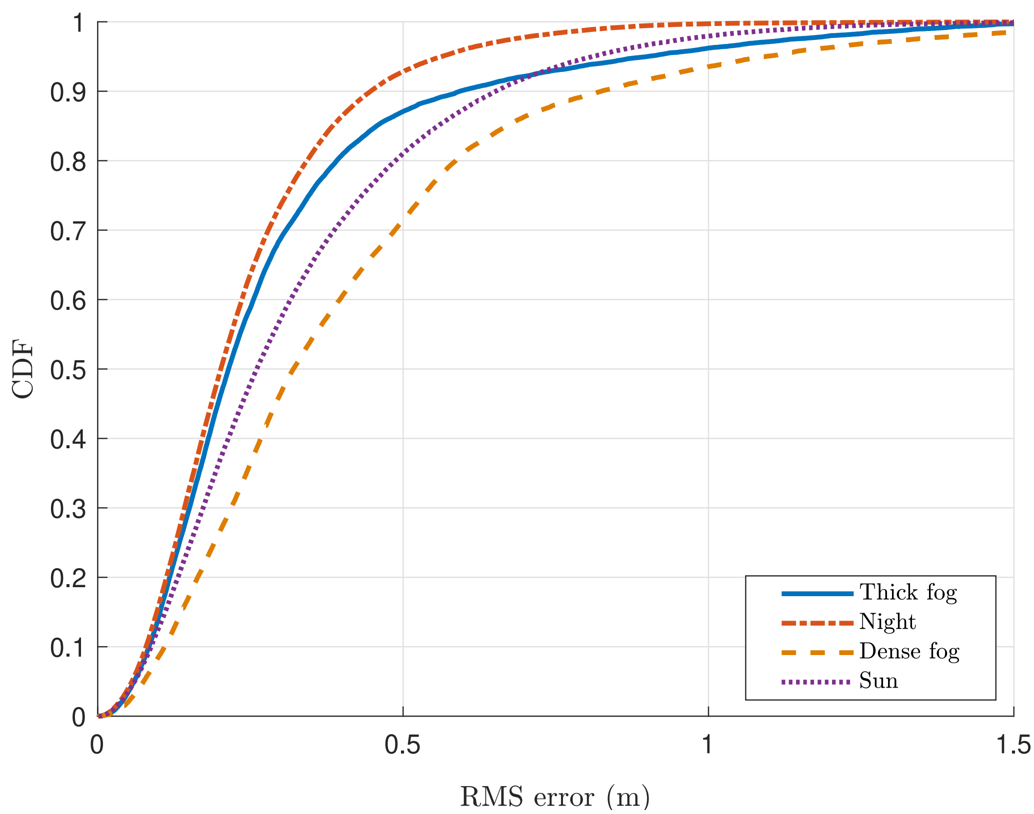

Figure 6.12: *CDF analysis at different weather conditions.*

different SNR values starting from 30 dB to 70 dB during the day. The model yields RMS error values above 0.4 m until it reaches 46 dB. A further drop in RMS error is noticed from 46 dB to 60 dB where an average RMS error below 0.19 m is achieved. Thereafter, no significant change in the gradient is noticed until an average RMS error of 0.13 m is recorded at 70 dB.

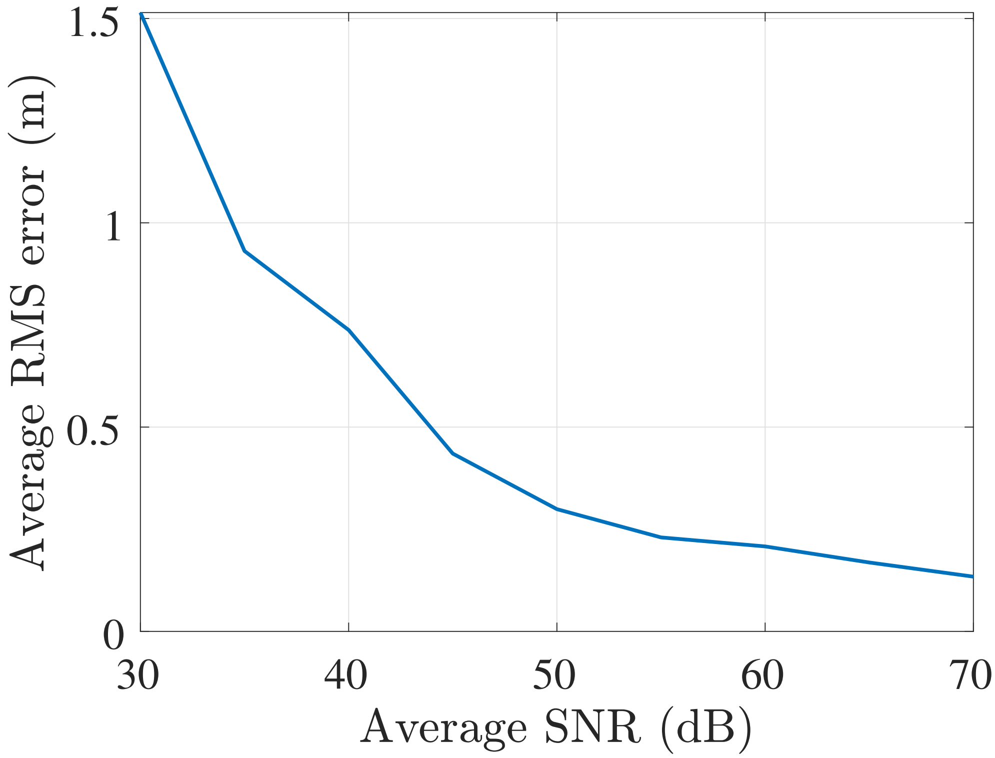

Figure 6.13: *Average SNR versus average RMS error.*

6.7.3 Different Road Scenarios

The proposed VLP design in this chapter is for autonomous vehicle applications. In most urban cities, different roads entail different transmitter locations (single-sided or double-sided), streetlight height and road width, as seen in [128]. In this section, different road scenarios are covered (see Table 6.4) to analyse the performance of the proposed model in urban cities. All the scenarios are analysed based on average RMS

Table 6.4: *Different road dimensions in urban cities [115].*

	Height	**Spacing**	**Road width**	**Transmitter position**	**RMS error**	**RMS error at** 95% **CI**
Case I	7 m	30 m	5 m	Single-sided	0.22m	0.72m
Case II	7 m	15 m	5 m	Single-sided	0.16 m	0.67 m
Case III	7 m	20 m	15 m	Double-sided	0.27 m	0.97 m
Case IV	8 m	15 m	10 m	Double-sided	0.09 m	0.29 m
Case V	8 m	30 m	10 m	Double-sided	0.27 m	1.21 m

error and (RMS error at 0.95 CDF) as shown in Table 6.4. By comparing Case I and Case II, reducing the transmitter spacing and the road width improves system performance. In Case III, streetlights are located on both sides of the road. Though the transmitter setup is distributed, the link distance is still long with 20 m transmitter spacing and 15 m wide road. When a 5 m reduction is made on both the transmitter spacing and road width, though increasing the transmitter height by 1 m as seen in Case IV, the performance of the system increases by 67%. Using the same transmitter height but increasing the transmitter spacing to 30 m in Case V provides similar performance in Case III. The system performs better on smaller roads, and providing a distributed transmitter (double-sided) enhances system performance.

6.8 Traffic light-based VLP using ANN

In the preceding section, streetlight based VLP has been proposed, designed and critically evaluated using ANN. However, streetlights are not the only possible transmitter sources available in the outdoor environment. In [127], the authors proposed the use of lights available tunnels for positioning. The study proposed using an image processing technique to determine the position of a vehicle based on three spatially distributed transmitters. However, the transmitter design used is not universal. To use a transmitter source that is widely available in most urban roads, Bai et al. in [42] proposed the use of an LED traffic light and two PDs. The study uses the TDOA and coplanar rotation based on the traffic lights for positioning. The research shows that Autonomous vehicles can use traffic light for proximity positioning in ITS application. Autonomous vehicles can use this to detect approaching distances to crossroads. Hence, in this section, MLP-ANN for 2-D traffic light-based VLP is proposed.

Figure 6.14 shows the traffic light-based VLP model. Similar simulation parameters are adopted from the literature as seen in [42]. A 6 m long traffic light with a 30 W LED is considered, with the traffic lights placed at the side of the road. Note that the colour of the LED light or its effect on VLP is not considered. Two PDs are placed on the vehicle, each facing the direction of travel. Each simulation assumes direct sunlight without an optical filter unless stated otherwise. The rest of the simulation parameters are presented in Table 6.5.

Note the same optimised ANN structure in Section 6.3 provides optimum near optimum ANN structure and is used in this section; thus, the same ANN design works for street light and traffic light-based VLP. In the following subsections, the performance of the ANN is analysed using single and multiple (two) traffic lights.

6.8.1 Single Traffic Light

In this subsection, the performance of the model will be analysed using a single traffic light. By considering a road dimension of 40 m $\times$5 m, the traffic light has a transmitter coordinate of $(0, 0)$ m (right side of the road). The vehicle is assumed to travel towards

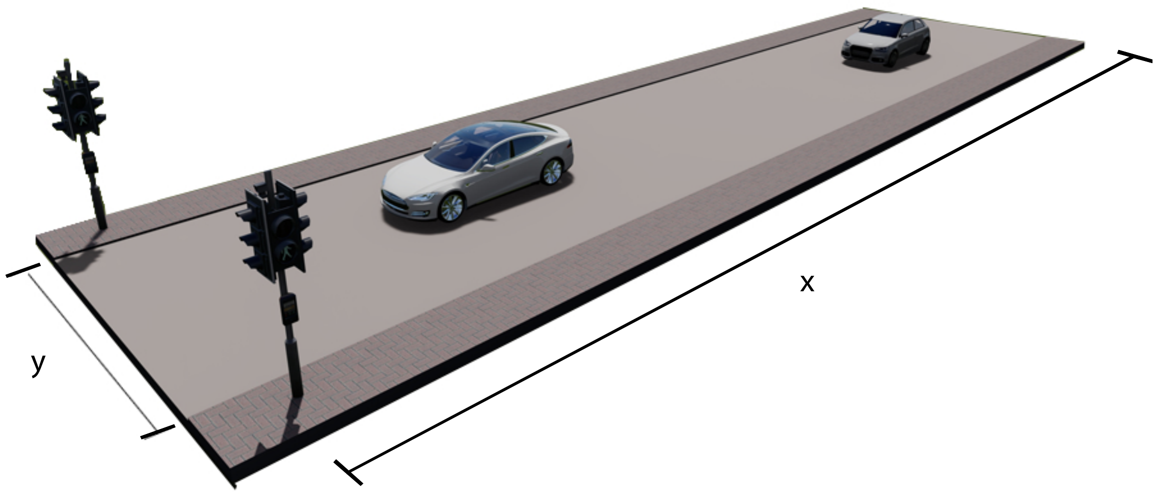

Figure 6.14: *Traffic light based VLP model.*

Table 6.5: *Parameters used for simulation*

Parameter	**Value**
Road parameters $[L \times W]$ (m)	40×5
Number of transmitters (M)	$[1 - 2]$
Transmitter height (m)	7
Transmitter power P_t (W)	60
Transmitter semi-angle (degree)	60
No. of receiver (N)	2
Receiver area, A (mm^2)	1
Optical filter gain	1
Noise bandwidth, B (MHz)	1
Noise bandwidth factor (I_2)	0.562
FET channel noise factor Γ	1.5
Fixed capacitance of PD (pF/cm^2)	112
Noise bandwidth factor (I_3)	0.0868

the transmitter with two PDs placed on the top. Figure 6.15 shows the RMS error distribution across the road. The model yielded an RMS error of 0.33 m and 1.26 m across the x and y-axis, respectively. An average RMS error of 1.33 m is calculated across the road. The higher RMS error on the y-axis shows that it is difficult for the model to identify the lane in which the vehicle is rather than its respective distance in the x-axis. As seen in Figure 6.15, there is a high positioning error on the left side of the road where a traffic light is not present. In the following subsection, a second

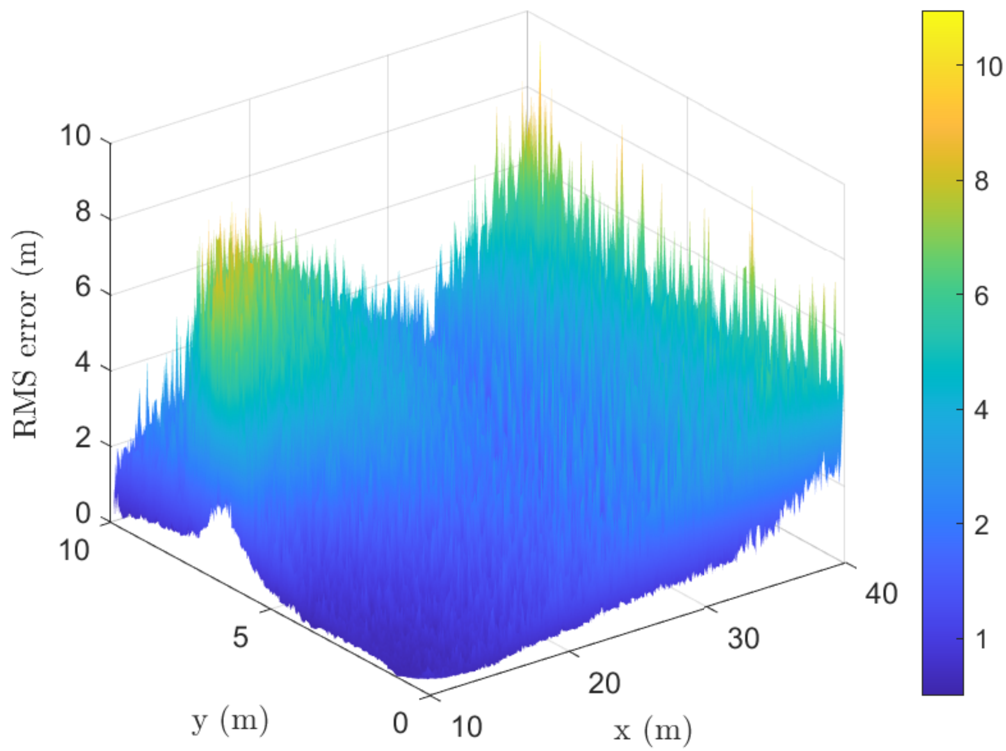

Figure 6.15: *RMS error across the road using single traffic light.*

traffic light is introduced.

6.8.2 Double Traffic Light

The performance of the system is analysed when a second traffic light is introduced across the street and the respective RMS error distribution is shown in Figure 6.16. The model yielded an RMS error of 0.04 m and 0.20 m in the x and y-axis, respectively. An average RMS error of 0.21 m is calculated. It is noted that the introduction of a second traffic light drastically reduced the RMS error by more than 1 m.

Based on the analysis using single and double traffic lights, it is noticed that the system performance starts degrading at distances beyond 30 m from the traffic light. This directly relates to the SNR values at the farther points, i.e. the more distant the length from the traffic light, the lower the SNR value. The relationship between SNR and VLP performance is shown in Chapter 4.9.2. Though using two traffic lights provides similar performance with streetlight based VLP in the preceding section, the traffic light-based VLP leverages a shorter road dimension with 40 m as compared to 60 m. Moreover, the traffic light-based VLP provides a better directionality between the transmitter and receiver as they are perpendicular to each other at all times in this

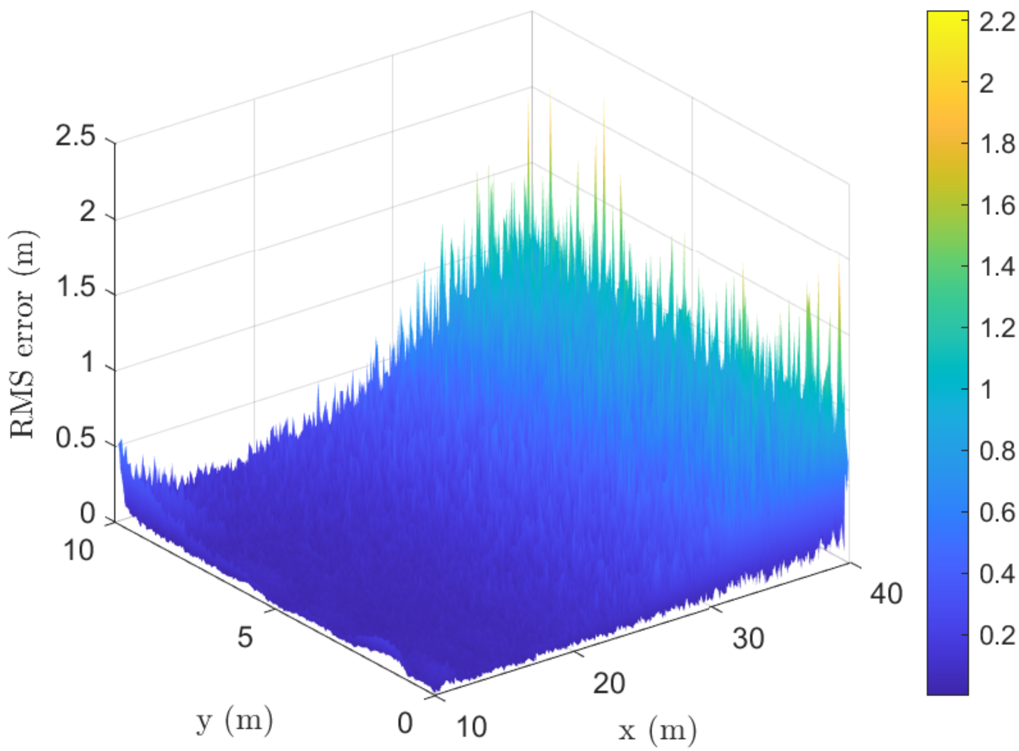

Figure 6.16: *RMS error across the road using dual traffic lights.*

study. However, at a closer x-axis but farther y-axis distance from the transmitter, the system performance decreases due to lower SNR values caused by limited receiver FOV (60°).

The proposed RSS model in this thesis outperforms the TDOA model proposed in [42]. Note that a near-optimum and more practical receiver spacing of 0.4 m is used in this study as compared to 2 m receiver spacing defined in the aforementioned study. Using single and double traffic lights, comparatively, the model in this work reduces the RMS error from 5.9 m to 1.33 m and 0.4 m to 0.21 m, respectively.

6.9 Summary

This chapter has presented a vehicular VLP solution based on ANN using the spatial and angular diversity receiver. Detailed system optimisation was presented, ranging from the ANN structure, the number of receivers, receiver angles and receiver separation. By using four PDs as the receiver and three streetlights as the transmitters, the received signal was identified using TDM or FDM. The distance between each transmitter-receiver link was calculated using the RSS. Using CMD, the model yielded an average RMS error of 6.84 m, which is high due to the collinear setup of the transmitter. ML algorithms were introduced to reduce this effect in VLP. Analysing the different ML algorithms such as GRU, sRNN, LSTM and ANN, it was found that MLP-ANN outperformed the rest with an average RMS error of less than 0.27 m under direct sunlight conditions on different road scenarios. Furthermore, the performance of the system is tested under different weather conditions to show the system's capability in adverse weather conditions. In clear weather, dense fog and at night, the system yielded an average RMS error of 0.22 m, 0.29 m and 0.14 m. Using just the forward-facing receivers (two-PDs), traffic lights were used as transmitters for 2-D VLP. The proposed model yielded an RMS error of 1.33 m and 0.21 m using single and double traffic lights on the road, respectively. This work proves that ANN with spatial and angular diversity receiver can overcome the collinearity condition in VLP using streetlight.

Chapter 7

Conclusions and Future Work

7.1 Conclusion

This research aimed to explore techniques to overcome the existing challenges that limit the realisation of VLP for indoor and outdoor applications. The literature study in Chapter 2 has identified the following gaps in research. Companies including Philip have deployed light positioning techniques to support user navigation focusing on relative positioning. However, VLP for actual positioning, where users can obtain their exact coordinates with respect to the environment, is more challenging. Research conducted in indoor 3-D VLP has not always considered the effect of multipath propagation to provide accurate and realistic channel modelling. VLP has been proposed to exploit the existing road infrastructure and street lighting. However, limited studies considered the wide range of streetlights alignment and relative positions concerning various road scenarios. The use of streetlights for VLP assumes that there are always distributed transmitters (on both sides of the road). However, this is not the case in some urban roads where streetlights are only on one side of the road. This thesis recognises this issue and proposes suitable methods and techniques to solve them.

In Chapter 3, the visible light channel model, including channel gains for LOS and NLOS were presented for a Lambertian source. The noise models used in indoor (shot) and outdoor (with sunlight) were detailed. The details of the proposed and benchmarked algorithms such as ANN, LSTM, GRU, RNN and CMD were described. Finally, the statistical methods of analysis such as RMS error, CDF, CI, percentage difference and percentage increase were stated.

Chapter 4, described ANN-based VLP with receiver diversity to improve performance in the presence of NLOS. The ANN used is trained using Levenberg-Marquardt back-propagation algorithm. The optimum ANN structure is found at 2 hidden layers, each with 16 neurons and a Log-sigmoid transfer function. The simulation studies found the best VLP link configuration with non directed LOS to use two receivers with a 60°. Increasing the receiver FOV from 40° to 60° offers performance improvement. The presence of NLOS was seen in the literature to reduce the performance of VLP systems by approximately 90%. Using more than one receiver in this study enabled the adoption of a receiver diversity scheme, which improved system performance by 15% from one to two receivers. A direct correlation is noted with the accuracy of the VLP system and the number of receivers and the receiver separation. However, a system with two receivers with a spacing of 0.02 m offers the best trade-off between performance and system structure. Overall, it was shown that the proposed scheme, together with MLP-ANN, improved the VLP performance and reduced the effect of reflection from a difference of 87% to 5.8%. Another contribution is applying the proposed MLP-ANN to dark VLP, where positioning is established despite the LED lights appearing 'OFF' to the human eye. Dark VLP is achieved by using a very low PWM duty cycle. The very low PWM duty cycles negatively affect existing VLP algorithms, such as CMD, for VLP applications. However, MLP-ANN can still work at duty cycles as low as 0.007% and improve positioning by 70% compared to CMD for duty cycles of 6.25%.

Chapter 5 studies passive VLP where transmitters and receivers are located in the room ceiling. The ray-tracing technique was used to calculate the received power across the PDs that were placed on the ceiling. The model considers different reflections on the walls and the respective object to be localised based on RSS change across different points. The simulation study presented in Chapter 5 demonstrated that using receivers on the ceiling and walls improves the passive VLP performance by a significant 25% with an accuracy of 0.23 m compared to placing them on the ceiling only. This is achievable with an object size of 0.3 m $\times$0.3 m $\times$1.6 m in a room of 5 m $\times$5 m $\times$3 m. Moderately sized objects are easier to localise with a minimum object height of 0.2 m. A negative correlation pattern is noted between system performance and objects reflectivity.

In chapter 6, the work achieved in the indoor environment is extended to an outdoor setting for vehicle application. Outdoor VLP, however, comes with more challenges such as weather conditions, greater link distances and lack of distributed transmitters. Streetlights are considered as transmitters as they are primarily and continuously available on urban and rural roads. A demanding scenario was considered where the street lights were situated in a straight line. This scenario made it challenging to apply traditional positioning algorithms. The setup proposed in this thesis addressed those challenges by using an angular and spatial receiver diversity scheme with ANN. By adopting the aforementioned diversity scheme, higher SNR was attained for each vehicle location, thus improving the system performance. The optimum vehicular VLP structure comprised 4 receivers situated 0.2 m apart. The optimum ANN structure included 2 hidden layers, each with 36 neurons. ANN offers a 96% improvement compared to CMD, 18% as compared to GRU and LSTM, and 32% when compared to sRNN. The difference in performance does not relate to the superiority of ANN, but it shows that ANN is the most suitable for understanding such data structures. The robustness of ANN is analysed by evaluating its performance in different weather conditions. The worst performance is recorded during dense fog with less than 50 m of visibility, resulting in a 31% reduction in performance compared to sunny conditions.

This still leads to an RMS error value of 0.29 m.

A contribution also made in Chapter 6, is traffic lights based VLP using PDs. Traffic light-based VLP was achieved using the RSS information in the forward-facing PDs, thus using the same system structure as provided in the literature. The near optimum and a more practical receiver spacing was adopted, which are situated 0.2 m apart. The application of ANN on traffic lights based VLP with the traffic lights provided a 77% and 48% improvement in system performance compared to the existing state of the art techniques.

7.2 Future Work

Though a diverse study has been conducted in this thesis ranging from indoor active VLP, indoor passive VLP and outdoor VLP, it is essential to state the further work that needs to be done to bring ML-based VLP to a reality. Promising results were obtained, but further research needs to be conducted for its realisation.

The most crucial improvement under all these studies will be a practical implementation. The channel model and the ANN training are simulation-based, and results are obtained via offline training. Offline training is generally used just for verification purposes.

A diverse study is conducted in Chapter 4 in studying and reducing the effect of NLOS in VLP. The impact of NLOS was decreased from 87% to 5.8% using receiver diversity with ANN. Further enhancement can be obtained through the transmitter and or receiver tilting to reduce the difference further to $< 5\%$, i.e. not significant.

In chapter 5, a study is conducted using ray-tracing software to model the passive VLP channel. With a 67% difference in accuracy with a different simulation-based study, it is essential to initiate a practical implementation of the specific room and object type to validate the reason for performance deviation. Filling this gap will improve the validity of the ray-tracing based channel model for VLP.

In chapter 6, the feasibility of vehicular VLP was shown using streetlights and traffic lights. To move from streetlights to traffic lights-based VLP, the directionality of the receivers needs to be changed. A strategy needs to be developed to either optimise the receiver angle for both transmitters set up or include a different transmitters for traffic light positioning.

Bibliography

[1] M. A. Al-Ammar, S. Alhadhrami, A. Al-Salman, A. Alarifi, H. S. Al-Khalifa, A. Alnafessah, and M. Alsaleh, "Comparative survey of indoor positioning technologies, techniques, and algorithms," in *Proceedings - 2014 International Conference on Cyberworlds, CW 2014*. Institute of Electrical and Electronics Engineers Inc., 12 2014, pp. 245–252.

[2] Philips, "Carrefour in France Installs Philips LED-Based Indoor Positioning System." 2015. [Online]. Available: http://www.lighting.philips.com/main/cases/cases/food-and-large-retailers/carrefour-lille.html

[3] Acuity Brands, " Indoor Positioning System." 2015. [Online]. Available: http://www.acuitybrands.com/solutions/services/bytelight-services-indoor-positioning

[4] M. N. Kamel Boulos, "Location-based health information services: A new paradigm in personalised information delivery," *International Journal of Health Geographics*, vol. 2, 1 2003.

[5] C. Jeffrey, *An Introduction to GNSS*, 2nd ed. Calgary: NovAtel, 2015.

[6] R.-C. Alexandru and L. Elena-Simona, "Comparison of detection techniques for multipath propagation of pseudolite signals used in dense industrial environments," *Procedia Engineering*, vol. 100, pp. 1294–1300, 2015.

[7] P. Yang and W. Wu, "Efficient particle filter localization algorithm in dense passive rfid tag environment," *IEEE Transactions on Industrial Electronics*, vol. 61, no. 10, pp. 5641–5651, 2014.

[8] R. Guan and R. Harle, "Towards a crowdsourced radio map for indoor positioning system," in *2017 IEEE International Conference on Pervasive Computing and Communications Workshops (PerCom Workshops)*, 2017, pp. 207–212.

[9] J. Nieminen, C. Gomez, M. Isomaki, T. Savolainen, B. Patil, Z. Shelby, M. Xi, and J. Oller, "Networking solutions for connecting bluetooth low energy enabled machines to the internet of things," *IEEE Network*, vol. 28, no. 6, pp. 83–90, 2014.

[10] Y. Zhuang, Z. Syed, J. Georgy, and N. El-Sheimy, "Autonomous smartphone-based WiFi positioning system by using access points localization and crowd-sourcing," *Pervasive and Mobile Computing*, vol. 18, pp. 118–136, 4 2015.

[11] Y. Zhuang, Z. Syed, Y. Li, and N. El-Sheimy, "Evaluation of two wifi positioning systems based on autonomous crowdsourcing of handheld devices for indoor navigation," *IEEE Transactions on Mobile Computing*, vol. 15, no. 8, pp. 1982–1995, 2016.

[12] Y. Zhuang and N. El-Sheimy, "Tightly-coupled integration of wifi and mems sensors on handheld devices for indoor pedestrian navigation," *IEEE Sensors Journal*, vol. 16, no. 1, pp. 224–234, 2016.

[13] C. Zhang, M. J. Kuhn, B. C. Merkl, A. E. Fathy, and M. R. Mahfouz, "Real-time noncoherent UWB positioning radar with millimeter range accuracy: Theory and experiment," *IEEE Transactions on Microwave Theory and Techniques*, vol. 58, no. 1, pp. 9–20, 1 2010.

[14] P. Cheong, A. Rabbachin, J.-P. Montillet, K. Yu, and I. Oppermann, "Synchronization, toa and position estimation for low-complexity ldr uwb devices," in *2005 IEEE International Conference on Ultra-Wideband*, 2005, pp. 480–484.

[15] Y. Almadani, M. Ijaz, W. Joseph, S. Bastiaens, S. Rajbhandari, B. Adebisi, and D. Plets, "A novel 3D visible light positioning method using received signal strength for industrial applications," *Electronics*, vol. 8, no. 11, pp. 1311–1312, 2019.

[16] J. Armstrong, Y. A. Sekercioglu, and A. Neild, "Visible light positioning: a roadmap for international standardization," *IEEE Communications Magazine*, vol. 51, no. 12, pp. 68–73, 2013.

[17] Z. Ghassemlooy, W. Popoola, and S. Rajbhandari, *Optical wireless communications: System and channel modelling with MATLAB®*. Florida USA: CRC Press, 2017.

[18] T. H. Do and M. Yoo, "An in-depth survey of visible light communication based positioning systems," *Sensors (Switzerland)*, vol. 16, no. 5, 5 2016.

[19] W. Gu, M. Aminikashani, P. Deng, and M. Kavehrad, "Impact of Multipath Reflections on the Performance of Indoor Visible Light Positioning Systems," *Journal of Lightwave Technology*, vol. 34, no. 10, pp. 2578–2587, 5 2016.

[20] H. Kaushal and G. Kaddoum, "Underwater Optical Wireless Communication," *IEEE Access*, vol. 4, pp. 1518–1547, 2016.

[21] S. Pradhan, P. K. Sahu, R. K. Giri, and B. Patnaik, "Inter-satellite optical wireless communication system design using diversity techniques," *2015 International Conference on Microwave, Optical and Communication Engineering, ICMOCE 2015*, pp. 250–253, 6 2016.

[22] S. Rajbhandari, "Spatial and wavelength division multiplexing for high-speed VLC systems: An overview," in *10th International Symposium on Communication Systems, Networks and Digital Signal Processing, Prague, Czech Republic*, 2016, pp. 1–6.

[23] B. Busan, H. Kim, and Y.-H. Chung, "Maritime Visible Light Communication with Sea Spectrum Models View project," Tech. Rep., 2020. [Online]. Available: https://www.researchgate.net/publication/280027617

[24] H. Chun, A. Gomez, C. Quintana, W. Zhang, G. Faulkner, and D. O'Brien, "A Wide-Area Coverage 35 Gb/s Visible Light Communications Link for Indoor Wireless Applications," *Scientific Reports*, vol. 9, no. 1, 12 2019.

[25] C. Sun, H. Zhao, W. Feng, and S. Du, "A frequency-domain multipath parameter estimation and mitigation method for BOC-modulated GNSS signals," *Sensors (Switzerland)*, vol. 18, no. 3, 3 2018.

[26] R. Mautz and E. Zurich, "Combination of Indoor and Outdoor Positioning," in *1st International Conference on Machine Control & Guidance*, Zurich, 2008, pp. 1–10.

[27] O. Popoola, S. Sinanović, W. Popoola, and R. Ramirez-Iniguez, "Optical Boundaries for LED-Based Indoor Positioning System," *Computation*, vol. 7, no. 1, pp. 1–7, 2019.

[28] A. Franca and L. Nollet, *Spectroscopic Methods in Food Analysis.* CRC Press, 12 2017.

[29] B. Gayral, "LEDs for lighting: Basic physics and prospects for energy savings," *Comptes Rendus Physique*, vol. 18, no. 7-8, pp. 453–461, 9 2017.

[30] T. Cevik and S. Yilmaz, "An Overview of Visible Light Communication Systems," *International journal of Computer Networks & Communications*, vol. 7, no. 6, pp. 139–150, 11 2015.

[31] C. Medina, M. Zambrano Nuñez, M. Zambrano, and K. Navarro, "LED Based Visible Light Communication: Technology, Applications and Challenges-A Survey magnetic suceptibility in liquids View project Construction and implementation of LDPC Convolutional Codes," *International Journal of Advances in Engineering & Technology*, vol. 8, pp. 482–495, 2015. [Online]. Available: https://www.researchgate.net/publication/281408421

[32] Y. Almadani, D. Plets, S. Bastiaens, W. Joseph, M. Ijaz, Z. Ghassemlooy, and S. Rajbhandari, "Visible Light Communications for Industrial Applications—Challenges and Potentials," *Electronics 2020, Vol. 9, Page 2157*, vol. 9, no. 12, p. 2157, 12 2020. [Online]. Available: https://www.mdpi.com/2079-9292/9/12/2157/htmhttps://www.mdpi.com/2079-9292/9/12/2157

[33] G. A. Mapunda, R. Ramogomana, L. Marata, B. Basutli, A. S. Khan, and J. M. Chuma, "Indoor Visible Light Communication: A Tutorial and Survey," *Wireless Communications and Mobile Computing*, vol. 2020, 2020.

[34] S. Demiguel, N. Li, X. Li, X. Zheng, J. Kim, J. C. Campbell, H. Lu, and A. Anselm, "Very High-Responsivity Evanescently Coupled Photodiodes Integrating a Short Planar Multimode Waveguide for High-Speed Applications," *IEEE Photonics Technology Letters*, vol. 15, no. 12, pp. 1761–1763, 12 2003.

[35] J. . Randall, O. . Amft, J. . Bohn, M. Burri, J. Randall, A. E. Oliver, A. Ae, J. Rgen, and B. Ae, "LuxTrace: indoor positioning using building illumination ETH Library LuxTrace: indoor positioning using building illumination," 2007. [Online]. Available: https://doi.org/10.3929/ethz-b-000412780

[36] E. Raaijmakers, "Philips Lighting installs first supermarket with indoor positioning in Germany - Philips Lighting," 2017. [Online]. Available: https://www.signify.com/global/our-company/news/press-release-archive/2017/20170306-philips-lighting-installs-first-supermarket-with-indoor-positioning-in-germany

[37] S. Somanath, "Lumicast lights the way to a more personal retail experience | Qualcomm," 2016. [Online]. Available: https://www.qualcomm.com/news/onq/2017/03/20/lumicast-lights-way-more-personal-retail-experience

[38] V. Renaudin, O. Yalak, P. Tomé, and B. Merminod, "Indoor Navigation of Emergency Agents," Tech. Rep. 3, 2007. [Online]. Available: https://www.researchgate.net/publication/37450461

[39] Y. Zhuang, L. Hua, L. Qi, J. Yang, P. Cao, Y. Cao, Y. Wu, J. Thompson, and H. Haas, "A survey of positioning systems using visible LED lights," *IEEE Communications Surveys and Tutorials*, vol. 20, no. 3, pp. 1963–1988, 7 2018.

[40] S. Savasta, S. Member, M. Pini, and G. Marfia, "Performance Assessment of a Commercial GPS Receiver for Networking Applications," in *2008 5th IEEE Consumer Communications and Networking Conference.*

[41] H. Tae-Hyun, J. In-Hak, and C. Seong-Ik, "Detection of traffic lights for vision-based car navigation system," in *Proceedings of the First Pacific Rim Conference on Advances in Image and Video Technology*, ser. PSIVT'06. Berlin, Heidelberg: Springer-Verlag, 2006, p. 682–691. [Online]. Available: https://doi.org/10.1007/11949534_68

[42] B. Bo, C. Gang, X. Zhengyuan, and F. Yangyu, "Visible Light Positioning based on LED Traffic Light and Photodiode," in *2011 IEEE Vehicular Technology Conference (VTC Fall)*, 2011, pp. 1–5.

[43] P. G. R. Roberts and S. Rathi, "Visible light positioning: Automotive use case," in *2010 IEEE Vehicular Networking Conference*, 2010, pp. 309–314.

[44] T. H. Do and M. Yoo, "Visible light communication based vehicle positioning using LED street light and rolling shutter CMOS sensors," *Optics Communications*, vol. 407, pp. 112–126, 2018.

[45] N. Faulkner, F. Alam, M. Legg, and S. Demidenko, "Smart wall: Passive visible light positioning with ambient light only," *I2MTC 2019 - 2019 IEEE International Instrumentation and Measurement Technology Conference, Proceedings*, vol. 2019-May, pp. 1–6, 2019.

[46] Y. Cai, W. Guan, Y. Wu, C. Xie, Y. Chen, and L. Fang, "Indoor high precision three-dimensional positioning system based on visible light communication using particle swarm optimization," *IEEE Photonics Journal*, vol. 9, no. 6, pp. 1–20, 12 2017.

[47] Y. Chapre, P. Mohapatra, S. Jha, and A. Seneviratne, "Received signal strength indicator and its analysis in a typical WLAN system (short paper)," in *Proceedings - Conference on Local Computer Networks, LCN*. IEEE Computer Society, 2013, pp. 304–307.

[48] S.-Y. Jung, D.-H. Kwon, S.-H. Yang, and S.-K. Han, "Inter-cell interference mitigation in multi-cellular visible light communications," *Optics Express*, vol. 24, no. 8, pp. 8512–8526, 2016.

[49] H. S. Kim, D. R. Kim, S. H. Yang, Y. H. Son, and S. K. Han, "Mitigation of inter-cell interference utilizing carrier allocation in visible light communication system," *IEEE Communications Letters*, vol. 16, no. 4, pp. 526–529, 4 2012.

[50] H. H. Chou, C. Y. Tsai, and J. S. Jiang, "An experimental study of a micro-projection enabled optical terminal for short-range bidirectional multi-wavelength visible light communications," *Sensors (Switzerland)*, vol. 18, no. 4, pp. 983–988, 2018.

[51] L. Tamazirt, F. Alilat, and N. Agoulmine, "A Visible Light Communication based positioning system for intuitive advertising in supermarkets," in *5th International Workshop on ADVANCEs in ICT Infrastructures and Services*, 2017. [Online]. Available: https://hal.archives-ouvertes.fr/hal-01775324

[52] S. Yamaguchi, V. V. Mai, T. C. Thang, and A. T. Pham, "Design and performance evaluation of VLC indoor positioning system using optical orthogonal

codes," in *2014 IEEE 5th International Conference on Communications and Electronics, IEEE ICCE 2014*. Institute of Electrical and Electronics Engineers Inc., 10 2014, pp. 54–59.

[53] H. Zhang, J. Cui, L. Feng, A. Yang, H. Lv, B. Lin, and H. Huang, "High-Precision Indoor Visible Light Positioning Using Deep Neural Network Based on the Bayesian Regularization with Sparse Training Point," *IEEE Photonics Journal*, vol. 11, no. 3, 6 2019.

[54] H. Chen, W. Guan, S. Li, and Y. Wu, "Indoor high precision three-dimensional positioning system based on visible light communication using modified genetic algorithm," *Optics Communications*, vol. 413, pp. 103–120, 4 2018.

[55] W. Gu, M. Aminikashani, and M. Kavehrad, "Indoor visible light positioning system with multipath reflection analysis," in *2016 IEEE International Conference on Consumer Electronics, Las Vegas, NV, USA*, 2016, pp. 89–92.

[56] H. H. Heqing Huang, A. Y. Aiying Yang, L. F. Lihui Feng, G. N. Guoqiang Ni, , P. Guo, and P. Guo, "Artificial neural-network-based visible light positioning algorithm with a diffuse optical channel," *Chinese Optics Letters*, vol. 15, no. 5, pp. 050 601–50 605, 5 2017.

[57] I. Alonso-González, D. Sánchez-Rodríguez, C. Ley-Bosch, and M. A. Quintana-Suárez, "Discrete indoor three-dimensional localization system based on neural networks using visible light communication," *Sensors (Switzerland)*, vol. 18, p. 1040, 2018.

[58] J. He, C.-W. Hsu, Q. Zhou, M. Tang, S. Fu, D. Liu, L. Deng, and G.-K. Chang, "Demonstration of high precision 3D indoor positioning system based on two-layer ANN machine learning technique," in *Optical Fiber Communication Conference (OFC) 2019*. Optical Society of America, 2019, p. Th3I.2. [Online]. Available: http://www.osapublishing.org/abstract.cfm?URI=OFC-2019-Th3I.2

[59] F. M. Alsalami, Z. Ahmad, S. Zvanovec, P. A. Haigh, O. C. Haas, and S. Rajbhandari, "Indoor intruder tracking using visible light communications," *Sensors (Switzerland)*, vol. 19, no. 20, 10 2019.

[60] T. Li, C. An, Z. Tian, A. T. Campbell, and X. Zhou, "Human sensing using visible light communication," in *Proceedings of the Annual International Conference on Mobile Computing and Networking, MOBICOM*, vol. 2015-September. Association for Computing Machinery, 9 2015, pp. 331–344.

[61] T. Li, Q. Liu, and X. Zhou, "Practical human sensing in the light," in *MobiSys 2016 - Proceedings of the 14th Annual International Conference on Mobile Systems, Applications, and Services*. Association for Computing Machinery, Inc, 6 2016, pp. 71–84.

[62] V. Nguyen, M. Ibrahim, S. Rupavatharam, M. Jawahar, M. Gruteser, and R. Howard, "EyeLight: Light-and-shadow-based Occupancy Estimation and Room Activity Recognition," in *IEEE INFOCOM 2018 - IEEE Conference on Computer Communications*, 2018, pp. 351–359.

[63] N. Faulkner, F. Alam, M. Legg, and S. Demidenko, "Watchers on the Wall: Passive Visible Light-Based Positioning and Tracking with Embedded Light-Sensors on the Wall," *IEEE Transactions on Instrumentation and Measurement*, vol. 69, no. 5, pp. 2522–2532, 5 2020.

[64] D. Konings, N. Faulkner, F. Alam, E. M. Lai, and S. Demidenko, "FieldLight: Device-Free Indoor Human Localization Using Passive Visible Light Positioning and Artificial Potential Fields," *IEEE Sensors Journal*, vol. 20, no. 2, pp. 1054–1066, 1 2020.

[65] K. Majeed and S. Hranilovic, "Performance Bounds on Passive Indoor Positioning Using Visible Light," *Journal of Lightwave Technology*, vol. 38, no. 8, pp. 2190–2200, 4 2020.

[66] M. I. Jais, P. Ehkan, R. B. Ahmad, I. Ismail, T. Sabapathy, and M. Jusoh, "Review of angle of arrival (AOA) estimations through received signal strength indication (RSSI) for wireless sensors network (WSN)," in *I4CT 2015 - 2015 2nd International Conference on Computer, Communications, and Control Technology, Art Proceeding*. Institute of Electrical and Electronics Engineers Inc., 8 2015, pp. 354–359.

[67] S. Lee and S. Y. Jung, "Location awareness using Angle-of-arrival based circular-PD-array for visible light communication," in *APCC 2012 - 18th Asia-Pacific Conference on Communications: "Green and Smart Communications for IT Innovation"*, 2012.

[68] G. B. Prince and T. D. Little, "Two-phase framework for indoor positioning systems using visible light," *Sensors (Switzerland)*, vol. 18, no. 6, pp. 1971–1972, 2018.

[69] Y. Muhammad and H. Siu-Wai, "Indoor Positioning System Using Visible Light and Accelerometer," *IEEE*, vol. 32, no. 19, pp. 3306–3316, 2014.

[70] M. Yasir, S. W. Ho, and B. N. Vellambi, "Indoor position tracking using multiple optical receivers," *Journal of Lightwave Technology*, vol. 34, no. 4, pp. 1166–1176, 2016.

[71] A. Arafa, S. Dalmiya, R. Klukas, and J. F. Holzman, "Angle-of-arrival reception for optical wireless location technology," *Optics Express*, vol. 23, no. 6, p. 7755, 3 2015.

[72] F. Chu, J. Su, T. Liang, J. Chen, X. Wang, and X. Ma, "Least Angle Regression Adaptive Incremental Broad Learning System," in *Proceedings - 2020 Chinese Automation Congress, CAC 2020*. Institute of Electrical and Electronics Engineers Inc., 11 2020, pp. 7153–7157.

[73] G. Cossu, M. Presi, R. Corsini, P. Choudhury, A. M. Khalid, and E. Ciaramella, "A Visible Light localization aided Optical Wireless system," in *2011 IEEE GLOBECOM Workshops, GC Wkshps 2011*, 2011, pp. 802–807.

[74] B. Soner and S. C. Ergen, "Vehicular Visible Light Positioning with a Single Receiver," in *IEEE International Symposium on Personal, Indoor and Mobile Radio Communications, PIMRC*, vol. 2019-September. Institute of Electrical and Electronics Engineers Inc., 9 2019.

[75] T. H. Do and M. Yoo, "TDOA-based indoor positioning using visible light," *Photonic Network Communications*, vol. 27, no. 2, pp. 80–88, 2014.

[76] G. Cossu, A. M. Khalid, P. Choudhury, R. Corsini, E. Ciaramella, and . M. Zhang, "Visible light communications-recent progresses and future outlooks," in *2010 Symposium on Photonics and Optoelectronics*, vol. 4, no. 5, 2010, pp. 1–6.

[77] T. Q. Wang, Y. A. Sekercioglu, A. Neild, and J. Armstrong, "Position accuracy of time-of-arrival based ranging using visible light with application in indoor localization systems," *Journal of Lightwave Technology*, vol. 31, no. 20, pp. 3302–3308, 2013.

[78] T. Akiyama, M. Sugimoto, and H. Hashizume, "Time-of-arrival-based smartphone localization using visible light communication," in *2017 International Conference on Indoor Positioning and Indoor Navigation (IPIN)*, 2017, pp. 1–7.

[79] S.-Y. Jung, S. Hann, and C.-S. Park, "TDOA-Based Optical Wireless Indoor Localization Using LED Ceiling Lamps," Tech. Rep. 4, 2011.

[80] Y. Xu, J. Zhao, J. Shi, and N. Chi, "Reversed three-dimensional visible light indoor positioning utilizing annular receivers with multi-photodiodes," *Sensors (Switzerland)*, vol. 16, no. 8, pp. 1254–1256, 2016.

[81] Y. Kim, Y. Shin, and M. Yoo, "VLC-TDOA using sinusodial pilot signal," in *2013 International Conference on IT Convergence and Security, ICITCS*, 2013, pp. 1–3.

[82] S. Y. Pyun, H. Widiarti, Y. J. Kwon, J. W. Son, and D. H. Cho, "Group-based channel access scheme for a V2I communication system using smart antenna," *IEEE Communications Letters*, vol. 15, no. 8, pp. 804–806, 2011.

[83] J. H. Nah, R. Parthiban, and M. H. Jaward, "Visible light communications localization using TDOA-based coherent heterodyne detection," in *4th International Conference on Photonics, ICP 2013*, 2013, pp. 247–249.

[84] C. Huang and X. Zhang, "Impact and feasibility of darklight LED on indoor visible light positioning system," in *2017 IEEE 17th International Conference on Ubiquitous Wireless Broadband, ICUWB 2017 - Proceedings*, vol. 2018-January. Institute of Electrical and Electronics Engineers Inc., 1 2018, pp. 1–5.

[85] K. Panta and J. Armstrong, "Indoor localisation using white leds," *Electronics Letters*, vol. 48, pp. 228–230, 02 2012.

[86] U. Nadeem, N. U. Hassan, M. A. Pasha, and C. Yuen, "Indoor positioning system designs using visible LED lights: Performance comparison of TDM and FDM protocols," *Electronics Letters*, vol. 51, no. 1, pp. 72–74, 1 2015.

[87] X. Liu, H. A. Ounifi, A. Gherbi, Y. Lemieux, and W. Li, "A Hybrid GPU-FPGA-based Computing Platform for Machine Learning," *Procedia Computer Science*, vol. 141, pp. 104–111, 1 2018.

[88] J. Xu, H. Shen, W. Xu, H. Zhang, and X. You, "LED-Assisted Three-Dimensional Indoor Positioning for Multiphotodiode Device Interfered by Multipath Reflections," in *2017 IEEE 85th Vehicular Technology Conference (VTC Spring)*. Sydney, NSW, Australia: IEEE, 2017, pp. 1–6.

[89] Z. Zhang, S. W. Ko, R. Wang, and K. Huang, "Millimeter-wave multi-point vehicular positioning for autonomous driving," in *2019 IEEE Global Communications Conference, GLOBECOM 2019*. Institute of Electrical and Electronics Engineers Inc., 12 2019, pp. 1–6.

[90] U. Onyekpe, V. Palade, and S. Kanarachos, "Learning to Localise Automated Vehicles in Challenging Environments Using Inertial Navigation Systems (INS)," *Applied Sciences*, vol. 11, no. 3, p. 1270, 2021.

[91] Y. Almadani, M. Ijaz, B. Adebisi, S. Rajbhandari, S. Bastiaens, W. Joseph, and D. Plets, "An experimental evaluation of a 3D visible light positioning system in an industrial environment with receiver tilt and multipath reflections," *Optics Communications*, vol. 483, 3 2021.

[92] A. J. Moreira, R. T. Valadas, and A. de Oliveira Duarte, "Optical interference produced by artificial light," *Wireless Networks 1997 3:2*, vol. 3, no. 2, pp. 131–140, 1997. [Online]. Available: https://link.springer.com/article/10.1023/A:1019140814049

[93] Y. Almadani, "Visible Light Positioning using Received Signal Strength for Industrial Environments," Ph.D. dissertation, Manchester Metropolitan University, 2020.

[94] M. Ijaz, Z. Ghassemlooy, J. Pesek, O. Fiser, H. Le Minh, and E. Bentley, "Modeling of fog and smoke attenuation in free space optical communications link under controlled laboratory conditions," *Journal of Lightwave Technology*, vol. 31, no. 11, pp. 1720–1726, 2013.

[95] L. Rejfek, V. Brazda, and O. Fiser, "Device for Measurement of Optical Visibility," in *13th Conference on Microwave Techniques COMITE, Pardubice, Czech Republic*. Pardubice, Czech Republic: IEEE, 2013, pp. 90–94.

[96] Z. Chen and J. Wang, "GROF: Indoor localization using a multiple-bandwidth general regression neural network and outlier filter," *Sensors (Switzerland)*, vol. 18, no. 11, 11 2018.

[97] S. S. Haykin and S. S. Haykin, *Neural networks and learning machines*. Prentice Hall/Pearson, 2009.

[98] M. T. Hagan and M. B. Menhaj, "Training Feedforward Networks with the Marquardt Algorithm," *IEEE TRANSACTIONS ON NEURAL NETWORKS*, vol. 5, no. 6, pp. 989–993, 1994.

[99] S. Gouravaraju, J. Narayan, R. A. Sauer, and S. S. Gautam, "A Bayesian regularization-backpropagation neural network model for peeling computations," *ArXiv*, vol. abs/2006.16409, 6 2020. [Online]. Available: http://arxiv.org/abs/2006.16409

[100] N. M. Nawi, A. Khan, M. Z. Rehman, H. Chiroma, and T. Herawan, "Weight Optimization in Recurrent Neural Networks with Hybrid Metaheuristic Cuckoo Search Techniques for Data Classification," *Mathematical Problems in Engineering*, vol. 2015, pp. 1–12, 2015.

[101] K. Cho, B. van Merrienboer, C. Gulcehre, D. Bahdanau, F. Bougares, H. Schwenk, and Y. Bengio, "Learning Phrase Representations using RNN Encoder–Decoder for Statistical Machine Translation," in *Proceedings of the 2014 Conference on Empirical Methods in Natural Language Processing (EMNLP)*. Stroudsburg, PA, USA: Association for Computational Linguistics, 2014, pp. 1724–1734.

[102] C. D'Andrea and M. Sombra, "The Cayley-Menger determinant is irreducible for n less than or equal to 3," *Siberian Mathematical Journal*, vol. 46, no. 1, pp. 71–76, 2005.

[103] F. Thomas and L. Ros, "Revisiting trilateration for robot localization," *IEEE Transactions on Robotics*, vol. 21, no. 1, pp. 93–101, 2 2005.

[104] S. H. Yang, H. S. Kim, Y. H. Son, and S. K. Han, "Three-dimensional visible light indoor localization using AOA and RSS with multiple optical receivers," *Journal of Lightwave Technology*, vol. 32, no. 14, pp. 2480–2485, 2014.

[105] H. Steendam, “A 3-D Positioning Algorithm for AOA-Based VLP with an Aperture-Based Receiver,” *IEEE Journal on Selected Areas in Communications*, vol. 36, no. 1, pp. 23–33, 1 2018.

[106] M. Yasir, S. W. Ho, and B. N. Vellambi, “Indoor positioning system using visible light and accelerometer,” *Journal of Lightwave Technology*, vol. 32, no. 19, pp. 3306–3316, 10 2014.

[107] D. P. Nicolella, L. Torres-Ronda, K. J. Saylor, and X. Schelling, “Validity and reliability of an accelerometer-based player tracking device,” *PLoS ONE*, vol. 13, no. 2, 2018. [Online]. Available: https://doi.org/10.1371/journal.pone.0191823

[108] J. Jiang, W. Guan, Z. Chen, and Y. Chen, “Indoor high-precision three-dimensional positioning algorithm based on visible light communication and fingerprinting using K-means and random forest,” *Optical Engineering*, vol. 58, no. 1, 2019.

[109] D. Kim, J. K. Park, and J. T. Kim, “Three-Dimensional VLC Positioning System Model and Method Considering Receiver Tilt,” *IEEE Access*, vol. 7, pp. 132 205–132 216, 2019.

[110] Y. Almadani, M. Ijaz, S. Rajbhandari, U. Raza, and B. Adebisi, “Dead-Zones Limitation in Visible Light Positioning Systems for Unmanned Aerial Vehicles,” in *International Conference on Ubiquitous and Future Networks, ICUFN*, vol. 2019-July. IEEE Computer Society, 7 2019, pp. 419–421.

[111] X. J. Yu, Y. L. Ho, L. Tan, H. C. Huang, and H. S. Kwok, “LED-based projection systems,” *IEEE/OSA Journal of Display Technology*, vol. 3, no. 3, pp. 295–303, 9 2007.

[112] Y. Wu, X. Liu, W. Guan, B. Chen, X. Chen, and C. Xie, “High-speed 3D indoor localization system based on visible light communication using differential evolution algorithm,” *Optics Communications*, vol. 424, pp. 177–189, 2018.

[113] D. Plets, Y. Almadani, S. Bastiaens, M. Ijaz, L. Martens, and W. Joseph, “Efficient 3D trilateration algorithm for visible light positioning,” *Journal of Optics (United Kingdom)*, vol. 21, no. 5, 2019.

[114] Z. Tian, K. Wright, and X. Zhou, “The DarkLight rises: Visible Light Communication in the dark,” in *Proceedings of the Annual International Conference on Mobile Computing and Networking, MOBICOM*, vol. 0, no. 1. Association for Computing Machinery, 10 2016, pp. 2–15.

[115] Z. Tian, K. Wrighty, and X. Zhou, “Lighting up the internet of things with DarkVLC,” in *HotMobile 2016 - Proceedings of the 17th International Workshop on Mobile Computing Systems and Applications.* Association for Computing Machinery, Inc, 2 2016, pp. 33–38.

[116] G. Deak, K. Curran, and J. Condell, "A survey of active and passive indoor localisation systems," pp. 1939–1954, 9 2012.

[117] Z. Zhang, X. Gao, J. Biswas, and K. W. Jian, "Moving targets detection and localization in passive infrared sensor networks," in *2007 10th International Conference on Information Fusion*, 2007, pp. 1–6.

[118] J. Kemper and H. Linde, "Challenges of passive infrared indoor localization," in *5th Workshop on Positioning, Navigation and Communication 2008, WPNC'08*, 2008, pp. 63–70.

[119] C. Zhang, J. Tabor, J. Zhang, and X. Zhang, "Extending mobile interaction through near-field visible light sensing," in *Proceedings of the Annual International Conference on Mobile Computing and Networking, MOBICOM*, vol. 2015-September. Association for Computing Machinery, 9 2015, pp. 345–357.

[120] F. Lichtenegger, C. Leiner, C. Sommer, A. P. Weiss, and F. P. Wenzl, "Ray-tracing based channel modeling for the simulation of the performance of visible light communication in an indoor environment," in *2019 Second Balkan Junior Conference on Lighting (Balkan Light Junior)*. Institute of Electrical and Electronics Engineers Inc., 9 2019, pp. 1–6.

[121] B. Lyon, N. Hudson, M. Twycross, D. Finn, P. Steve, and Z. Maklary, "Automated Vehicles Do We Know Which Road To Take?" North Sydney, Tech. Rep., 2017. [Online]. Available: www.advisian.com

[122] J. Xiong, "Pushing the Limits of Indoor Localization in Today's Wi-Fi Networks," Ph.D. dissertation, University College London, 2015.

[123] S. Bauer, Y. Alkhorshid, and G. Wanielik, "Using high-definition maps for precise urban vehicle localization," in *IEEE Conference on Intelligent Transportation Systems, Proceedings, ITSC*. Institute of Electrical and Electronics Engineers Inc., 12 2016, pp. 492–497.

[124] H. P. Intelligence. (2019) High-precision GPS for Autonomous Vehicles. [Online]. Available: https://www.novatel.com/industries/autonomous-vehicles/

[125] Z. Ghassemlooy, L. N. Alves, S. Zvánovec, and M. A. Khalighi, *Visible light communications: Theory and applications*. CRC Press, 2017.

[126] "Lighting," 12 2019. [Online]. Available: https://ec.europa.eu/info/energy-climate-change-environment/standards-tools-and-labels/products-labelling-rules-and-requirements/energy-label-and-ecodesign/energy-efficient-products/lighting_en

[127] B. W. Kim and S. Y. Jung, "Vehicle positioning scheme using V2V and V2I visible light communications," in *2016 IEEE 83rd Vehicular Technology Conference (VTC spring)*, 2016, pp. 1–5.

[128] L. Leo, "Projects of LED Street Lights," Lighting Orient, Shenzhen, Tech. Rep., 2019.